DISSERTATION

DEVELOPMENT OF ADVANCED COMBUSTION STRATEGIES FOR HEAVY DUTY LPG ENGINES TO ACHIEVE NEAR-DIESEL EFFICIENCY

Submitted by

Toluwalase Jude Fosudo

Department of Mechanical Engineering

In partial fulfillment of the requirements

For the Degree of Doctor of Philosophy

Colorado State University

Fort Collins, Colorado

Fall 2024

Doctoral Committee:

Advisor: Daniel B. Olsen

Bret Windom
Dan Wise
Neil Grigg

ABSTRACT

DEVELOPMENT OF ADVANCED COMBUSTION STRATEGIES
FOR HEAVY DUTY LPG ENGINES TO ACHIEVE NEAR-DIESEL EFFICIENCY

As the transportation sector evolves in response to increasingly stringent emissions regulations and economic realities in the wake of the decarbonization drive, several no/low carbon fuel options have emerged as viable options for internal combustion engines. Among these fuels, Liquefied Petroleum Gas (LPG) is uniquely positioned for spark ignited engine operation due to its favorable physical and chemical properties. Currently, much of its use as an engine fuel is limited to light-duty applications, dual fuel applications, or retrofitted gasoline engines, with a lesser degree of penetration into the heavy-duty sector where diesel fuel still dominates. A key reason for this is the deficit in performance and efficiency between diesel and other low carbon fuels, including LPG, necessitating the need for targeted research aimed at bridging this gap, and positioning LPG as a fuel of choice in the heavy-duty sector. Two prominent drawbacks responsible for this gap between diesel and LPG engine performance are the dearth of specialized fuel injection hardware and tailored injection strategies, and knock, which limits the performance of spark ignited engines. This work seeks to address these and other limitations and achieve near diesel efficiency on a heavy-duty engine platform. Two engine platforms were employed in this study. A cooperative fuel research (CFR) spark-ignited engine was used to study the knock dynamics and the performance, combustion, and emissions behavior of the LPG fuel in relation to key engine parameters, the LPG fuel composition, and other low carbon fuel options. Compression ratio, engine load, exhaust gas recirculation percents, and a novel combustion control tool, the

combustion intensity metric (CIM), were all varied on the CFR engine and a computational fluid dynamics (CFD) model calibrated and validated. Key findings were then transferred to a heavy-duty engine platform, the Cummins ISX15L single cylinder engine. The engine is a converted 6-cylinder diesel engine with diesel brake thermal efficiency (BTE) of 44%. A baseline evaluation was conducted with liquid LPG port-injected at 16bar and 9.3:1 compression ratio. Then the engine was switched to direct injection (DI) configuration with a fuel delivery system capable of delivering liquid LPG at pressures up to 200bar. Three principal configurations were developed for operation of the heavy-duty engine employing a gasoline direct injector (GDI) with nozzle patterns adapted for optimal distribution of the LPG fuel in the combustion chamber, a GDI modified for higher LPG flow and a double-injector port-fuel injection (PFI) system optimized for injection location, and charge cooling and distribution. The experiments and modeling contained in this study demonstrate the impact of LPG composition on engine performance, the mitigating effect of EGR on knock and NOx emissions, the potential for a better controlled combustion using the CIM tool and the advantages in terms of knock, performance, and emissions of designing an injection strategy tailored to the LPG fuel. The results show that the heavy-duty engine operated on LPG achieved the target efficiency of 44% BTE at high EGR, high compression ratio, and high load conditions for both DI and PFI configurations. The outcomes of this study advance the literature on knock, end-gas autoignition, emissions, and EGR related to LPG and its use as a choice fuel for heavy-duty applications and advances the development of specialized fuel delivery hardware and injection strategies for the LPG fuel.

ACKNOWLEDGMENTS

It is with deep gratitude to Almighty God that I acknowledge everyone who was a part of my journey, everyone He set on my path. It really took a village. I also acknowledge the U.S. Department of Energy's Office of Energy Efficiency and Renewable Energy (EERE) who provided funding for this research under the award number DE-EE0009198. I would also like to thank the Colorado State University Energy Institute and its Powerhouse Energy Campus for providing the research facility and resources.

DEDICATION

I dedicate the entirety of this work to my glorious wife, Abisola, the star of my life, Mure, my best friend and brother, Temi, the greatest to ever do it, Tumininu. Also, to my brother Tomiwa, and my parents Prof. Sola and Yetunde Fosudo, for their ever-present love and encouragement, and for giving me a chance, Dr. Olsen.

TABLE OF CONTENTS

LIST OF TABLES

LIST OF FIGURES

LIST OF DEFINITIONS

AFR	-	Air-Fuel Ratio
AHRR	-	Apparent Heat Release Rate
aTDC	-	After Top Dead Center
bTDC	-	Before Top Dead Center
BMEP	-	Brake Mean Effective Pressure
bs	-	Brake Specific
BSFC	-	Brake Specific Fuel Consumption
BTE	-	Brake Thermal Efficiency
c-EGAI	-	Controlled End-Gas Auto-Ignition
CA50	-	50% Burn Crank Angle
CAD	-	Crank Angle Degrees
CFR	-	Cooperative Fuel Research
CIM	-	Combustion Intensity Metric
CNG	-	Compressed Natural Gas
CO	-	Carbon Monoxide
CO_2	-	Carbon Dioxide
CO_2eq	-	Equivalent CO_2
COV	-	Coefficient of Variation
CR	-	Compression Ratio
DI	-	Direct Injection
EGAI	-	End-Gas Auto-Ignition
EGR	-	Exhaust Gas Recirculation
EOI	-	End of Injection
EVC	-	Exhaust Valve Closing
EVO	-	Exhaust Valve Opening
f-EGAI	-	Fraction of End-Gas Auto-Ignition
FFT	-	Fast Fourier Transform

FID	-	Flame Ionization Detection
FTIR	-	Fourier Transforms Infrared
GDI	-	Gasoline Direct Injector
GHG	-	Greenhouse Gases
HC	-	Hydrocarbons
IMAP	-	Intake Manifold Air Pressure
IMEP	-	Indicated Mean Effective Pressure
IVC	-	Intake Valve Closing
IVO	-	Intake Valve Opening
KI	-	Knock Integral
KOCA	-	Knock Occurrence Crank Angle
Lambda (λ)	-	Excess air ratio
LECM	-	Large Engine Control Module
LFS	-	Laminar Flame Speed
LHV	-	Lower Heating Value
LNG	-	Liquefied Natural Gas
LPG	-	Liquefied Petroleum Gas
LPP	-	Location of Peak Pressure
LSI	-	Liquid Sequential Injection
MAT	-	Manifold Air Temperature
MBT	-	Maximum Brake Torque timing
MFB	-	Mass Fraction Burned
MN	-	Methane Number
NMHC	-	Non-Methane Hydrocarbons
NMNEHC	-	Non-Methane Non-Ethane Hydrocarbons
NOx	-	Oxides of Nitrogen
ON	-	Octane Number
PFI	-	Port Fuel Injection
PM	-	Particulate Matter
ppm	-	parts per million

RON	-	Research Octane Number
RSM	-	Response Surface Method
SCE	-	Single Cylinder Engine
SI	-	Spark Ignited
SOI	-	Start of Injection
STP	-	Standard Temperature and Pressure
TDC	-	Top Dead Center
THC	-	Total Hydrocarbons
UHC	-	Unburned Hydrocarbons
VOC	-	Volatile Organic Compounds

CHAPTER 1. INTRODUCTION

1.1 Background

The transportation sector, which contributed ~37% of the total end-use carbon dioxide (CO_2) emissions in the US in 2021 [1] and almost half of the NOx emissions in Europe in 2016 [2], has realized the need to evolve in a bid to survive stringent emissions regulations and rising fuel costs. Of the 120 billion GGEs of energy consumed by light duty vehicles in 2019, about 550 million were from alternative, relatively cleaner sources, LPG and electricity [3]. In the middle/heavy trucks and buses sector which accounts for 20% of energy consumed in the transportation sector, a more encouraging yet still minute fraction, 380 million of the 51 billion GGEs of energy consumed, were supplied by alternative sources, mostly by Natural Gas and LPG [3]. These numbers suggest that one of the viable pathways for this evolution, especially in the hard to transition transportation sectors like the heavy-duty sector is the use of alternative fuels such as LPG and CNG. Of the two fuels, LPG has the physical advantage of being easily liquefied at moderate pressures [4] and can therefore be stored and transported using the current extensive network of global and local infrastructures making it an attractive low-carbon alternative fuel option for transportation applications. Figure 1.1 shows the NOx and CO_2 contribution of the transportation sector relative to other sectors.

Chemically, LPG consists mostly of Propane and n-butane. It is sourced either as a by-product of crude oil refining, or during the extraction of natural gas or crude oil [5]. As a result of this variation in sources, coupled with seasonal requirements, a specific country's standard definition of the fuel etc., [6], the composition of LPG can vary wildly. Several studies [7 - 9] have shown that this variation in LPG composition can impact the performance characteristics of the fuel in an engine

environment. Saleh [8] conducted experimental investigations to determine the effect of LPG composition on the performance and emissions of a dual fuel diesel engine. They tested LPG blends containing propane and n-butane only and found that the LPG composition impacted exhaust gas temperatures, efficiency, and emissions [8]. They also found that butane as high as 30% in the LPG blend maximized the dual fuel engine overall performance to levels comparable to that of a conventional diesel engine [8]. Elnajjar et al. [9] also studied the effect of engine parameters and varying amounts of butane and propane on the performance of a dual fuel diesel engine [9]. They found a significant composition effect on combustion noise levels in the engine [9]. However, there are even fewer studies on the effect of LPG composition on a single fuel spark-ignited (SI) engine as these aforementioned studies were conducted in a dual fuel engine configuration. Also, only the effects of varying amounts of n-butane and propane in the constitution of the LPG fuel were studied without consideration for the effects of ethane and propylene, for example, which are also commonly found in LPG.

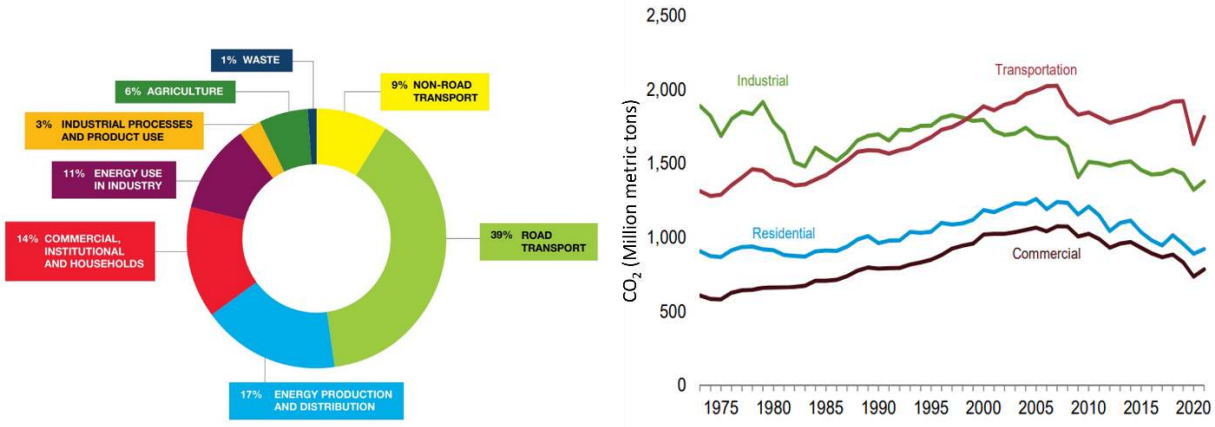

Figure 1.1. Left - NOx emissions by sources. Right - CO_2 emissions from end-use sectors [1 - 2]

A key fuel property which establishes LPG position as an ideal candidate for SI engines operation is its octane number (ON), which is a measure of a fuel's ability to resist knock. Knock is an abnormal undesirable combustion event and the higher the ON, the less likely it is for knock to

occur [10]. LPG has a higher ON relative to gasoline, which accounts for almost half of the transport energy consumed globally [4]. As a result of this higher resistance to knock, LPG fueling can enable engine operation at higher compression ratios which in turn leads to comparable or higher efficiencies to the conventional SI engine fuel, gasoline [11, 12]. Similar to ON for liquid fuels, methane numbers (MN) were formulated to define the resistance to knock for gaseous fuels where a lower MN means a gaseous fuel is more likely to knock than a fuel with a higher MN. Malenshek and Olsen conducted experiments on a CFR engine to determine the methane number of eight gaseous alternative fuels including reformed natural gas [13]. Wise et al. [14] also conducted studies to characterize the MN of several blends of producer gas and the effect of engine operating conditions on the determined MN [14]. Both studies found that the chemical composition of the fuels impacts the measured MN substantially, and consequently, impacted the knock tendency of the fuels [13, 14]. A method developed in the literature was used to calculate the MN of the gaseous LPG blends in this work [15].

While knock, which results from pressures oscillations as the end-gas ahead of the flame front in the cylinder is compressed and auto-ignited, is undesirable and ultimately destructive, there are instances where auto-ignition of the fuel-air mixture may be desired. Hampson et al. [16] distinguishes between knock where several pockets of end-gases auto-ignite randomly, and a spark triggered scenario where all the end-gas regions auto-ignite at the same time or volumetrically [16]. They introduced a novel control tool, the combustion intensity metric (CIM) which used a combination of combustion design and feedback to affect this controlled end-gas auto-ignition concept and applied it a natural gas engine with high EGR rates [16]. Their results showed improved combustion stabilities and faster burn durations even at high EGR rates, reduced unburned hydrocarbons in the form of CH_4, and the ability to operate at elevated compression

ratios using the CIM tool [16]. Several studies have studied knock and end-gas auto-ignition for different alternative fuels of interest including CNG [17-20] and LPG [7, 21-24].

Krieck et al. [21] investigated the knock and pre-ignition behavior of a spark-ignited engine fueled with LPG of different compositions and at three different compression ratios of interest [21]. They found that compared to gasoline, the LPG fuels demonstrated a more improved behavior in terms of auto-ignition [21]. They also found that MN showed a more consistent correlation to auto-ignition than the calculated motor octane number (MON) for LPG [21]. Their results indicated all the LPG fuels investigated enhanced knocking resistance compared to gasoline and thus achieved higher compression ratios of up to 3 units [21]. In terms of emissions, their results showed significantly reduced HC emissions for all the LPG blends tested on the engine compared to a reference E5 gasoline with a RON of 95 [21].

Morganti et al. [23] conducted numerical investigations on the auto-ignition of LPG blends consisting of Propane, iso-Butane, n-Butane, and Propylene on an SI engine [23]. They found that the composition of the residual gas and heat transfer inside the cylinder affected the auto-ignition characteristics of the LPG fuels [23]. Importantly, they showed that nitric oxide (NO) concentrations correlated strongly to the occurrence of auto-ignition and that including this chemistry improved the models [23]. They also showed that HC and carbon monoxide (CO) concentrations had an insignificant impact on the auto-ignition of the tested cases when compared to the NO effect [23].

Despite the previous works, studying knock and end-gas autoignition remains a key aspect of engine combustion study and as such an integral part of this work especially geared towards applying the controlled end-gas auto-ignition concept to an LPG engine for the first time on a CFR

engine [24] and then on the heavy-duty engine platform. Figure 1.2 presents the pressure traces for three distinct stages of knock on an engine.

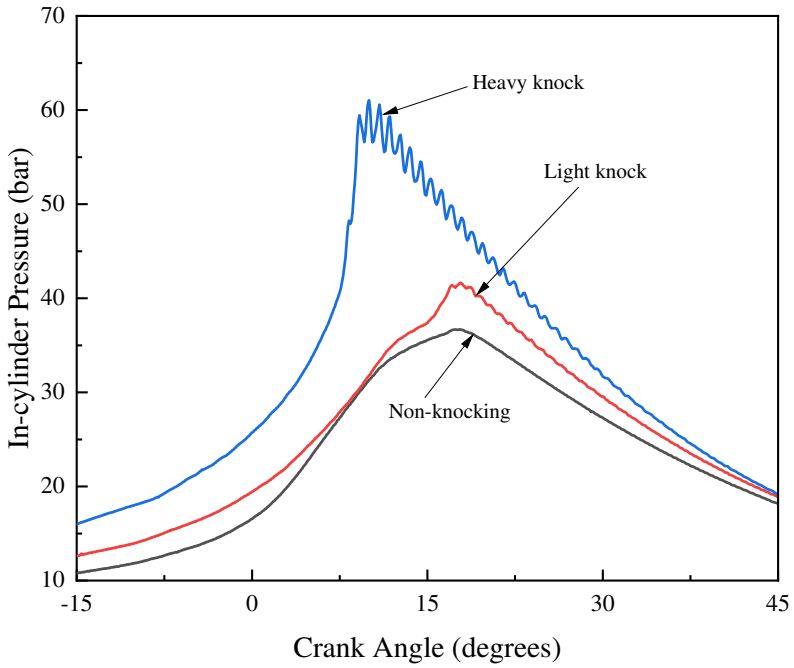

Figure 1.2. Single cycle in-cylinder pressure traces showing the progression of knock from a non-knocking condition to heavy knock as a single engine parameter (compression ratio) was varied

While the preceding discussion on the application of the CIM tool describes the potential benefits of controlling the combustion and end-gas auto-ignition and how this can lead to increased efficiency, there are other strategies in the literature than can affect this increase in performance as well. For example, LPG has been used in dual fuel engine operation either as the primary fuel or as the secondary fuel and the benefits in terms of fuel consumption, emissions and performance documented in the literature [25-27]. Nutu et al. [25] conducted experimental investigations on a compression engine operated in dual fuel configuration with diesel and varying amounts of LPG substituted in [25]. The experiments were conducted on a 10.3L turbocharged engine and LPG was substituted in to match the energy of the displaced diesel thus maintaining the engine power [25]. Their results indicated an almost 25% reduction in NOx and a ~20% reduction in energetic

consumption at an LPG substitution ratio of 25% [25]. On the other hand, Cinar et al. [26] investigated the introduction of acetylene in dual fuel configuration on an SI engine operating with LPG as the primary fuel [26]. They conducted their tests at four equivalence ratios ranging from lean to stoichiometric to rich conditions, at a compression ratio of 10:1 and with the engine at 25% and 50% load [26]. They found that the acetylene addition improved thermal efficiencies and reduced CO emissions especially at lean conditions [26]. However, they discovered that acetylene was detrimental to the NOx emissions causing a significant increase in the criteria pollutant especially at conditions just lean of stoichiometric [26].

Another key advantage of LPG is its high EGR dilution tolerance. It is in the literature [10,28] that the use of cooled EGR as a diluent can lead to knock mitigation, a substantial reduction of NOx emissions and improvement in thermal efficiency, and several investigations have supported this claim by conducting experiments on different LPG engines [29-31]. Boronat et al. [29] investigated the possibility of improving the efficiency of a DI SI engine run on three separate fuels including LPG [29]. Their investigations involved the use of EGR and a high stroke-to-bore ratio engine design as well as varying other engine parameters [29]. They found that the combined effect of late intake valve closing and EGR produced the highest benefits in terms of efficiency [29]. Ravi et al. [30] studied the effect of cooled EGR on a lean burn SI LPG engine with compression ratio 10.5:1 [30]. Their results demonstrated significant NOx reductions, but the increased possibility of misfire especially around the lean limits [30]. Kar et al. [31] went further to show the effect of EGR and LPG composition on an SI engine using both numerical and experimental methods [31]. They discovered a relationship between the LPG blend composition and the extent of EGR knock mitigation [31].

More recently, Ge et al. [32] conducted a numerical study of the dilution tolerance of LPG relative to gasoline [32]. They studied the premixed flames of iso-octane and LPG at engine relevant conditions, comparing the influence of dilution and turbulence intensity on both fuels by using a two-dimensional direct numerical simulation approach [32]. They found that LPG demonstrated higher dilution tolerances compared to gasoline which they linked possibly to differences in their low temperature chemistry, flame surface areas, and Lewis numbers [32]. However, Ge et al. recommended that further work be conducted to determine the relationship with Lewis number by comparing the dilution tolerances of LPG and a lower Lewis number fuel like Methane [32]. The author believes that this high EGR dilution tolerance of LPG could be harnessed to produce higher thermal efficiencies, lower knock intensities, and fewer emissions.

The previous discussions centered on the combustion and chemistry perspective and while the discussions are applicable to heavy-duty scenarios they have largely been on light and medium duty applications. Therefore, as research studies begin to trend towards heavy-duty engines, perhaps the most beneficial gains in thermal efficiency could be achieved in terms of hardware reconfiguration tailored to the properties of the LPG fuel. In this regard, Sawut et al. [33] conducted studies on the development of a return-less LPG fuel delivery system optimized for efficient energy consumption especially in low load conditions [33]. Tuan et al. [34] suggested the implementation of a heating element to tackle the issue of freezing of the LPG injector tip because of the thermodynamic process occurring in that region as LPG vaporizes rapidly [34]. In engine operation, Pradeep et al. [35] investigated the advantages of port fuel injected LPG over the carburetion fueling system showing an increase in performance and a decrease in HC and CO emissions [35]. Pradeep et al. [36] then further showed the advantage of direct injected (DI) LPG

over the manifold injection case on a 2-stroke SI engine as the DI operation demonstrated improved efficiency and reduced HC emissions but indicated higher CO emissions [36].

However, these studies were conducted with LPG in the gaseous form and the literature suggests that liquid phase port-fuel and especially direct injection could have further volumetric efficiency and power density benefits [10]. For example, Watson and Phuong demonstrated that liquid port-injected LPG minimized brake specific fuel consumption compared to their gaseous port-injected counterparts in their experiments on a CFR engine [37]. Tukiman et al. [38] presented results of an experimental study on a 1.6L engine comparing multi-point sequential port injection of liquid to gasoline showing that the LPG engine achieved higher thermal efficiencies than the gasoline configuration [38]. Splitter et al. [39] performed comparative experiments on the performance of DI LPG and gasoline in an SI engine and found that DI LPG indicated almost no soot and FSN [39]. Dube et al. [40] carried out experiments on a 2-stroke SI LPG fueled engine in which they compared the influence of single and multiple hole direct injections, and single hole manifold injection of liquid LPG [40]. They found that the DI modes improved efficiency and lowered HC emissions and that the end of injection timing had a significant effect on BTE, HC and NO in DI mode [40].

Krieck et al. [41] conducted experiments using different LPG blends in a 4-cylinder boosted DI SI engine and a single cylinder research engine [41]. They demonstrated measures to improve the high-pressure DI system including a recommended upper limit on the C3 content of the fuel and controlling the fuel rail temperatures using cooling designs [41]. Finally, their results showed some HC sensitivity with LPG fuel temperature but an overall advantage over a RON 95 gasoline E5 blend in terms of the HC emissions [41]. De Ojeda and Wu [42] successfully developed a high-pressure injection system for propane-DME on a 2.2L 85mm bore engine considering factors such

as fluid properties and pump design [42]. The propane system demonstrated insignificant cyclic variations in terms of injection rate and rail pressure and their developed models were capable of predicting injection rates and hydraulic delays to high fidelity [42]. Other studies comparing DI LPG on an SI engine to a diesel CI engine for medium-duty minibus applications [43] and DI gasoline and LPG on a light duty vehicle [44] have demonstrated the clear advantage of LPG in terms of HC, PM, and NOx emissions. Baek et al. [43] showed that the diesel configuration generated almost 20% more sub-23-nm particles than the DI-LPG engine in the world harmonized drive cycle mode [43] while the DI LPG engine exhibited around 50% lower NOx + THC than the gasoline configuration in the results presented by Myung et al. [44].

Despite the increasing study of liquid LPG injection, its use on heavy-duty engines is still sparse in the literature especially related to experimental direct injection engines. A few studies have demonstrated the influence of LPG injection parameters such as injection timing, injector spray characteristics, in-cylinder charge motion, and combustion chamber design on mixing and homogeneity inside the cylinder and how these affect performance but these works have mostly been numerical and focused on light-duty applications [45 - 47]. Boretti and Watson [48] developed a computational model for DI LPG engines that showed they could achieve better efficiencies than gasoline with the attendant CO_2 emission advantages [48]. However, they concluded that a massive obstacle in the actualization of these improved LPG engines would be the development of a specialized fast-acting high-pressure injector [48]. They also added that extensive experimental and numerical studies on the combustion and spray characteristics of these LPG engines would be required to make the technology practical [48]. Finally, Krieck et al. [21,41] provided some insight into some of the hinderances in developing heavy-duty LPG engines

including changes in the phase of the liquid LPG during hot soak and hot idle conditions and how these may affect the direct injector and engine performance [21,41].

1.2 Research Motivation

Over $32 billion worth of cargoes are freighted every day by vehicles in the US [49] with the transportation sector relying on petroleum for 90% of its energy as at 2021 [50]. This reliance on petroleum is even more glaring with the transportation sector accounting for about 67% of total US petroleum use in 2021 [50], 20% of which the US imports, costing over $15 billion per month [49]. In finer details, medium and heavy-duty trucks accounted for almost 25% of US transportation energy use in 2019 [50] but as illustrated in Figure 1.3, they consumed over 3 times the fuel in gallons per vehicle compared to light duty vehicles in 2020 [1].

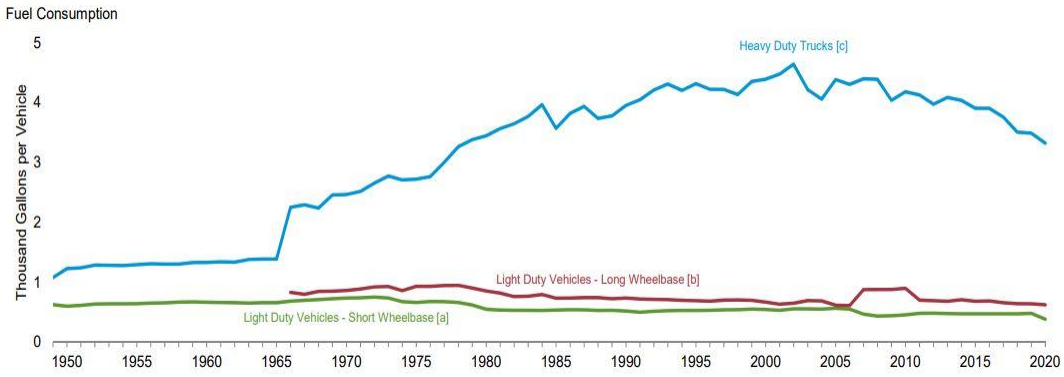

Figure 1.3. Motor vehicle fuel consumption [1]

Perhaps the biggest concern with this reliance on petroleum is the environmental and health impact of its emissions. Between 1990 and 2020, the CO_2 emissions from the Americas increased by just about 8% [50], however, global CO_2 emissions have continued to trend upwards as can be seen in Figure 1.4. In the US, the transportation sector was responsible for 35% and 28.8% of the total US CO_2 and GHG emissions respectively in 2019, second only to the industrial sector [50]. Of these

transportation sector CO_2 emissions, heavy-duty engines accounted for 25% in the same year, while they were responsible for 45% of the total NOx and 51% of total PM-2.5 from high-way vehicles in 2017 [50]. The US is currently working towards an 80% reduction in GHG relative to 2005 levels by 2050 and the adoption of low-carbon fuels is one of the key strategies in this regard as shown in Figure 1.4 [51].

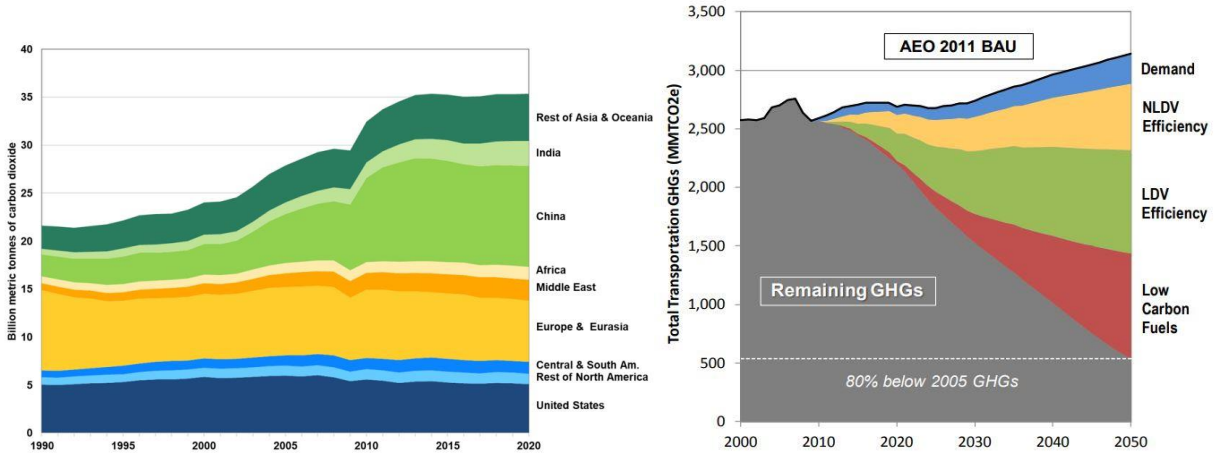

Figure 1.4. Left: World carbon dioxide emissions. Right: Depiction of low-carbon GHG reductions scenario [50, 51]

Therefore, transitioning the heavy-duty sector to locally available cleaner alternative fuels whilst improving their engine efficiency is a key pathway to enabling economic growth, attaining environmental sustainability targets and making transport more affordable. This work is based on a project funded by the Department of Energy Vehicle Technologies Office and one of the set goals for their Advanced Combustion Engines and Fuels R&D Program is to "improve heavy-duty engine efficiency by 35% relative to a 2009 baseline vehicle and identify cost-effective high-performance fuels that can further increase efficiency up to an additional 4%" by 2030 [49]. To this end, the VTO incentivizes fuel diversification by supporting early-stage research including those seeking to understand and control the combustion processes that improve efficiency and reduce emissions for internal combustion engines. Propane or liquefied petroleum gas (LPG) has

been identified as a viable fuel option for heavy-duty engine operation capable of achieving comparable efficiencies to the conventional heavy-duty engine fuel, diesel, for several key reasons. The US became the largest exporter of propane globally in 2014, exporting 6.5 billion gallons of the low-carbon fuel, a remarkable growth from 2005 when it imported over 20% of its propane supply and 2011 when it finally achieved net export status for propane [52]. A direct deduction from this is that propane is a locally available resource of which the US has a healthy surplus, with net exports projected to exceed 13 billion gallons by 2025, and the fuel is already popular in the internal combustion engines (ICE) market with ICE related sales projected to rise from 640 million gallons in 2014 to almost 2 billion gallons by 2025 [52]. Propane's popularity in the ICE applications is backed by a number of factors such as costs, physical properties, emissions reduction potential etc. For example, LPG has a higher H:C ratio than both diesel and gasoline which can be harnessed for lower GHG emissions, LPG is a liquid at pressures as low as 900kPa which enables it to be easily transported, stored, and dispensed using the extensively developed liquid fuel infrastructure. In addition, Bae and Kim [5] noted further physical and chemical advantages of the LPG fuel including having a higher octane number than gasoline which makes higher compression ratios and their attendant increase in BTE possible, wider spray angles, shorter penetration of liquid, and better atomization in liquid injection which promotes mixing and prevents well wetting compared to gasoline [5]. This availability, superior properties, and extensive infrastructure trickles down to the end-user in terms of cost as depicted in Figure 1.5 with propane and natural gas maintaining an average cost over 10 years that was ~54% less than gasoline and ~63% less than diesel over that same time period [53].

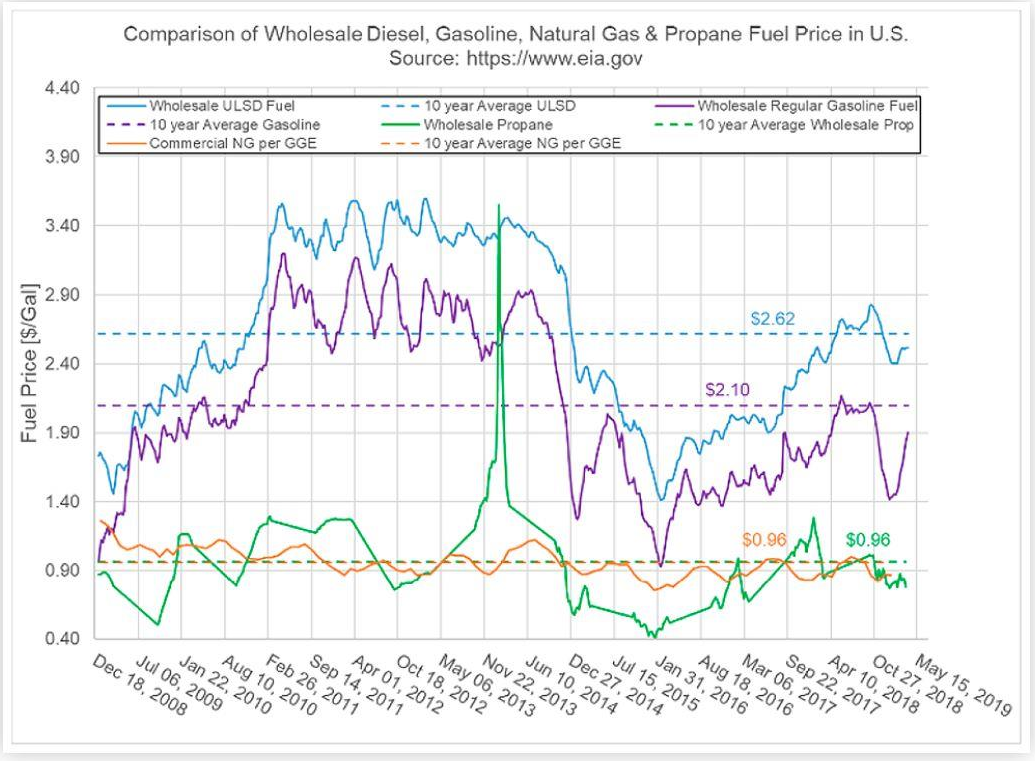

Figure 1.5. Comparison of wholesale diesel, gasoline, natural gas and propane prices [53]

In terms of emissions, TM Leuven [54] performed tank-to-wheel analyses to illustrate the potential savings with widespread propane adoption in the transportation sector over the period from 2007 to 2020 compared to a baseline [54]. They demonstrated 340,000 tons of NOx saved, 11,000 tons of PM, and over 314 million tons of CO_2 avoided resulting in a total savings in materialized costs of over $20 billion [54]. There also exists renewable pathways for the synthesis of propane (renewable propane) from waste greases, vegetable and plant oils, animal fat which are cost effective and can deliver even further emissions reduction in the march towards carbon neutrality [55].

1.3 Research Questions and Objectives

The preceding review of the literature and research motivation section suggests there is keen interest regarding the use of LPG for heavy-duty applications but that there are several gaps or sparse information in knowledge regarding the use of the fuel in the liquid port-injected and to an even lesser degree, liquid direct injected configuration, on these heavy-duty engines. The pertinent questions to be answered are as follows.

1. How does LPG compare with the other popular alternative fuel options in the heavy-duty sector, natural gas, and how does variability in the composition of the LPG fuel affect engine performance?
2. How much engine modification is required to operate an engine optimally on gaseous premixed and liquid PFI and DI LPG?
3. What are the advantages and disadvantages of direct liquid injection and liquid port-fuel injection on a heavy-duty engine platform, and can we design injection strategies tailored to the properties of the fuel?
4. Can we design controls and advanced combustion strategies for LPG including the use of high EGR, tailored injection strategies, innovative spark plug and computationally optimized combustion chamber design?
5. Can we optimize the heavy-duty engine efficiency operating on LPG to match the diesel benchmark within the prescribed limits of knock and misfire using the developed combustion strategies?

Considering the research questions, the overall objectives of this work are to contribute to the development of specialized fuel delivery and injection hardware for the LPG fuel, to develop avenues to improve combustion and mitigate knock whilst avoiding misfire, to achieve the target

44% brake thermal efficiency on the heavy-duty LPG engine platform, and to guarantee lower emissions, all compared to the conventional heavy-duty diesel platform. Generally, several pathways exist to increase efficiency for spark-ignited engines as presented by Szybist et al. [28], however, this work seeks to bridge the gap in performance with the strategies presented in Figure 3.

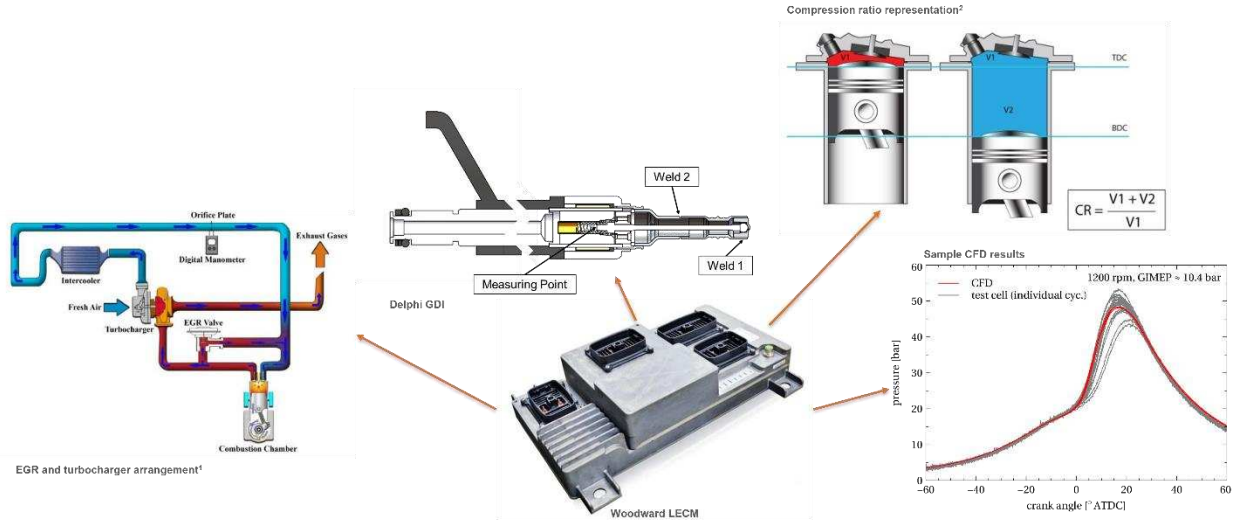

Figure 1.6. Strategies to achieve near diesel efficiency on the heavy-duty engine platform [56 - 58]

First, critical preliminary studies will be conducted on a CFR engine operated with premixed gaseous LPG and natural gas to understand the combustion characteristics of the LPG fuel and the impact of the fuel composition on engine limits, performance, and control. Then, a baseline evaluation of the heavy-duty Cummins X15 engine platform on LPG, replicating readily available liquid port-fuel injection technology on two sample LPG buses: The Bluebird and Navistar buses, will be performed. Following this, CFD models which have been calibrated and validated using the preliminary work on the CFR engine will be updated with the baseline data. Then, a baseline direct injector for liquid LPG will be developed and tested on the engine and optimized based on flow patterns, injection durations, and mixture homogeneity. Next, the compression ratio will be

increased from the baseline case to maximize efficiency whilst avoiding knock and misfire. The CFD models will guide this innovative piston design process. Finally, high percentages of EGR will be introduced into the system at turbocharged conditions in an attempt to increase power density and efficiency, lower emissions and mitigate knock. All the while, a real-time feedback control module on the engine will provide combustion control and access to an embedded novel combustion control parameter, the combustion intensity metric (CIM) which has been shown to improve combustion and performance [16, 20, 24, 59]. This process will be iterative, with CFD and GT-Power capabilities constantly applied to reduce time and cost and will continue until diesel efficiency parity is achieved on the heavy-duty engine with LPG.

1.4 Dissertation Overview

This dissertation is largely a combination of independent articles published in different journals and conference proceedings over the course of the work. The work transitions from preliminary studies done on the CFR engine to baseline evaluations on the heavy-duty Cummins X15 engine to optimization tests on the heavy-duty platform geared at achieving the target efficiency. The work employs learnings and tools from the literature, preliminary experiments, computational studies, high-pressure spray diagnostics, and injector hardware development all conducted in parallel during the course of the research study. The flow of the dissertation is presented below.

1. Chapter 1 presents a background on the fuel of interest, LPG, and its current applications and limitations in internal combustion engines. The objectives of the research study are laid out and summarized at a high level.
2. The experimental set-up is then described in detail in Chapter 2. The Chapter includes details on the engines used as well as the ancillary systems such as the exhaust gas

recirculation system, the liquid fuel delivery system etc. Finally, the chapter concludes with a discussion on key methods of combustion data analysis employed during the study.

3. The first results and discussions chapter, Chapter 3, is an excerpt from a published journal article which compares the combustion, emissions and performance characteristics of the two popular low-carbon fuels in use in the heavy-duty sector, LPG and natural gas, on the CFR engine with exhaust gas recirculation. The chapter begins with a quick overview that introduces the work to be discussed in the chapter and ends with a summary of the key findings in the Conclusions subsection.
4. Chapter 4 follows the same pattern as Chapter 3. The results and discussions are mostly culled from a published conference proceeding that described the influence of the LPG fuel composition on engine performance, combustion, and emission characteristics. Like the preceding chapter, this study was also conducted on the CFR engine with several engine parameters varied.
5. The dissertation then transitions to heavy-duty engine operation and discussions in Chapter 5. The engine is configured to replicate the performance of a medium/heavy-duty liquid PFI LPG engine currently in operation in the US. The efficiency results are designated as the baseline for the rest of the study and improvements are then investigated with a DI system which includes an injector developed specially for optimal distribution of the LPG spray on this research engine platform. The results and discussions in this chapter are sourced from an article currently submitted for review and publication with a journal.
6. The discussion in Chapter 6 then focuses on the results of the optimization experiments that were conducted to achieve the target efficiency on the heavy-duty engine platform. The chapter includes data obtained from several different configurations in terms of

injection configuration, injection strategy, compression ratios, and spark plugs. This chapter is the culmination of all the previous chapters and concludes the work done during this study.

7. A general conclusion chapter in Chapter 7 ties the entire results and discussion chapters together and provides a consistent thread of findings, takeaways, and contributions to the literature through the different conducted studies. The chapter concludes with a sortie into the possible directions for future research and recommendations for subsequent related studies.

CHAPTER 2. EXPERIMENTAL METHODS

This project began with extensive work on the cooperative fuels research (CFR) engine providing the data with which LPG combustion was modeled using CONVERGE CFD, computational and experimental results were then transferred to the single cylinder heavy-duty Cummins X15L engine on which optimization experiments were finalized.

2.1 The CFR Engine Test Cell[1]

The engine used for preliminary gaseous LPG investigations was a single cylinder, 4-stroke CFR F-2 engine. The SI research engine produced by Waukesha Motor Company, was designed as a variable compression ratio engine for defining gasoline fuel quality in a standardized set-up. The test engine specifications are provided in Table 2.1.

Table 2.1. CFR engine specifications

Displaced volume (L)	0.6117
Stroke (m)	0.1143
Bore (m)	0.0826
Connecting Rod (m)	0.254
Compression ratio	Adjustable 4:1 – 18:1 by cranked worm shaft – worm wheel drive in cylinder clamping sleeve
Number of Valves	2
EVO	140° ATDC
EVC	15° ATDC
IVO	10° ATDC
IVC	146° BTDC
Cylinder type	Cast Iron, Flat Combustion Surface, Integral Coolant Jacket
Ignition	Capacitive discharge through coil to spark plug

[1] Section 2.1 extracted from published manuscripts,
[7] Fosudo, T., Kar, T., Marchese, A., Windom, B., Olsen, D. (2022). The Impact of LPG Composition on Performance, Emissions, and Combustion Characteristics of a Pre-mixed Spark-Ignited CFR Engine. SAE Technical Paper 2022-01-0476, 2022. doi:10.4271/2022-01-0476.
[24] Fosudo, T., Kar, T., Windom, B., Olsen, D. (2024). Low-carbon fuels for spark-ignited engines: A comparative study of compressed natural gas and liquefied petroleum gas on a CFR engine with exhaust gas recirculation. Fuel (360) 2024, 130456. https://doi.org/10.1016/j.fuel.2023.130456.

Several modifications were made to the original test engine to allow operation on gaseous fuels. This customization included the installation of several measuring instruments at specific locations to obtain accurate measurement of engine operating parameters and results. A detailed description of the measurement devices and methods used in this study is provided below.

A Yaskawa U1000 regenerative variable frequency drive was installed to ensure accurate speed control. The industrial MATRIX drive can maintain speeds between 600 and 1200 RPM. All the tests in this study were performed at 900 RPM engine speed. A BEI model L25 incremental optical encoder was also installed on the crankshaft to provide crank angle position with a tenth of a degree resolution. Three Kistler high-speed pressure transducers were used in this study; a 6061B water-cooled piezoelectric transducer provided in-cylinder pressure readings, while dynamic intake and exhaust pressure measurements were made with the 4007D and 4049B piezoresistive transducers respectively. Several absolute pressure transducers from Omega Engineering and K-type thermocouples were installed at strategic locations to measure pressure and temperature of the fuel, oil, coolant, and intake and exhaust buffer volumes at all engine operating conditions. To maintain a constant vapor pressure inside the LPG cylinder irrespective of fluctuations in the ambient conditions, a heated blanket was wrapped around the tank and an electrically heated Swagelok K-series pressure regulator and heat trace were introduced on the fuel delivery line to preserve the fuel supplied to the engine in the gas phase. A Micromotion CMF series Coriolis mass flow meter downstream of the heated regulator was used to measure the flow rate of the fuel while a wide-band LSU 4.9 lambda sensor with operating range lambda (λ) 0.65 to ∞ and exhaust temperatures up to 930^{o}C located downstream of the exhaust buffer volume provided a measure of the air-fuel ratio in the engine. A schematic of the CFR engine test cell layout is presented in Figure 2.1.

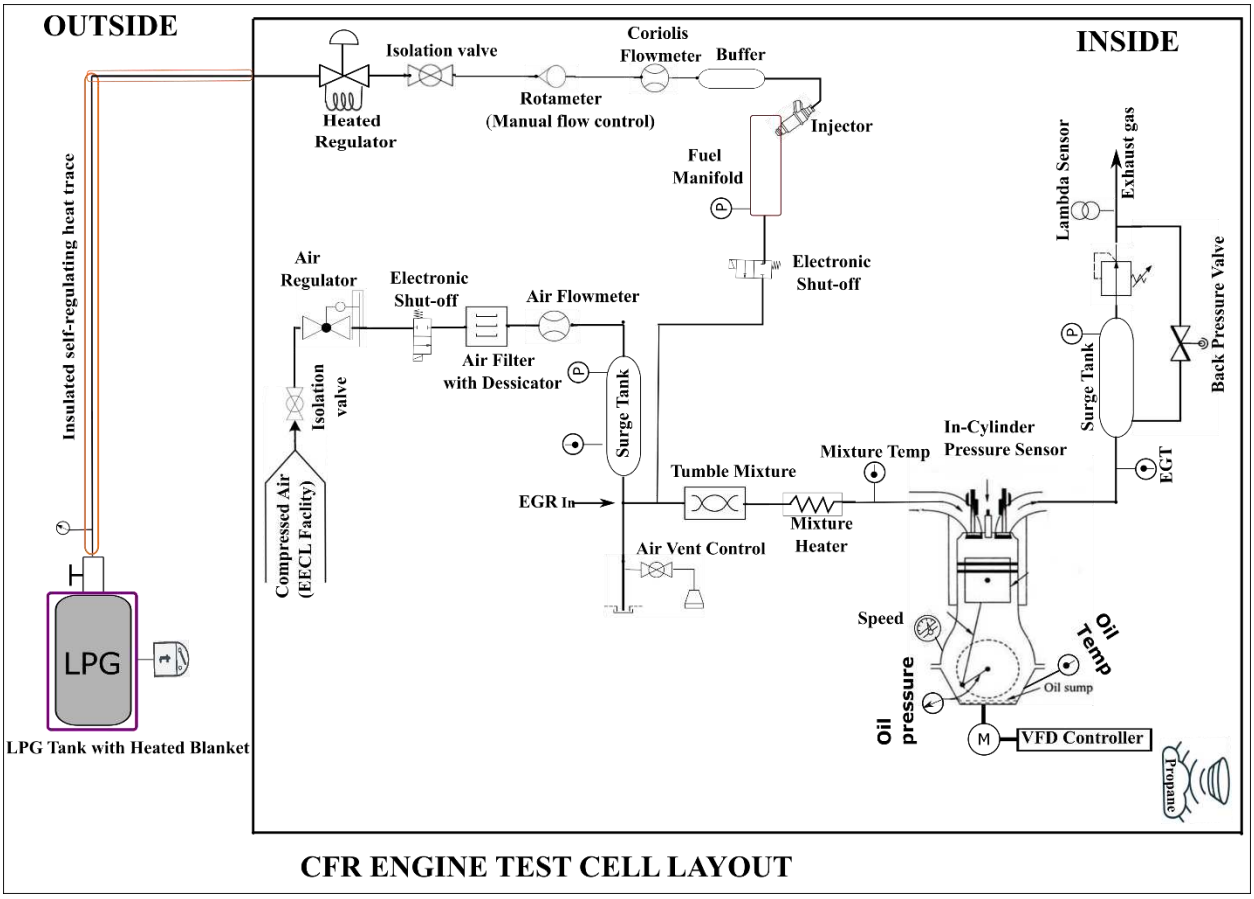

Figure 2.1. Schematic of the CFR engine test cell.

The CFR test cell upgrade also includes a 10kW NK APT-TH series power transducer to measure electrical power output from the engine and a Woodward Large Engine Control Module (LECM) and LabView program interface to achieve real-time CFR engine control, monitoring and performance analysis. A National Instruments PCI 6251 high speed data acquisition card was used to collect in-cylinder pressure data. Combustion and manifold pressure data were logged at 54kHz ($1/10^{th}$ degree resolution) for 1000 cycles (2-3 min). Combustion data logged for 200 cycles on the Woodward LECM was used for ignition control. Other parameters such as temperatures, fuel flowrate, and electrical power were logged at 10 Hz for 3 minutes. A picture of the CFR test cell showing all the integral components is shown in Figure 2.2.

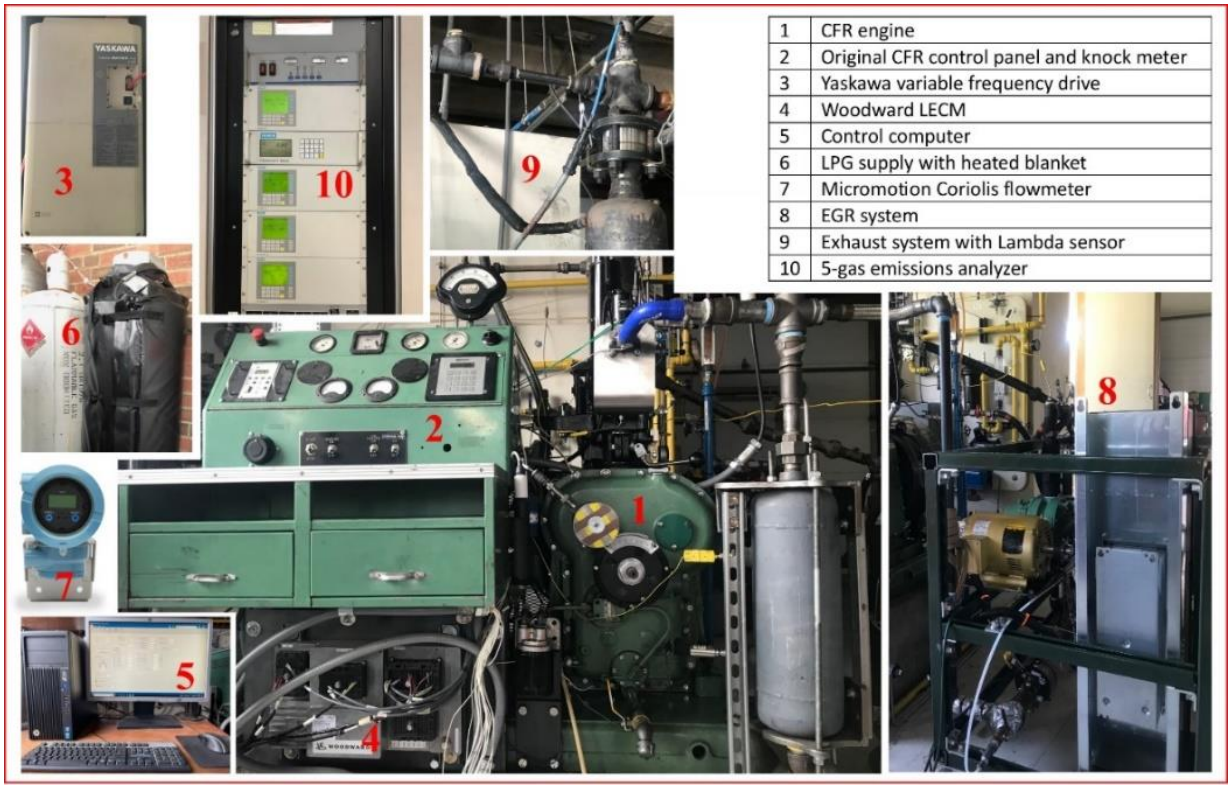

Figure 2.2: The CFR test cell

2.2 The Single Cylinder Cummins ISX15L Test Cell[2]

The second single cylinder engine used in this study was a converted Cummins ISX15L 6-cylinder diesel engine. The conversion involved replacing five of the six original pistons with carefully machined dummy pistons to provide balance on the crankshaft as the active piston, the piston in cylinder number 6 in this case, was operated. The cylinder head was modified to accommodate a spark plug in the location originally intended for the diesel direct injector. The turbocharger, fuel pump, exhaust gas recirculation (EGR) components, and other diesel-allied components were also uninstalled from the original engine. The SCE is water-cooled and has the capability to run at

[2] Sections 2.2 and 2.3 extracted from published manuscript
[60] Fosudo, T., Kar, T., Windom, B., Schlagel, J. et al. Performance, Combustion and Emissions Evaluation of Liquid Phase Port-Injected LPG on a Single Cylinder Heavy-Duty Spark Ignited Engine. SAE Technical Paper 2023-01-0245, 2023. doi:10.4271/2023-01- 0245

higher loads using compressed air from the research facility. A friction model which was based on an analysis of the production diesel engine was used to account for the other cylinders thus allowing brake mean effective pressures to be calculated from the indicated mean effective pressures. Exhaustive details of the conversion and required modifications that were carried out on the original ISX15L diesel engine can be found in the experimental studies done by Rodriguez et al. [19]. A detailed specification of the heavy-duty SCE is presented in Table 2.2.

Table 2.2. The heavy-duty Cummins X15 SCE specifications.

Displacement volume (L)	2.5
Stroke (mm)	169
Bore (mm)	137
Connecting Rod (mm)	261.5
Compression ratio	9.3, 11.9, 14
Number of Valves	4
Exhaust Valve Open	19° BBDC
Exhaust Valve Close	2° BTDC
Inlet Valve Open	11° BTDC
Inlet Valve Close	155° BTDC

Apart from the modifications that were made to the engine hardware, several upgrades were made to the SCE and its test cell to facilitate the collection and analysis of combustion data, and determination of the performance of the engine under different operating conditions. In-cylinder pressure measurements were made with an AVL GH14DK pressure transducer (range 0-300bar) and an AVL QC34C pressure transducer (range 0-250bar) installed in the active cylinder. High speed manifold pressure measurements were performed using a Kistler 4007D piezoresistive pressure transducer and a water-cooled Kistler 4049B piezoresistive pressure transducer for intake and exhaust pressures, respectively. A BEI H25 series encoder with 0.1 crank angle resolution and LabView based high-speed National Instrument hardware (NI PXIe 6363) were used to record and analyze combustion and manifold pressure signals. A Woodward large engine control module

(LECM) was used to control injection, ignition, combustion, and air-fuel ratio while giving real-time updates on the state of combustion in the cylinder. The LECM received a lower resolution position signal using a hall effect crank sensor. A schematic of the X15 engine showing the converted single cylinder is shown in Figure 2.3.

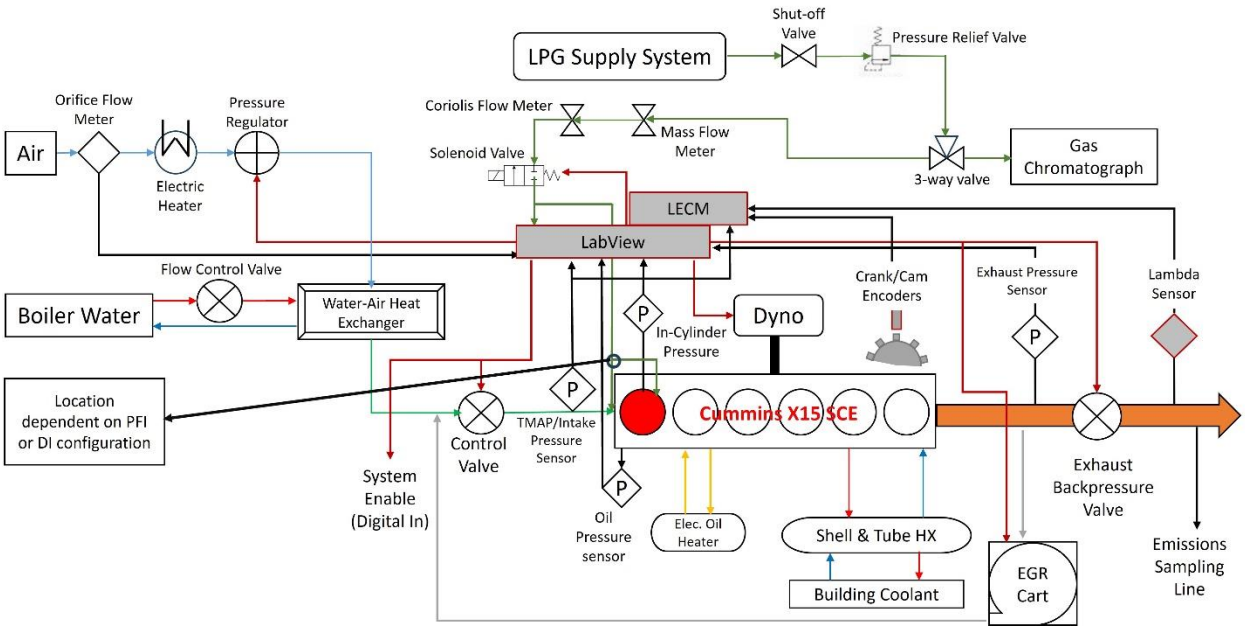

Figure 2.3. Schematic of the X15 engine test cell

Key performance parameters were also recorded on LabView software platform using the NI 6224 and 6704 modules and on the LECM. These measurements include fuel flow rate measured using a Bronkhorst M15 Coriolis flow meter, air-fuel ratio measured with a wide-band lambda sensor LSU 4.9 (application range: lambda 0.65 to ∞), and pressure and temperatures measurements made at the required locations using absolute pressure transducers and K-type thermocouples. The engine speed was controlled by an Eaton SVX variable frequency drive (VFD) which turned the engine during motoring and applied a load during combustion. This VFD was controlled by LabView, and its output recorded in LabView as well. The high-speed combustion and manifold pressure data were logged for 1000 cycles, while 200 cycles of combustion data were logged on

the LECM. Other parameters such as the fuel flowrate, engine speed, and fuel pressure were logged at a slower rate of 2Hz for 2-3 minutes.

2.2.1 Piston Configuration Design

Three pistons were installed on the heavy-duty Cummins engine namely.

1. The baseline 9.3:1 piston
2. The 11.9:1 “Natural Gas” piston
3. The CFD-optimized high-squish 14:1 piston

The pistons were designed with CAD software and fabricated at the Colorado State University powerhouse research facility using a 3-axis computer numerical control (CNC) milling machine. The 9.3:1 CR piston was chosen to enable the baseline operation of the Cummins SCE on liquid LPG replicate the performance of current LPG engines. Two of such identified LPG engines currently on the market are the Power Solutions International 8.8L-V8 engine and the Roush Cleantech Ford 6.8L-V10, used in the Navistar 44 CE Series and Blue Bird school buses, respectively. These engines have compression ratios of 9.1:1 and 9.2:1 respectively. The 11.9:1 piston was designed for natural gas operation on the X15 engine and adopted for LPG applications to provide useful data on the performance of the engine at compression ratios higher than the baseline piston. The high-squish 14:1 piston was then developed using combustion models calibrated and validated with engine data obtained at 9.3 and 11.9 compression ratio to computationally optimize combustion chamber design, piston bowl shape, in-cylinder charge motion and homogeneity and compression ratio for peak thermal efficiency and knock mitigation. A blank stock piston with the required cooling gallery was provided by Cummins and then machined to achieve the required compression ratio. Cummins also provided technical assistance

on the minimum recommended piston crown and bowl thickness for an assumed maximum peak pressure of 7MPa for the 9.3:1 piston which had a target brake mean effective pressure (BMEP) of 900kPa to match the output of the Blue Bird LPG engine at naturally aspirated conditions. The 11.9 and 14 compression ratio pistons were designed for higher peak pressures and BMEP. The target compression ratios were achieved by milling material off the blank piston to obtain the designed bowl shape and required clearance volume (V_c), shown in Equation 1.

$$V_c = \frac{V_d}{(CR_t - 1)} \tag{1}$$

Where:

V_d is the displacement volume = 2.49 x 10^{-6}mm^3

CR_t is the target compression ratio = 9.3, 14

Figure 2.4 shows the CAD model and pictures of the piston configurations used on the X15 LPG engine. The cooling galleries have been filled out in the CAD section views.

2.2.2 Spark Plug Configuration Options

Three sparkplug options shown in Figure 2.5 were considered for heavy-duty operation during the course of this study. The Altronic L1863B massive 3-prong nickel sparkplug was used as the baseline sparkplug. The sparkplugs were designed for large, and medium bore stoichiometric and lean-burn engines. These low-cost sparkplugs were developed to be very reliable in conventional stoichiometric engines with high compression ratios and could be used in either pre-chamber or open chamber configuration [61]. They were used in open chamber configuration for the duration of this study. One of the key advanced combustion strategies used in this work was the

passive pre-chamber combustion enabled by the Woodward FTI pre-chamber sparkplug. The FTI igniter which was developed for large bore lean-burn engines and designed for high in-cylinder pressures generates a multi-jet flame front from the holes on its surface to provide a faster, more stable combustion in these large bore engines [62]. The sparkplug operation produces an in-chamber turbulence of its own which enhances in-cylinder turbulent dynamics in the engine and promotes flame development while avoiding flame kernel quenching. The pre-chamber FTI sparkplug was especially important in this work in mitigating misfire and knock thus extending the EGR tolerance limit and increasing engine efficiency at high EGR-diluted in-cylinder mixture operation. A regular J-Gap sparkplug was also tested to demonstrate the improvements with the 3-prong and FTI sparkplugs.

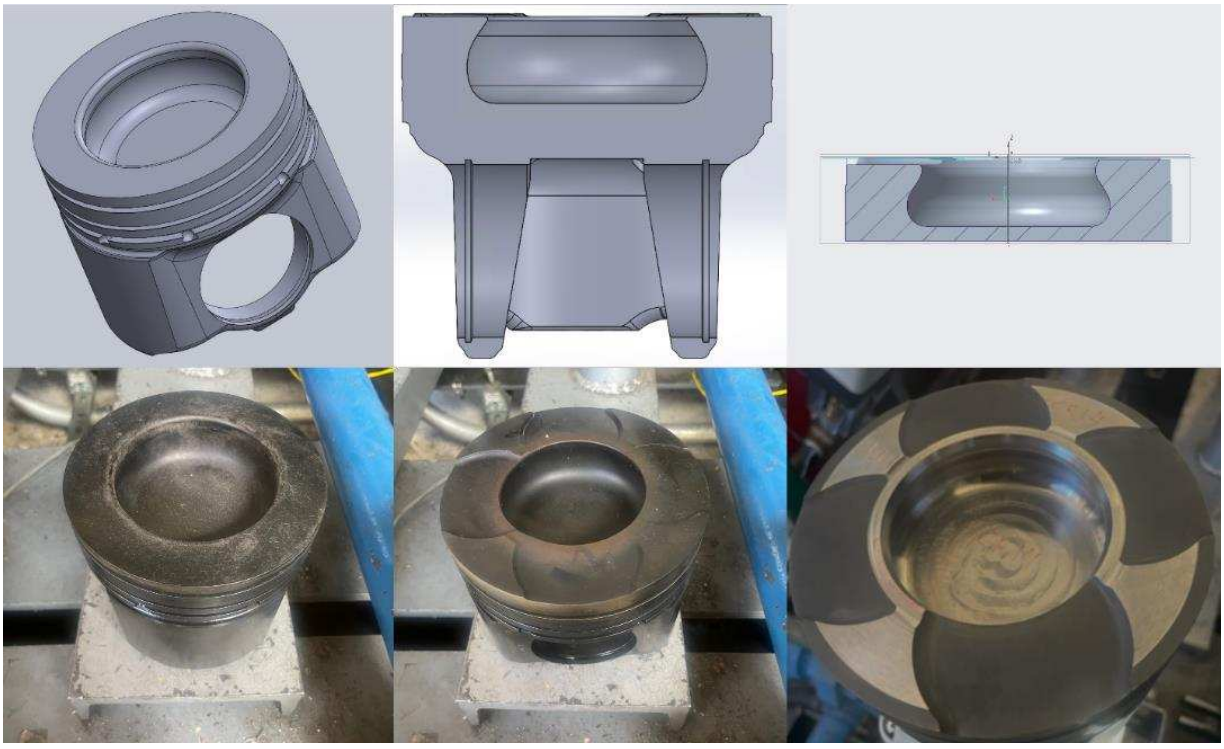

Figure 2.4. Compression ratio optimization direction on the X15 LPG engine showing the CAD model (top) and pictures (bottom) of the pistons for Left: The baseline 9.3:1 piston, Middle: The 11.9:1 "Natural Gas" piston, Right: The CFD-optimized high-squish 14:1 piston.

Figure 2.5. Spark plug options for the heavy-duty LPG engine operation Left: The Woodward Fast Turbulent Igniter (FTI) Pre-chamber sparkplug, Middle: The Altronic L1863B 3-prong massive nickel sparkplug, Right: The regular J-Gap sparkplug.

2.2.3 Injector Configuration Options

The engine operation on direct injection mode required a more involved process as the engine cylinder head had to be redesigned to accommodate the direct injector due to the centrally located sparkplug. The redesigned cylinder head was fabricated by Cummins and installed on the engine along with the direct injector optimized for high-pressure LPG injection. A picture of both cylinder heads used in this work during a cylinder head swap is presented in Figure 2.6.

The “original” cylinder head was used for the port-fuel injection configuration while the redesigned head was used in direct injection mode. Three main injector configurations were tested on the heavy-duty engine. Firstly, the baseline configuration as well as other high compression ratio configurations involved port-fuel liquid LPG injection using a Siemens DEKA injector. The initial set-up for the baseline study had one DEKA injector slightly upstream of the intake ports, however, this design was optimized for high-load engine operation to a double-injector set-up with valve targeting. Secondly, a Delphi 7-hole gasoline direct injector (Volkswagen 06M906036AE) was modified for LPG use as the baseline DI injector on the engine. The modification involved a metrology of two choice gasoline direct injectors (GDI) to understand seat dimensions, nozzle

orifice dimensions, flow restrictions associated with the injectors. The Delphi injector was then chosen for its ease of modification and form (long-body type injector). Next, a dynamic model of the injector was created and recommended only injector nozzle orifice modification to achieve the desired high LPG flow rate required for high load operation of the heavy-duty engine and mitigate pressure losses. Based on the injector off-center location constraint and the required flow rate at peak load, 1200RPM, target efficiency conditions, a new 5-hole nozzle was machined and welded onto the stock Delphi injector to replace the 7-hole tip. The 5-hole nozzle pattern was designed to guarantee LPG spray distribution to the center of the combustion chamber despite the off-center location constraint. Finally, a commercially available high-flow LPG short-body injector (XDI 6-hole injector) was physically modified for operation on the heavy-duty engine. The nozzle and spray pattern remain unchanged; however, the injector was tweaked to ensure installation was possible on the Cummins SCE. Details of the injectors and the injection configurations are presented in Table 2.3 and Figure 2.7.

Figure 2.6. Engine cylinder head and manifolds swap in progress

Table 2.3. Injection configuration details

Injector Type	**Hole Number**	**Injection duration @ nominal conditions***	**Current Profile**		**Average flow rate (g/s) at relevant injection pressures (MPa)**			
			Peak (A) [duration (ms)]	Hold (A)	1.6	14	16	17
Delphi	5	9ms	15 [3]	10	N/A	16.24	17.74	18.95
XDI	6	4.8ms	17 [3]	4		30.87		33.97
Siemens DEKA	1	11ms	5 [2.5]	2.5		N/A		

*** Nominal conditions are 1200RPM, naturally aspirated, $\phi = 1$, injection pressure: 17MPa for Delphi, 13MPa for XDI and 1.6MPa for the Siemens DEKA injector.**

The 3-hole injector was developed using CONVERGE CFD to optimize mixture homogeneity and achieve effective LPG distribution to the bottom of the piston bowl. This 3-hole design emerged as the best after simulations with other candidates at different engine operating conditions in terms of intake pressure, fuel temperature, injection rates, and spray break-up or flashing tendency. Actual testing of the developed 3-hole Delphi injector on the engine was designated as future work and will not be discussed further in this study. A composite picture of the heavy-duty Cummins ISX15L engine test cell and a few of its integral details are presented in Figure 2.8.

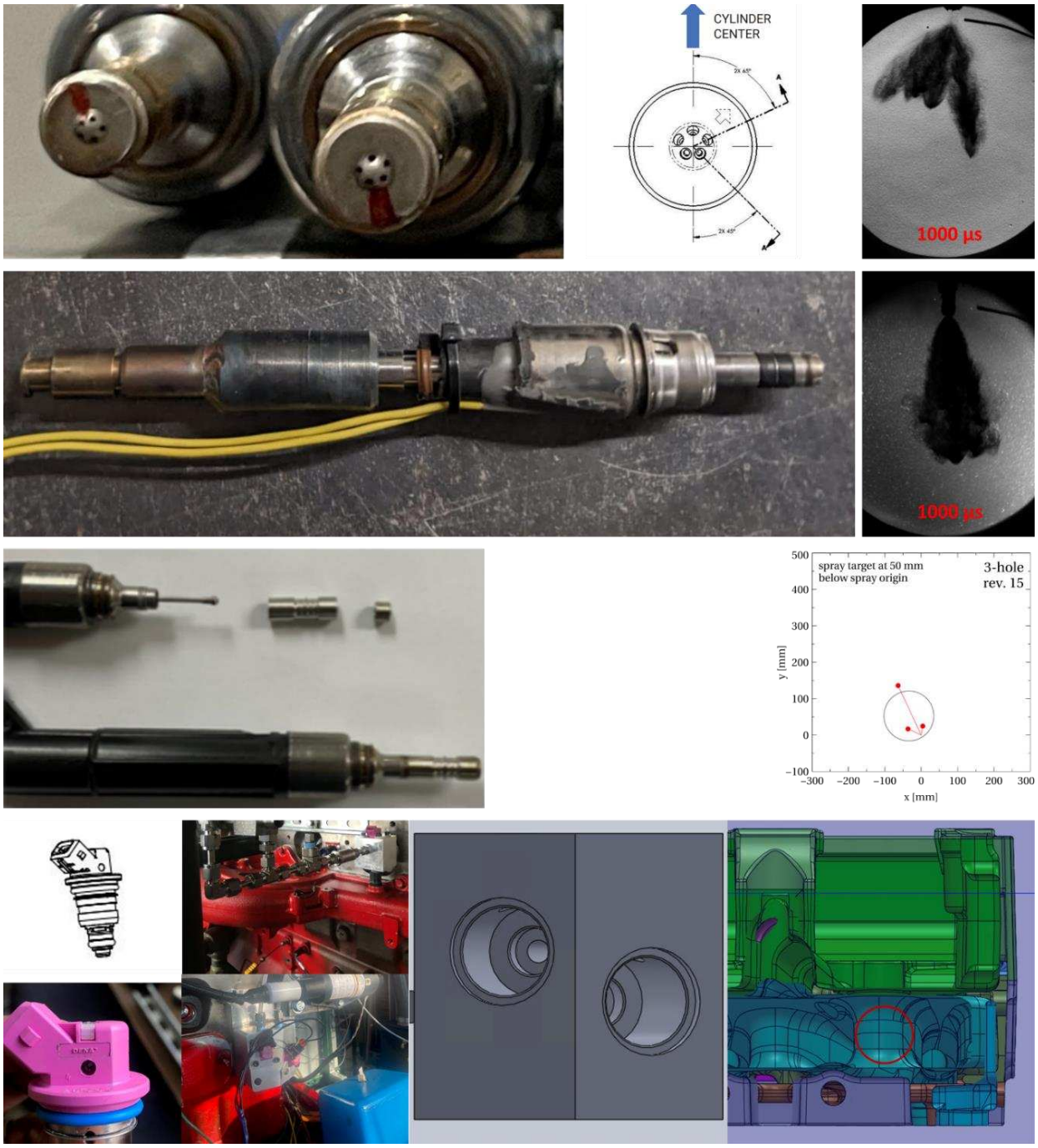

Figure 2.7. Injector configuration details showing all the essential features and considerations for Top: The modified Delphi 5-hole injector, its designed nozzle and spray schlieren image, Next: The high-flow XDI injector modified to long body form and its unmodified spray pattern, Next: The disassembled Delphi stock injector and a CFD optimized 3-hole spray pattern, Bottom: The PFI set-up showing the DEKA injector, both locations considered for this study, the optimized double-injector PFI mount and location designed for this engine.

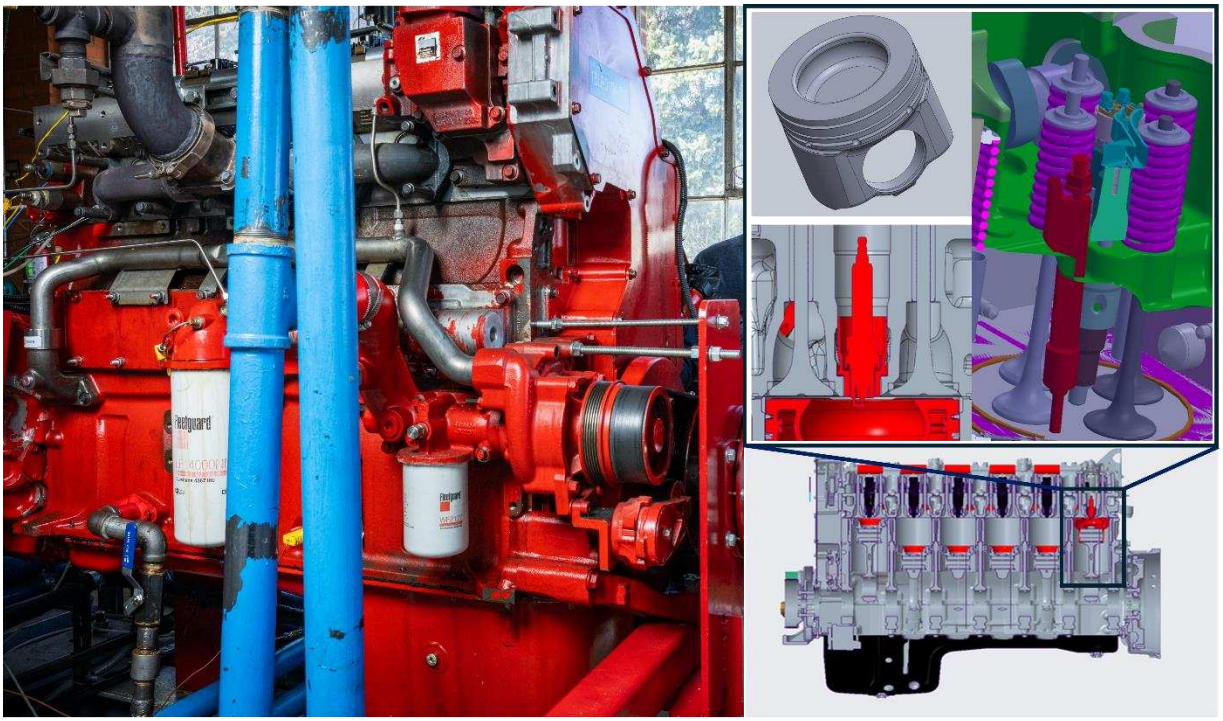

Figure 2.8. Left - X15 SCE; Top Right – Cut-out of key sections of the cylinder head showing the valves and the centrally located spark plug, off-center installed direct injector and baseline 9.3:1 piston; Bottom Right – CAD of the six-cylinder engine showing the active single cylinder, cylinder 6

2.3 The LPG Fuel Delivery System

2.3.1 Port Fuel Injection (PFI) System

The fuel injection system in Figure 2.9 was designed to ensure a steady supply of liquid LPG to an injector just upstream of the intake valve on the SCE. The LPG injector used in this work was the Siemens DEKA injector also used on the Roush Cleantech Ford 6.8L-V10 engine. The high impedance injector was controlled by the LECM and delivered the required amount of liquid fuel at all operating conditions. The liquid fuel delivery system consisted of a high-pressure nitrogen cylinder connected to the vapor port of an LPG tank. The nitrogen enters the LPG tank, through two sets of pressure regulators, at a pressure of ~1.6MPa. Several studies have shown that this pressure is sufficiently above the LPG vapor pressure to ensure liquid LPG all through the system [63, 64].

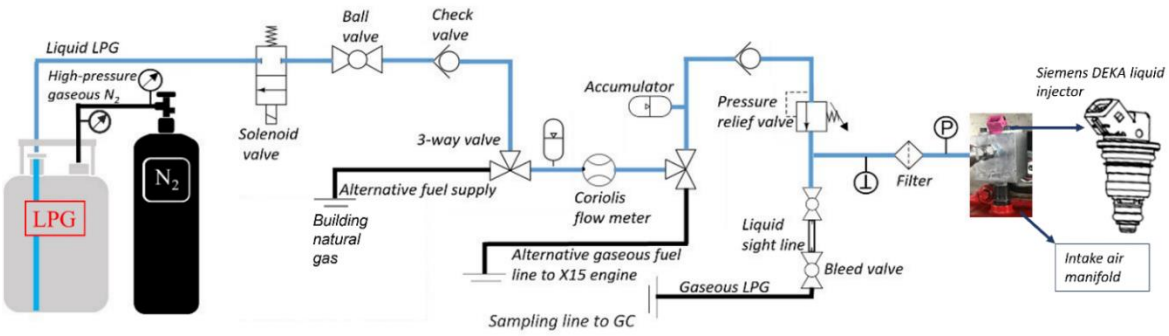

Figure 2.9. The schematic of the PFI system.

The system was designed to incorporate the possibility of alternative fueling options on the SCE with a 3-way valve installed just upstream of the Coriolis flow meter. Two accumulators were installed up and downstream of the Coriolis flow meter to dampen any pressure fluctuations and ensure a reliable fuel flow rate measurement with the flow meter. Density measurements were displayed by the visual interface of the Coriolis flow meter, and this was a useful tool to confirm the state of the LPG in the fuel line. A sight tube installed upstream of the engine also provided visual confirmation of the phase of the fuel. Downstream of the liquid sight tube and bleed valve, the fuel line was connected to an INFICON Micro gas chromatograph to give the real-time composition of the fuel entering the injector. Battino et al. [65] showed that nitrogen was soluble over time in LPG, so particular care was taken to eliminate this possibility in this work. The empty LPG tanks were purged of nitrogen before each refill and its contact time with the LPG minimized by only initiating the flow of the nitrogen gas into an LPG tank at the beginning of the test day.

2.3.2 Direct Injection (DI) System

The direct injection fuel delivery system expanded on the design and successful operation of the baseline PFI fuel delivery system. The schematic is shown in Figure 2.10.

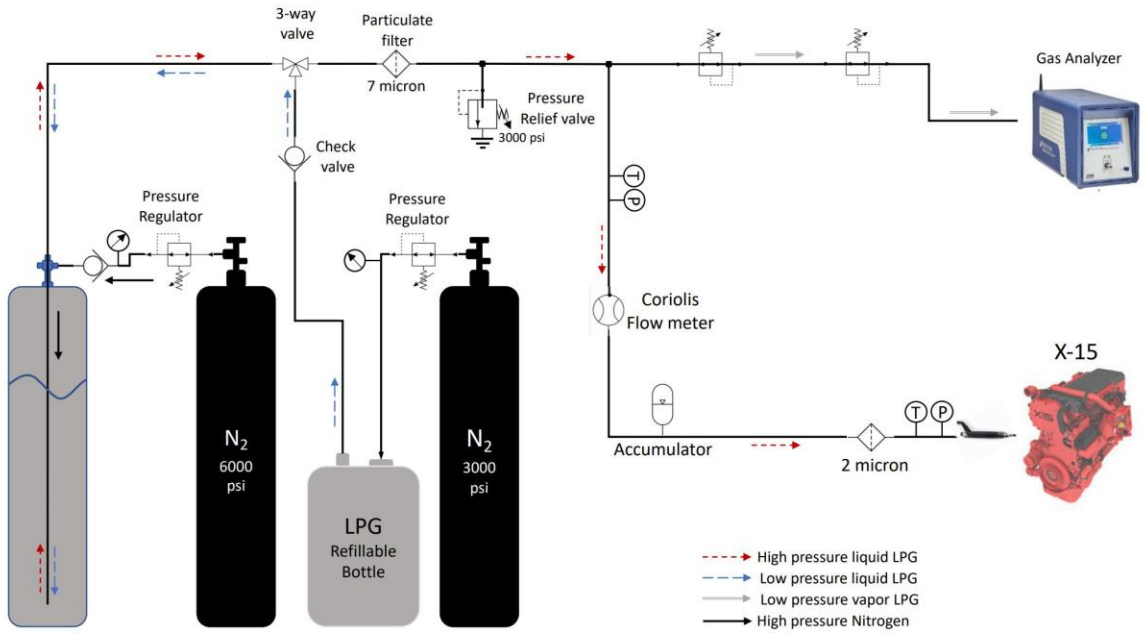

Figure 2.10. A schematic of direct injection system.

The direct injection system was designed with the capability to supply high-pressure liquid LPG at pressures up to 20MPa. Medium pressure liquid LPG is delivered into a cylinder rated to pressures as high as 41.36MPa and a secondary nitrogen supply at the desired injection pressure is flowed to compress the medium pressure liquid to the required injection pressure. Due to the higher nitrogen solubility at the higher DI pressures [65] compared to the PFI system, the DI system included a continuous fuel supply line to the Micro GC to provide real-time fuel composition data. A braided tube was also installed upstream of the injector to dampen any vibrations from the engine into the rigid high-pressure fuel supply line.

2.4 The Exhaust Gas Recirculation System

An existing exhaust gas recirculation system was modified for use on both the CFR and the Cummins X15 engine. The original cart used by Scott et al., on the CFR engine [20] was designed for EGR rates of up to 40% and included an Eaton VFD for speed control of an electric motor

connected directly by a shaft to a twin-screw positive displacement blower that then provides varying flow of exhaust gases, and an EGR cooler and a water heater to maintain temperatures to the desired levels. The cart was slightly modified for the LPG configuration of the CFR engine by including a valve at the inlet of the cart for effective isolation of the EGR system during engine operation and finer control of the EGR flow and installing thermocouples at the inlet and outlet of the cart for better thermal management of the exhaust gas flow properties as the AGA Report #3 flow measurements quoted in [20] were sensitive to flow properties. The cart was then modified for heavy-duty engine use notably with the introduction of a belt and pulley system between the electric motor and a Speedaire 3300H positive displacement blower capable of higher flows. The inlet valve was maintained on the cart while the water heater was disconnected due to the higher inlet pressure of the exhaust gases on the X15 engine negating the need for a heater. A final critical modification was the introduction of a real-time CO_2 balance EGR rate calculation that eliminated the uncertainties associated with the EGR flow rates calculation presented in [20] and ensured a more accurate and consistent measurement of the EGR rates. To achieve this real-time EGR rate measurement, a valve was introduced sufficiently downstream of the EGR entry point into the airstream to allow for adequate mixing and upstream of the cylinder in both PFI and DI configuration such that the CO_2 concentration in the mixture of the air and EGR could be measured by the exhaust sampling devices. This CO_2 concentration was compared relative to the CO_2 concentration in the air and the exhaust to determine the EGR rate. The equations and assumptions are described in section 2.5.5. A picture of the final modified EGR cart is shown in Figure 2.11.

Figure 2.11. The EGR cart

2.5 Combustion Data Acquisition and Analysis Methods

Several analysis methods and tools were common to both engines and are presented below:

2.5.1 Knock Quantification Method

The engine control programs were capable of quantifying engine knock in several ways. Details of these methods are contained in the work done by Bayliff et al. [20]. Two of these methods were used in this work. Using the rotary encoder, the in-cylinder piezoelectric pressure transducer provided high resolution pressure history that was analyzed in real time to get insight into the combustion process in the cylinder. With the knowledge of the operating speed (and therefore

sampling frequency) and the natural frequency of the engine, a bandpass filter was applied to the pressure data to calculate the high frequencies of pressure oscillations caused by end-gas autoignition. A fast Fourier transform (FFT) technique was then applied to this bandpass filtered data to obtain the power spectrum of the signal.

A time averaged approach was then used to establish a knock index and to provide an objective and repeatable metric for comparison of the overall intensity of knock experienced with different fuels under the same engine operating conditions. The term knock integral was used to refer to the area under the curve bounded by FFT power spectrum magnitude over a set number of combustion cycles and was the first of the methods used throughout this work especially on the CFR engine. The KI summation is given by Equation 2.

$$KI = Area_{bounded} = \sum_{i=0}^{n} \{KL(i+1) + KL(i)\}/2 \tag{2}$$

Where:

n = number of combustion cycles in a data set

KL(x) = knock level magnitude for a given combustion cycle, x.

The knock integral derived by summing the FFT power spectrum amplitudes (in kPa^2) was displayed real-time in LabView and logged for post-processing [14,20]. For this study, the knock integral is summed over 200 consecutive cycles and provided a useful tool for the determination of the intensity of knock during engine operation.

The second method involved a knock intensity calculation based on the Woodward LECM operation called the knock ripple sum (KRS). The KRS method was used primarily on the heavy-

duty Cummins engine and provided a consistent means of knock comparison across configurations. The KRS considers the 50 previous pressure traces of engine operation and takes an average of these traces to set as the reference. Knocking traces and their intensities can then be analyzed by subtracting the reference trace from the knocking trace in real-time, generating a history of pressure fluctuations vs crank angle degrees. The knock ripple sum is scaled on a 0 to 100% basis and thresholds of transition from no knock to light, medium and heavy knock were determined and set during engine operation. This method was especially important in that it effectively filtered out any engine noise without cutting out any low or high spectrum frequencies as may be the case with bandpass filter dependent knock quantification methods.

2.5.2 Emissions Measurement and Analysis

Pollutants from the engines were measured using two devices:

A Rosemount 5-gas emissions bench analyzer from Siemens Instruments measures CO, CO_2, THC, NOx and O_2. A condenser removes water from the exhaust sample before the gas enters the analyzer. A non-dispersive infrared (NDIR) approach is employed for the detection of CO and CO_2 concentrations. THC emissions are detected by a flame ionization detector (FID). NOx is measured using a chemiluminescence detector for NO, coupled with an inlet catalyst that converts NO_2 to NO. Finally, the O_2 concentration is measured based on a paramagnetic detection technique.

A Fourier transforms infrared (FTIR) spectrometer (an MKS Instruments, Inc. Model No. 2030) measures hazardous air pollutants and other compounds. Its working principle is based on the absorption of different wavelengths of an emitted IR beam by the different components in the exhaust gas. The signal is picked up by a detector and relayed to a computer where the Fourier transform technique is applied to produce a unique IR spectrum of the gas. Using Beer-Lambert's

law, absorbance is directly proportional to the concentration of the sample gas and the components of the gas can thus be identified by the IR absorption spectrum.

In order to capture NMHC and for consistency, only the MKS spectrometer results were presented in this work, however, the outputs were checked against the 5-gas analyzer output for reproducibility and consistency. Methods developed by Urban et al., [66] described the calculation of the air-fuel ratio using exhaust gas composition. Equations 3 - 5 from their work were applied as a further check to calculate the equivalence ratios in this study, and all checked stoichiometric conditions agreed to within 1% with the equivalence ratios output from the wide band lambda sensor used on the engine. This pointed to excellent control of the air-fuel ratio and the accuracy of fuel flow and exhaust measurements at all these conditions.

$$H2FAC = \frac{0.5 * y * (\%CO) * (\%CO + \%CO2)}{(3.5 * (\%CO2) + \%CO)} \tag{3}$$

$$A = 0.25 * y - 0.5 * z + \cdots$$

$$\ldots + \frac{\%C02+\left((0.5*z)-0.25*y\right)*\%HC+0.5*\%CO+0.5*\%NOx+\%O2-0.5*H2FAC}{\%CO2+\%CO+\%HC} \tag{4}$$

$$AFR = \frac{138.28 * A}{12.011 + 1.008 * y + 15.999 * z + 14.008 * f} \tag{5}$$

For the fuel $C_xH_yO_zN_f$

Where:

AFR = Air-fuel ratio

x = 1

H2FAC is the computed exhaust H_2 concentration.

In this work, engine-out emissions were mostly presented and analyzed in brake specific terms calculated from the measured ppm values using Equation 6 below.

$$bsi = \dot{m}_i/\dot{W}_b = \frac{\dot{m}_f * \alpha * Y_i * M_i}{M_f * \sum(Y_j * \alpha_j) * \dot{W}_b} \quad (6)$$

Where:

bsi is the brake specific value of specie i

$\dot{m}_i$ is the mass flow of specie i

$\dot{W}_b$ is the brake power

$\dot{m}_f$ is the fuel flow rate

α is the fuel carbon number

Y_i is the mole fraction of species i

M_i is the molar mass of specie i

M_f is the molar mass of the fuel

$\sum(Y_j * \alpha_j)$ is the sum of all carbon carrying species j in the exhaust

2.5.3 Heat Release Analysis

Heat release analysis was conducted using the single zone equation shown in Equation 7. On the X15 Cummins engine the specific heat ratio, γ, was deduced in real-time by the LECM using the polytropic relation. The γ of compression was calculated from 30 deg bTDC to 10 deg bTDC and the γ of expansion was determined from 10 deg after the location of peak pressure to 60 deg after the location of peak pressure for that engine operating condition. The average of the compression and expansion γ was then used in Eq. 7 to evaluate the apparent heat release rate (AHRR). On the CFR engine, a constant value of 1.35 was selected for the specific heat ratio and inserted in Eq. 7.

$$\frac{dQ}{d\theta} = \frac{\gamma}{\gamma - 1} P \frac{dV}{d\theta} + \frac{1}{\gamma - 1} V \frac{dP}{d\theta} \tag{7}$$

Where:

P is the in-cylinder pressure

Q is the heat release

V is the cylinder volume

2.5.4 Uncertainty Analysis

Nominal repeat tests were conducted for every day of testing at the same engine operating condition for the CFR and at a repeatable condition for each of the main configurations on the X15 heavy-duty engine to determine the random uncertainty with the assumption that system uncertainties remained constant on the unchanged test cell. The random uncertainty for each measured variable was then propagated to the results of interest using the root of summation of

squares equation [67] in Equation 8. Plots describing the consistency and repeatability of the engine under these nominal operating conditions can be found in the appendix.

$$w_R = (\sum_{i=1}^{n} [w_{x_i} \frac{\partial R}{\partial x_i}]^2)^{1/2} \tag{8}$$

Where:

w_R is the total uncertainty of the result

w_{x_i} is the uncertainty of the independent variable x_i

2.5.5 Exhaust Gas Recirculation

Exhaust gases were cooled and then recirculated back into the intake. The mass flow rates of the measured and/or calculated quantities in Equation 9 were used to determine the EGR rate.

$$EGR\% = \frac{\dot{m}_{EGR}}{(\dot{m}_{EGR} + \dot{m}_{air} + \dot{m}_{fuel})} \tag{9}$$

where $\dot{m}_{EGR}$, $\dot{m}_{air}$, and $\dot{m}_{fuel}$ are the mass flow rates (g/s) of the recirculated exhaust gases, air, and fuel respectively.

On the CFR engine, $\dot{m}_{EGR}$ was obtained using the measured flow properties and the calculations reported in [20], however, these calculations were susceptible to slight changes in the exhaust gas flow properties, so to improve this, CO_2 concentrations were used to calculate the $\dot{m}_{EGR}$ on the heavy-duty X15 engine using Equation 10.

$$\dot{m}_{air} * X_{CO_2{}_{air}} + \dot{m}_{egr} * X_{CO_2{}_{exh}} = \dot{m}_{egr+air\_mix} * X_{CO_2{}_{egr+air\_mix}}$$

$$\dot{m}_{egr} = \dot{m}_{air} * \frac{X_{CO_2{}_{air}} - X_{CO_2{}_{egr+air\_mix}}}{X_{CO_2{}_{egr+air\_mix}} - X_{CO_2{}_{exh}}}$$

(10)

Where:

$X_{CO_2{}_{air}}$ is the mass fraction of CO_2 in air

$X_{CO_2{}_{egr+air\_mix}}$ is the mass fraction of the CO_2 in the intake manifold air and EGR mixture

$X_{CO_2{}_{exh}}$ is the mass fraction of the CO_2 in the exhaust

The main assumptions allowing this equation to be used were that the mole fraction of CO_2 in air was 410ppm, the LPG fuel had no CO_2 in its composition (confirmed by all gas chromatographs results) and that the CO_2 already in the intake charge does not participate in any further reactions. The EGR rates obtained with this method were in agreement with the calculated AGA report #3 values and showed the desired consistency.

2.5.6 Brake Thermal Efficiency

On the CFR engine the NK APT-TH series 10kW power transducer was used to measure the electrical output from an induction motor connected to the engine. The generator efficiency of the motor was known, and the brake thermal efficiency was calculated using Equations 11 and 12.

$$\eta_b = \frac{\dot{W}_b}{\dot{m}_f * LHV}$$

(11)

$$\dot{W}_b = \dot{W}_e/\eta_{gen} \tag{12}$$

Where:

η_b is the brake efficiency.

$\dot{W}_b$ is the brake power calculated from Eq. (12).

$\dot{m}_f$ is the mass flow rate of the fuel.

LHV is the lower heating value of the fuel.

η_{gen} is the known generator efficiency, and

$\dot{W}_e$ is the electrical power

On the X15 engine, Equation 11 was also used to calculate the brake thermal efficiency, however, the brake power was obtained from the brake mean effective pressure which was obtained by subtracting the frictional mean effective pressure, calculated using the developed friction model, from the gross indicated mean effective pressure

2.5.7 Combustion Intensity Metric

The CIM is an advanced combustion tool which monitors the effects of several key combustion metrics in real-time to detect and control end gas auto-ignition in the cylinder to a desired fraction [16]. This EGAI fraction was reliably controlled by the CIM which is a linearly scaled combination of the metrics shown in Equation 13 with respect to a reference value.

$$CIM = A_1 \frac{P_{max}}{P_{max_{ref}}} + A_2 \frac{BD}{BD_{ref}} + A_3 \frac{PRR}{PRR_{ref}} + A_4 \frac{HRR_S}{HRR_{S_{ref}}} + A_5 \frac{KI}{KI_{ref}} \quad (13)$$

where A_x are calibration constants, P_{max} is the peak pressure (bar), BD is the burn duration (CAD), PRR is the pressure rise rate (bar/deg), HRR_s is the heat release rise rate slope (J/deg/deg), and KI is the knock intensity. The CIM which is an embedded parameter in the engine control module was recalibrated for engine operation on LPG due to the strong fuel effects on these five metrics.

CHAPTER 3. LOW-CARBON FUELS FOR SPARK-IGNITED ENGINES: A COMPARATIVE STUDY OF COMPRESSED NATURAL GAS AND LIQUEFIED PETROLEUM GAS ON A CFR ENGINE WITH EXHAUST GAS RECIRCULATION[3]

3.1 Overview

The foregoing review reveal that LPG and CNG are two of the forefront alternative, low-carbon fuels capable of addressing the emission burden of conventional fuels, diesel and gasoline, in the transportation sector, but they also reveal that further research is still required especially in the area of engine hardware development, exhaust gas recirculation, end-gas auto-ignition and the development of advanced combustion strategies before these fuels can gain substantial adoption and contribute to this end goal of fuel diversification and decarbonization. This chapter presents the first phase of the larger work with set goals to develop high efficiency alternative fuel heavy-duty engines.

As fleet managers consider several alternative fuel options in their decision-making process, this direct comparison of these two choice fuels provides useful insights and adds to the body of knowledge. This chapter first explores the combustion, performance, and emissions behavior of LPG and CNG across different compression ratios and engine loads on an SI cooperative fuel research (CFR) engine. The study then experimentally expands on recent numerical work done by Ge et al. [32] by comparing the EGR dilution tolerance of the two fuels, CNG and LPG, for a given load and at two compression ratios. Finally, this chapter extends previous work done exclusively with natural gas engines, by exploring the end-gas auto-ignition behavior and combustion benefit

[3] Chapter 3 extracted from published manuscript
[24] Fosudo, T., Kar, T., Windom, B., Olsen, D. Low-carbon fuels for spark-ignited engines: A comparative study of compressed natural gas and liquefied petroleum gas on a CFR engine with exhaust gas recirculation. Fuel (360) 2024, 130456.
https://doi.org/10.1016/j.fuel.2023.130456.

of using the CIM on an SI engine fueled with LPG. In the experimental investigations, pipeline natural gas (86% methane) and locally supplied LPG (95% propane) were used for the performance, emissions, and combustion comparison and the results discussed.

The chapter is extracted from a journal article [24] published in Fuel (Fuel 360 (2024) 130456) and begins with a quick overview. A brief section on the experimental methods and test matrices particular to the chapter follows, before a discussion of the results and a short conclusion brings the chapter to an end.

3.2 Experimental Methods

The CFR engine was operated on gaseous LPG and CNG to compare the performance, emissions, and combustion characteristics of both fuels on the engine. CNG supplied to the research facility and LPG with constituents conforming to the U.S. HD-5 standard was specified and certified by a local gas supplier to a ±2% accuracy. Fuel samples were collected and also constantly monitored during engine operation using an INFICON Micro GC to ensure constancy of fuel composition and provide gas chromatography results. The experiments involved a compression ratio sweep from 7:1 (non-knocking condition) to a knocking compression ratio for both fuels, then load was swept by increasing the intake manifold air pressure from just above atmospheric pressure to the engine load limit. EGR was then introduced at CR 8:1 and 9:1 and high engine loads. Finally, the CIM was calibrated for LPG use and varied from 0 to 80%. The properties and composition of the fuels used for the experiments in this chapter, and the test matrix are shown in Tables 3.1 and 3.2 respectively.

Table 3.1. Test fuel properties [68 – 70]

Composition (% vol)	**LPG**	**CNG**
Methane	-	86.01
Ethane	0.01	10.05
Propane	95.64	1.34
Propylene	2.53	-
n-Butane	1.75	0.15
i-Butane	0.05	0.09
n-Pentane	-	0.02
i-Pentane	-	0.02
Nitrogen	0.02	0.36
Carbon dioxide	-	1.96
Properties		
LHV (MJ/kg)	46.32	46.8
Laminar flame speed (cm/s)	40.32	36.65
Stoichiometric AFR	15.54	15.98
H:C ratio	2.65	3.69
Methane number	33	74
Autoignition temperature (°C)	454 - 510	540

Table 3.2. The test matrix

Variable	**LPG**	**CNG**
Compression Ratio (CR)	7 - 10	7 – 10, 12
Engine Load (bar)	8 - 11	8 - 11
EGR @ CR 8:1 (%)	10 - 30	10 - 25
EGR @ CR 9:1 (%)	10 – 30, 35	10 - 30
CIM (%)	0 - 80	0 - 80
Engine operating conditions: ϕ = 1, Speed = 900RPM, Coolant Temperature = 95^{o}C, Oil Temperature = 55 – 60^{o}C, Mixture Temperature = 60^{o}C, IMAP = 1.013bar, CA50 = 9.5^{o}aTDC*		

IMAP was varied based on load requirement

3.3 Results and Discussion

This study presents a comparison of the combustion, emission, and performance characteristics of two select low-carbon fuels: LPG and CNG, on a single cylinder CFR engine. Combustion parameters such as in-cylinder pressures and AHRR were analyzed, engine-out emissions like NOx were evaluated in a brake power normalized format, and performance was quantified in terms of brake thermal efficiencies (BTE). The investigations were performed at different compression ratios, engine loads, EGR rates, and CIM% for each fuel and the following results obtained.

3.3.1 Effect of Compression Ratio

This section discusses the effect of compression ratio on the characteristics of both fuels. First, Figure 3.1a presents a measure of the knock intensity as CR was increased from a non-knocking CR of 7:1 for both fuels. A subjective limit above which knock began to occur on the CFR engine was defined as KI = 6kPa^2. As CR was increased to 8:1, LPG began to experience incipient knock, developing rapidly to medium knock at CR 9:1 and on to heavy, destructive knock at 10:1.

Meanwhile, CNG did not experience any form of knock until CR 10:1 while also demonstrating a gentler rise, compared to LPG, to medium knock which was induced at CR 12:1. This variation in knocking tendency is due to the composition of both fuels. The longer carbon chains in the dominant component of the LPG, Propane, has a higher knocking tendency than that of the primary component of the CNG, Methane [10]. This difference can be quantified in terms of octane numbers (ON), where the higher ON for CNG (120) enables it to be more resistant to knock than LPG (104) [71, 72]. Also, since they were both introduced as gaseous fuels on the test cell, a comparison of methane number (MN) shown in Table 3.1 supports the higher knocking tendency of LPG over CNG. Results from Malenshek et al. [13] showed that fuels with similar MN to the LPG and CNG fuels used in this study experienced knock at approximately the same CR as those observed in the present study.

Next, the in-cylinder pressure traces and AHRR at CR 7:1, 10:1 and 12:1 (CNG only) are shown as a function of CR in Figure 3.1b. LPG combustion indicated a higher AHRR at all conditions with a shorter duration of heat release compared to CNG which translates to quicker fuel energy release and shorter combustion durations in favor of LPG. In terms of the in-cylinder pressures, LPG indicated peak pressures higher by 6% at CR 7:1 and then by 22% at CR 10:1 compared to CNG and also exhibited more advanced location of peak pressures (LPP) at both CR. However, it is desirable to increase CR, peak pressures, and advance LPP without the occurrence of destructive knock and CNG achieved the highest CR (i.e., CR 12:1) and peak pressures recorded during the CR tests with only medium knock. The steeper slope after the inflection point on the LPG pressure trace at CR 10:1 even compared to CNG at CR 12:1 indicated a rapid rate of pressure rise typically associated with end-gas auto-ignition.

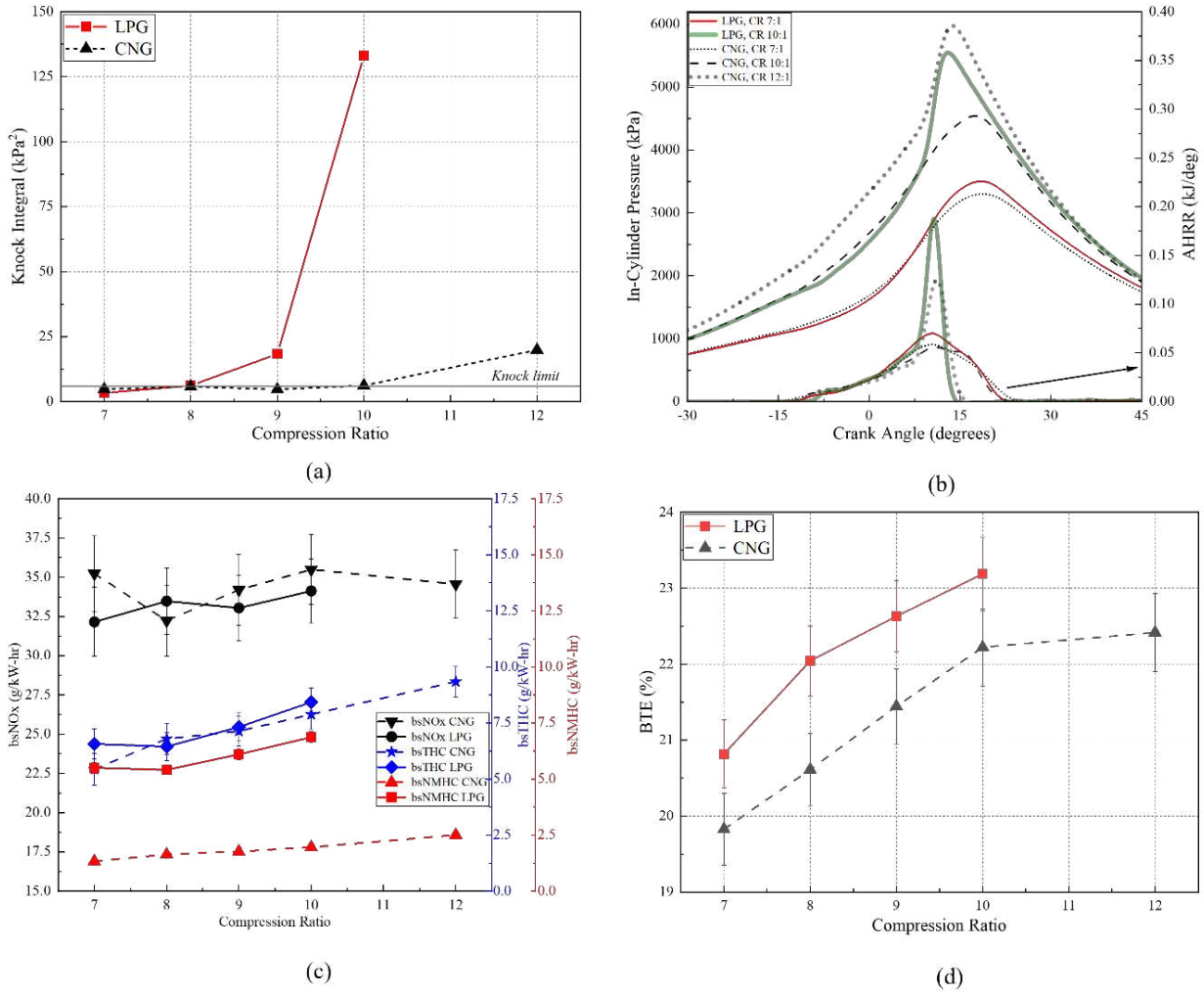

Figure 3.1. Variation of (a) Knock Integral (b) In-cylinder pressure and AHRR (c) brake specific emissions (d) BTE, with compression ratio for CNG and LPG

In addition, the brake specific (bs) NOx, THC and NMHC are graphed in Figure 3.1c. The exhaust sampling results showed that LPG produced slightly higher ppms of NOx compared to CNG; for example, at CR 9:1 LPG NOx emissions were recorded as 4078ppm compared to 3941ppm for CNG at the same CR. However, this trend was reversed upon normalization with brake power as presented in Figure 3.1c as a result of the higher brake powers generated by LPG at every CR. Since NOx chemistry is primarily determined by local in-cylinder temperatures, an approximation for the peak in-cylinder temperatures was determined using the ideal gas equation and this showed higher peak temperatures for LPG across all CR which supports the higher NOx ppm values for

LPG. In terms of the CR effect alone, as CR increases, pressure and temperature also increase with a consequent increase in NOx ppm observed in this study. However, this increasing effect was counteracted by the reducing effect of the normalization with higher brake powers at higher CR. The bsTHC emissions in Figure 3.1c described a more distinctive increasing trend with CR. This is likely largely due to the crevice volume effect, with the high in-cylinder pressures recorded at high CR forcing more gas into the crevices. This gas then rejoins the exhaust stream during the expansion stroke as unburned hydrocarbons (UHC).

Comparing both fuels, LPG indicated higher bsTHC than CNG except at CR 8:1, with the most being 8.4g/kW-hr at CR 10:1, 7% more than the bsTHC of CNG at this CR. Another important class of regulated emissions for SI LPG engines are NMHC, as such the bsNMHC emissions were also evaluated and plotted in Figure 3.1c. CNG operation reduced bsNMHC emissions compared to LPG by over half at every tested CR showing an almost 72% reduction at CR 10:1. This reduction was due to the composition of the CNG (i.e., 86% CH_4 by vol) and the fact that a larger percentage of its THC emission was made up of CH_4. However, CH_4 is a potent contributor to GHG and should also be minimized. The notable difference in Figure 3.1c between the bsTHC and the bsNMHC numbers is the bsCH_4, which increases with CR as observed from the divergence between the bsTHC and bsNMHC lines. This divergence is likely due to the greater rate of low temperature oxidation of higher hydrocarbons on reentry into the combustion chamber from the crevice volume compared to CH_4. Similar NMHC/CH_4 behavior of LPG and CNG has also been reported in the literature [73].

Finally, the performance metrics are presented in terms of BTE in Figure 3.1d, where BTE was observed to increase in tandem with CR due to improved cycle efficiency [7, 10]. LPG indicated a higher BTE value at every tested CR when compared with CNG, with a maximum relative

increase of 7% at CR 8:1, where LPG had an efficiency of 21.54% compared to 20.11% with CNG fueling. This can be attributed to the combined contribution of the reduced burn durations and higher AHRR for LPG compared to CNG which was shown in Figure 3.1b. These differences between the fuels were linked to the superior laminar flame speed (LFS) shown in Table 3.1 and the fuel energy density [71] of LPG compared to CNG. The LFS was calculated at STP using the ALPINE_153 mechanism in CHEMKIN [68].

3.3.2 Effect of Engine Load

Engine load, represented by the net IMEP, was swept at CR 8:1 from 8bar until the load limit of the engine at 11bar was reached. The results for both fuels are presented in this section. The in-cylinder pressures and AHRR for the LPG and CNG fueling configuration at 8bar and 11bar are shown in Figure 3.2a. The LPG pressure traces indicated higher peak in-cylinder pressures, 6.5% higher at 8bar engine load and 10% higher at 11bar, with LPP also closer to TDC than their CNG counterparts. Another feature of the in-cylinder pressure traces was the steeper slope observed for LPG as its rate of pressure rise differed markedly from that for CNG. Similar to the CR case in Section 3.3.1, LPG demonstrated faster AHRR with much higher peaks than CNG. For example, the peak AHRR at 11bar engine load was 0.24kJ/deg for LPG compared to 0.1kJ/deg for CNG. The shape of the AHRR curves, at 8bar engine load for LPG, with the distinctive shoulder also suggested the presence of a secondary combustion event typically associated with end-gas auto-ignition. These dissimilar combustion characteristics were due to the differences in reactivity of the primary constituents of both fuels, Propane for LPG, and Methane for CNG.

Figure 3.2b shows the knock integral (KI) characteristics of both fuels at the same engine operating conditions, CNG demonstrated a clear advantage owing to its ON/MN as previously discussed in Section 3.3.1, remaining below the knock limit at all engine loads. LPG on the other hand, started

to experience light knock from 8bar engine load as was suggested by the distinctive shoulder on the AHRR curve. LPG also indicated an exponential rise in knocking intensities as engine load was increased. For both fuels, however, the KI increased with increasing engine load.

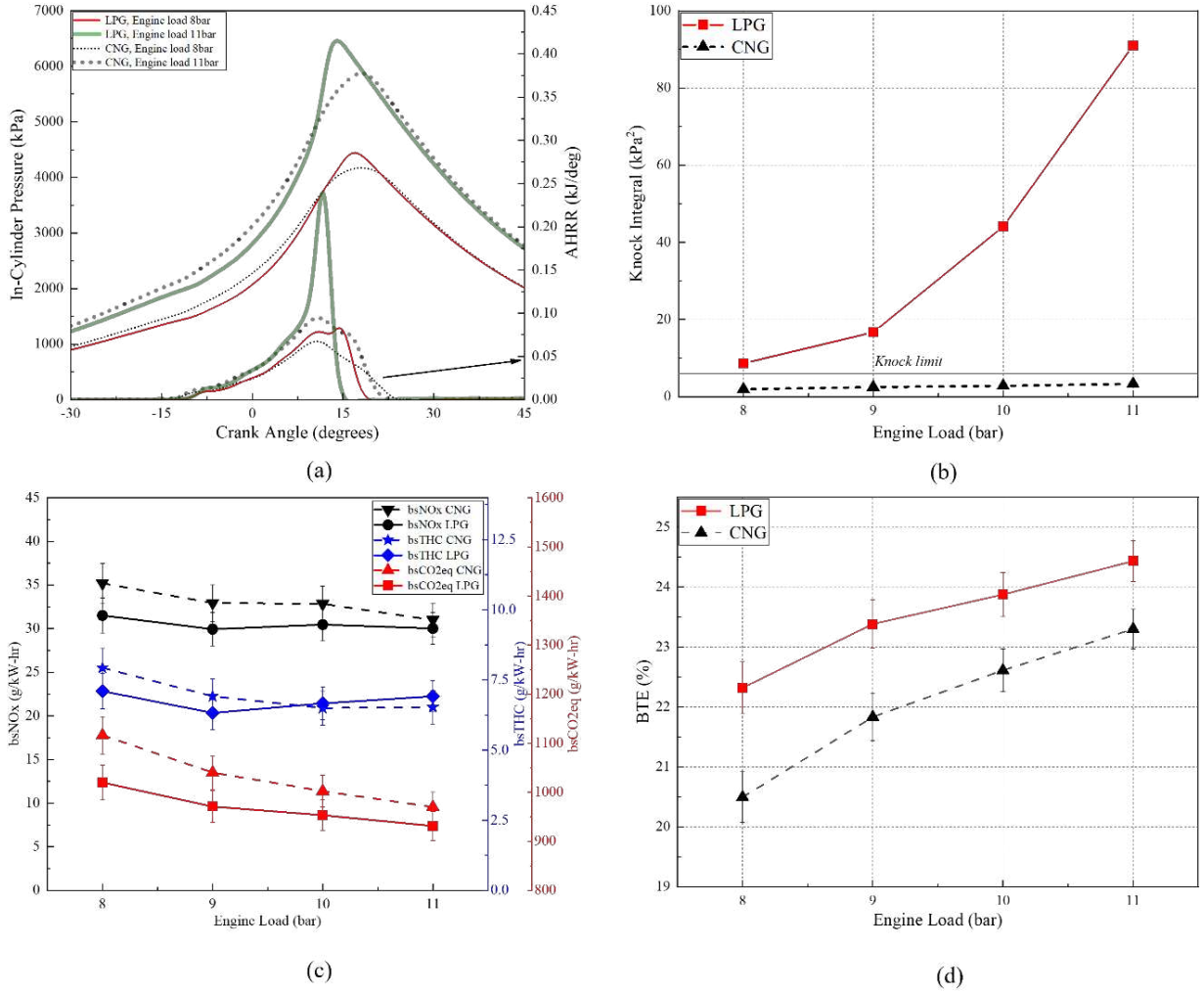

Figure 3.2. Variation of (a) In-cylinder pressure and AHRR (b) Knock Integral (c) brake specific emissions (d) BTE, with engine load for CNG and LPG

The brake specific NOx, THC and CO_2eq are shown in Figure 3.2c for both tested fuels. The bsNOx values for CNG were observed to be higher than for LPG at all engine loads. In addition to the in-cylinder temperature and brake power normalization discussions mentioned in Section 3.3.1, the N_2 present in the CNG fuel and quantified in Table 3.1 may be a possible contributor to the CNG NOx emissions. However, the normalization by a lower brake power remains the key

reason for the higher bsNOx emissions of CNG despite the higher ideal gas peak in-cylinder temperature of LPG compared to CNG (for example 2851K compared to 2744K at 8bar engine load) and its effect on the raw NOx ppm values. Figure 3.2c also illustrates the variation of the brake specific THC for both tested fuels across the engine loads. HC emissions are primarily due to the incomplete combustion of the fuel. From the results, CNG and LPG demonstrated opposing trends as load was increased; similar trends were also observed for CNG and LPG [27] and LPG only [36]. Finally, bsCO_2eq emissions are shown in Figure 3.2c. These composite GHG emissions combine the effect of CO_2, CH_4 with a 25-unit multiplier, and N_2O with a 298 multiplier to present a CO_2 equivalent emissions metric. These emissions, although dominated by the bsCO_2 emissions, demonstrate the importance of considering the CH_4 and N_2O emissions. Due to its higher H:C ratio shown in Table 3.1, the bsCO_2 emissions of CNG at all tested engine loads were considerably lower than the LPG bsCO_2 similar to results presented in the literature [73]. Nevertheless, CNG produced significantly higher bsCO_2eq emissions at all tested engine loads, showing a 10% increase at low engine loads and a 4% increase in bsCO_2eq at the engine load limit compared to LPG. This trend is a result of the higher concentrations of CH_4 emissions, a potent GHG, produced by CNG.

BTE, shown in Figure 3.2d, increased as engine load was increased as a result of minimized friction and pumping losses at the boosted engine conditions [28, 74]. Comparing CNG and LPG BTE values, LPG produced a maximum BTE of 24.4% at the engine load limit, a 5% relative improvement in efficiency compared to CNG at the same engine load. The largest improvement was recorded at 8bar engine load where CNG produced a BTE of 20.5%, 9% relatively lower than the LPG BTE at this condition. The fuel effect on BTE was discussed in Section 3.3.1 with another

possible contributor, captured in Figure 3.2a, being the proximity of the LPP to TDC with LPG combustion compared to CNG, which suggests increased work transfer to the piston.

3.3.3 Effect of Exhaust Gas Recirculation (EGR)

The results from the CR and engine load investigations were then analyzed and guided the EGR tests. This section presents the influence of EGR dilution on the performance, emission, and combustion behavior of both fuels. EGR was added to the fuel-air mixture at CR 8:1 and 9:1 with the engine load maintained at 10bar by varying the IMAP. Details of the combustion characteristics are presented in Figure 3.3. Figures 3.3a and 3.3b illustrate the interaction between the KI, the combustion stability expressed in terms of the $COV_{peak\ pressure}$, and the EGR rate. As EGR is added and the intake charge becomes more diluted and less reactive, the COV increases to a limit above which combustion can be said to be unstable, usually marked by high cycle-to-cycle variability. In this study, a $COV_{peak\ pressure}$ of 10% was adopted as the COV limit, and the EGR% at which this COV limit was reached referred to as the EGR limit.

Accordingly, as EGR% was increased in Figures 3.3a and 3.3b, the $COV_{peak\ pressure}$ also rose until it crossed the 10% limit for both CNG and LPG. LPG indicated a higher tolerance for dilution with EGR, with an EGR limit of 26% at CR 8:1, achieving a 13% relative improvement compared to the EGR limit for CNG. At CR 9:1 the dilution tolerance gap was even wider as LPG indicated an EGR limit of 28%, achieving double the relative improvement (27%) compared to CNG. This improvement in EGR tolerance could likely be due to the differences in early flame development and flame propagation times linked to the superior flame speed of LPG shown in Table 3.1. For example, at CR 9:1 and 30% EGR, the 10-90% mass fraction burned duration was calculated to be 22.3 CAD for LPG and 34.8 CAD for CNG. However, recent computational studies by Ge et al. [32] comparing two fuels of similar flame speed still showed significant differences in EGR

dilution tolerances and they proposed the Lewis number or low temperature chemistry as possible dominant factors in EGR dilution mechanics. Therefore, these experimental results suggest that fuel low temperature chemistry may possibly be a key factor in determining EGR dilution tolerance as despite the lower Lewis number of CNG, LPG still demonstrated substantially improved EGR dilution tolerances. These effects were likely amplified by increasing the CR for LPG in particular, as it was discovered that the CNG EGR limit remained approximately the same at both CR.

A documented desired effect of EGR is its mitigating effect on knock, thus allowing engine operation at higher CR and engine loads especially for fuels with high reactivity such as LPG. This effect was demonstrated especially for LPG, in Figure 3.3a, as the KI was reduced by 84% from medium knock levels to a stable, knock-free engine operation in the window between 22% EGR and the EGR limit at 26%. From Figure 3.3b, it is seen that the KI was reduced even more remarkably by 98% at the higher CR, as the engine was transitioned from heavy, destructive knock without EGR to light knock at the EGR limit. These effects were much less pronounced with CNG as the engine only experienced some level of incipient knock at CR 9:1 without EGR, and they were quickly counteracted by the increased dilution.

The in-cylinder pressure traces and AHRR at CR 8:1 and 9:1 are shown in Figures 3.3c and 3.3d. For LPG, the addition of EGR was observed to reduce the peak in-cylinder pressures and retard the LPP up until the EGR limit at both CR. In the case of CNG, a similar trend was observed at CR 9:1 with a slight difference at CR 8:1, where only the LPP trend was observed, and peak pressures remained approximately equal. The AHRR curves also described very definitive trends for both fuels. For LPG, the peak AHRR was reduced by 62%, from 0.19kJ/deg without EGR to 0.07kJ/deg around the EGR limit, at CR 8:1 and from 0.27kJ/deg without EGR to 0.08kJ/deg

around the EGR limit at CR 9:1. For CNG, a similar peak AHRR reduction trend was observed but by lesser amounts: 38% at CR 8:1 and 60% at CR 9:1. A key feature of the AHRR curves for both fuels was the longer AHRR duration as EGR was introduced, indicating longer burn durations in the combustion chamber. Ravi et al. [30] showed similar combustion behaviors in their study.

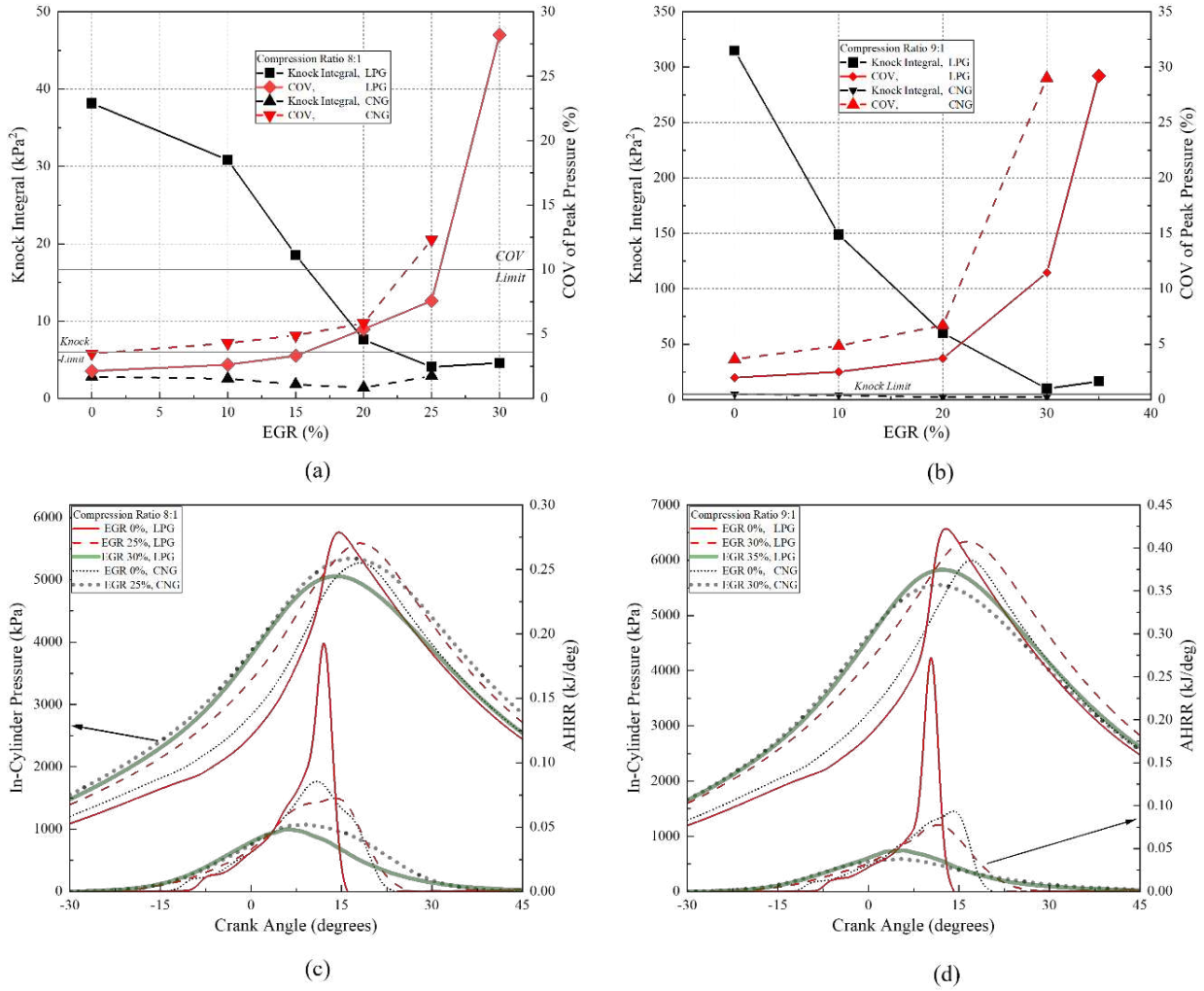

Figure 3.3. Various combustion metrics at different EGR rates for CNG and LPG and at different compression ratios: (a) Knock Integral and $COV_{peak\ pressure\ @CR8:1}$ (b) Knock Integral and $COV_{peak\ pressure\ @CR9:1}$ (c) In-cylinder pressures and AHRR $_{@CR8:1}$ and (d) In-cylinder pressures and AHRR $_{@CR9:1}$

In terms of brake specific emissions presented in Figures 3.4a and 3.4b, LPG bsNOx was reduced by 80% from 32.24g/kW-hr to 6.7g/kW-hr as EGR was introduced to the intake charge from 0% up to the EGR limit at CR 8:1. This reduction was furthered at CR 9:1, as bsNOx was minimized

by around 90% from 34g/kW-hr to 3.5g/kW-hr within the same EGR window, while the bsNOx was reduced by approximately 70% for CNG at both CR. This trend continued even after the EGR limit when combustion had become unstable. This EGR influence on NOx is a result of the elevated heat capacity of the cylinder charge due to introduction of exhaust gases, and the decreased flame temperatures, which effectively reduce NOx. This mitigating effect of EGR on NOx is outlined in the literature [10, 20, 30]. As combustion transitioned from slow burn w.r.t increasing EGR rates to misfire after the EGR limit, the bsTHC emissions remained fairly constant around 7g/kW-hr up until the EGR limit and then spiked to over 6 times that value to greater than 42g/kW-hr for both CNG and LPG at CR 9:1 suggesting misfire at those extremes. At CR 8:1, LPG bsTHC indicated similar trends to those exhibited at CR 9:1; however, while the bsTHC emissions for CNG increased after its EGR limit, it was not as dramatic as was observed for LPG. As discussed above, this EGR - bsTHC behavior resulted from decreased burn rates as combustion transitioned from slow burn to misfire, leading to the incomplete combustion of the fuel. These trends were also captured by Bayliff et al. [20].

Finally, bsCO_2eq emissions are shown for both fuels at CR 8:1 in Figure 3.4a while bsNMHC are shown for both fuels at CR 9:1 in Figure 3.4b. As discussed in Section 3.3.1, the bsNMHC for CNG was observed to be significantly lower compared to the bsNMHC of LPG, and this trend persisted as EGR rates were increased. Although CNG was mainly Methane, the presence of NMHC in its exhaust emissions is due to the recombination reactions to higher hydrocarbons which can be found in the low temperature chemistry of Methane. There are also the 10% by vol C_2H_6 and 1.3% by vol C_3H_8 present in the fuel shown in Table 3.1 which can escape as unburnt hydrocarbons from the crevice volumes or during misfires/partial combustion. After the EGR limit, this bsNMHC produced by CNG rose to approximately match the bsNMHC at the EGR limit of

LPG. In this regard, CNG had exceeded its EGR limit but still produced low enough bsNMHC at around 6.5g/kW-hr to match that of LPG even though LPG was still within its EGR limit. In Figure 3.4a, the bsCO_2eq emissions decreased with increased EGR, then began to rise a few percentages before the EGR limit for both fuels, suggesting that if all relevant emissions are considered, an optimal EGR amount may not necessarily exist at the EGR limit but slightly retarded from that EGR%.

Figures 3.4c and 3.4d present the BTE for both fuels at the two tested CR. BTE demonstrated an increasing trend up until the EGR limit for both fuels, this influence of EGR on BTE was likely a result of reduced pumping work and fuel consumption as well as reduced heat loss in the combustion chamber as temperatures were much lower [75]. For example, pumping work calculated from the in-cylinder pressure data was reduced by 11% from 98J at 0% EGR to 87J at the EGR limit for LPG at CR 8:1. After the EGR limit, however, BTE dropped sharply for both fuels due to the unstable combustion illustrated by the high $COV_{peak\ pressures}$ associated with high dilutions shown in Figures 3.3a and 3.3b. These high $COV_{peak\ pressures}$ underscored misfire/partial combustion which was responsible for the elevated bsTHC emissions in Figures 3.4a and 3.4b which in turn would have a deleterious effect on combustion efficiency and BTE. Comparing the fuels, the disparity in performance was more obvious for all EGR rates at CR 8:1 with LPG fueling responsible for a maximum 3% relative improvement over CNG at 25% EGR. Conversely, the brake thermal efficiencies of the fuels were more closely matched at CR 9:1, until a strong divergence point at 30% EGR, where LPG achieved a 25% relative improvement in performance as a result of its higher EGR tolerance. The maximum BTE recorded during this study was 25.2%, achieved with LPG fueling at CR 9:1, 10bar engine load, and 30% EGR.

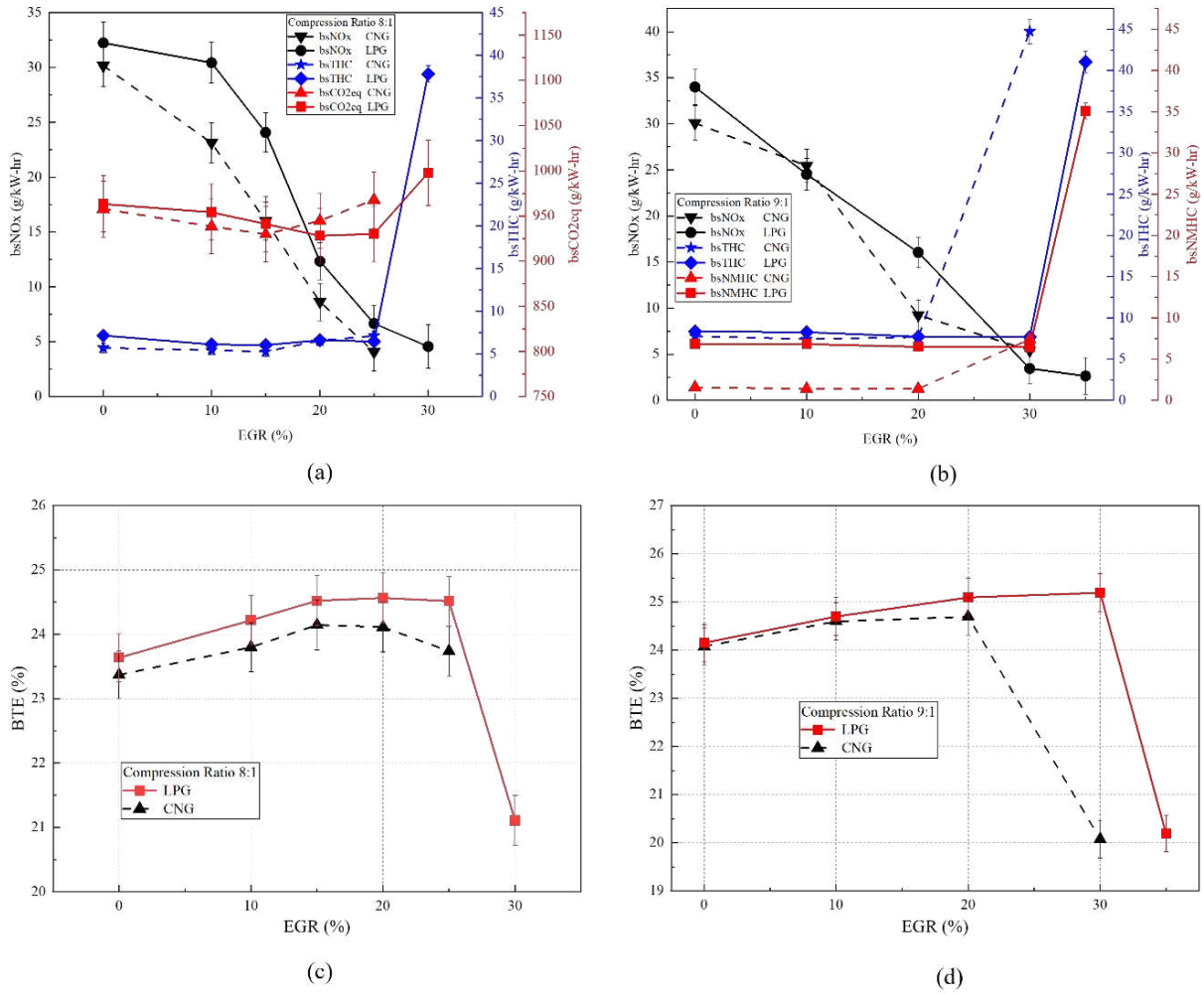

Figure 3.4. Plots of emission and performance metrics at various EGR rates for CNG and LPG and at different compression ratios showing (a) brake specific emissions $_{@CR8:1}$ (b) brake specific emissions $_{@CR9:1}$ (c) BTE $_{@CR8:1}$ and (d) BTE $_{@CR9:1}$

3.3.4 Combustion Intensity Metric (CIM)

Finally, this chapter preliminarily explores the possible benefits on the combustion and performance of LPG using the real-time ignition timing control tool, the combustion intensity metric (CIM). The CIM, a robust combustion control tool, which takes into account several key combustion metrics outlined in equation 13 had been previously applied for natural gas operation optimization [16, 76]. The CIM, which was to be used to initiate a desired fraction of end-gas auto-ignition (f-EGAI), was successfully recalibrated for use with LPG in this study. Figure 3.5a shows the relationship between CIM and f-EGAI for CNG and LPG. The CNG data, culled from previous

work on the CFR engine by Bayliff et al. [20] described a steeper relationship, 0.15 to 0.53 f-EGAI as CIM was varied from 20 to 80%, compared to the narrower control region indicated for LPG, 0.31 to 0.5 f-EGAI. This was an indication that LPG transitioned more suddenly into end-gas auto-ignition as opposed to CNG, which exhibited a steadier climb into end-gas auto-ignition. The fuel reactivity and knock resistance, discussed in Sections 3.3.1 and 3.3.2, are likely responsible for this trend.

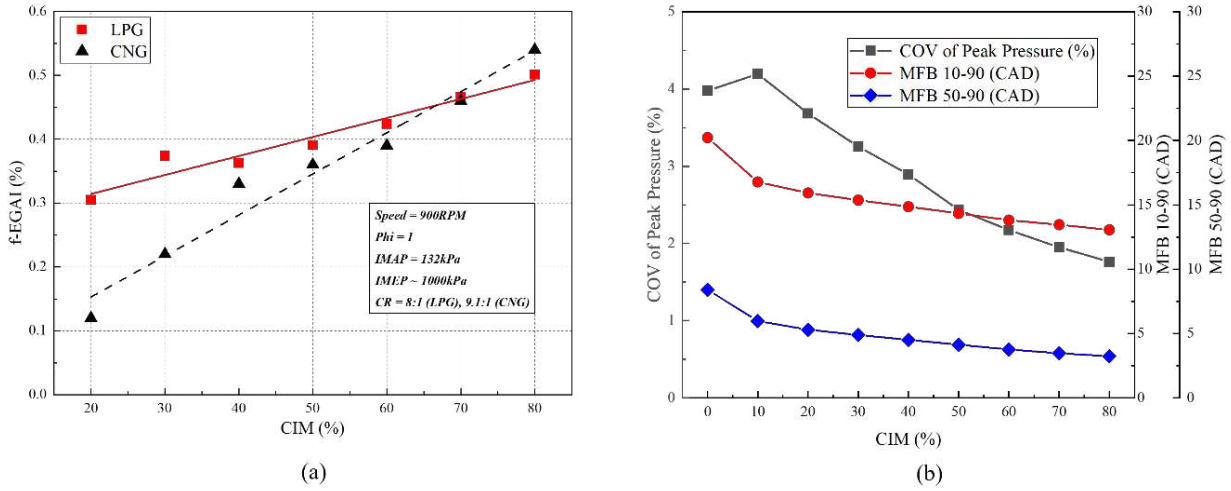

Figure 3.5. (a) fraction of end-gas auto-ignition vs CIM for CNG and LPG (b) $COV_{peak\ pressure}$, MFB 10-90% and MFB 50-90% vs CIM for LPG

In Figure 3.5b, the $COV_{peak\ pressure}$, MFB 10-90% and 50-90% are shown. Hampson et al. [16] suggested that CIM could be responsible for effecting a more controlled volumetric ignition as opposed to isolated harmful pockets of end-gas auto-ignition. They suggested that this could be achieved by shortening the combustion duration and especially, the 50-90% time during which end-gas auto-ignition is most likely to occur so that desirable auto-ignition is happening volumetrically all through the combustion chamber at approximately the same time. The trends showed that as CIM was increased, the 10-90% burn duration for LPG was reduced; however, more desirable was the reduction in 50-90% time, which even exhibited a slightly quicker decline compared to the 10-90% burn duration. The $COV_{peak\ pressure}$ was also shown to improve as CIM

was increased suggesting less cycle-to-cycle variability, linked to the more favorable combustion phasing, the quicker burn durations, and possibly, this controlled volumetric auto-ignition. Finally, the influence of CIM on performance is captured in Figure 3.6. The BTE increased from 23.1% at CIM 0% to a maximum at CIM 20% which corresponded to an f-EGAI of 0.31. Bayliff et al. [20] reported a similar result for CNG, with the maximum BTE w.r.t CIM observed at an f-EGAI of 0.33. This increase in BTE was the result of the advanced ignition timings as CIM was increased, which shifted the LPP closer to the TDC and increased work transfer to the piston.

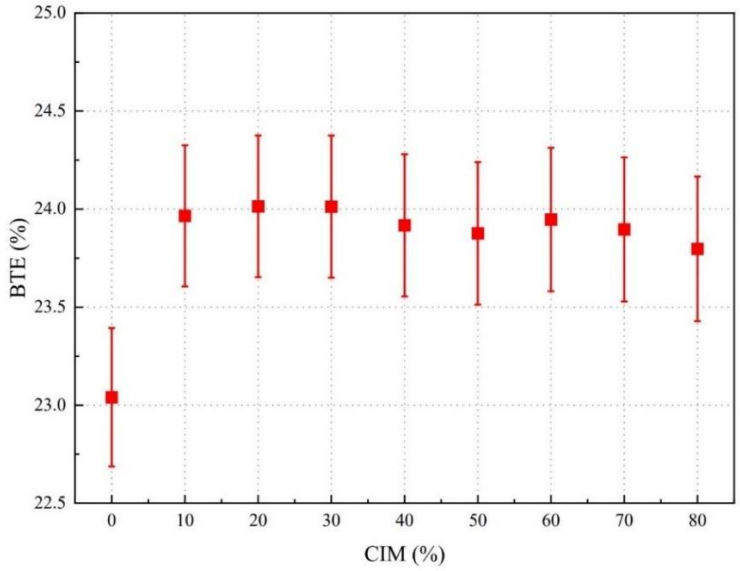

Figure 3.6. BTE vs CIM at ϕ = 1, CR = 8:1 and 10 bar engine load for LPG fueling

3.4 Conclusions

This chapter compared the combustion, emissions, and performance characteristics of two forefront low-carbon alternative fuels, LPG and CNG. Experimental investigations were conducted over a range of compression ratios, engine loads, and exhaust gas recirculation rates on a spark-ignited CFR engine. The application of a novel, robust combustion control tool was also

explored for LPG after having previously been studied with CNG in different works. The main findings are summarized below in this section.

CNG demonstrated an advantage in terms of engine operation at higher engine loads and compression ratios, allowing knock-free engine operation up until the engine load limit and only experiencing medium level of knock at CR 12:1. On the other hand, LPG began to exhibit knocking combustion at lower compression ratios and engine loads and demonstrated a steeper rise in knock intensity as the engine transitioned into heavy knock at CR 10:1 and at the engine load limit. In general, however, LPG consistently indicated enhanced combustion characteristics with faster and higher AHRR, shorter burn durations, higher peak pressures, and closer to TDC locations of peak pressure compared to CNG.

Despite the higher compression ratios achieved by CNG, LPG performed marginally better in terms of BTE, accounting for the highest BTE with 22.7% at CR 10:1 compared to 21.9% for CNG at CR 12:1. LPG also performed significantly better at all tested engine loads, producing a maximum efficiency of 24.4% compared to 23.3% for CNG at the engine load limit. CNG was observed to generate significantly higher $bsCO_2eq$ emissions, a direct consequence of its considerably higher CH_4 emissions despite indicating lower $bsCO_2$ emissions compared to LPG. For example, the CNG fuel was responsible for a 10% and 4% higher $bsCO_2eq$ at low engine loads and at the engine load limit respectively.

LPG indicated superior EGR tolerance compared to CNG at the two tested compression ratios with a maximum EGR limit of 28% at CR 9:1 compared to 22% for CNG at the same CR suggesting that fuel low-temperature chemistry and flame speeds had a more significant effect on EGR dilution tolerance than the Lewis number. This superiority was further demonstrated at the LPG EGR limits, as LPG accounted for a 3% relative improvement in BTE at CR 8:1 and a 25% relative

improvement at CR 9:1. EGR demonstrated a strong effect on bsNOx reducing the engine-out bsNOx at CR 8:1 by 80% from 32.24g/kW-hr without EGR to 6.7g/kW-hr at the EGR limit and exhibiting an even stronger effect at CR 9:1 by eliminating 90% of the bsNOx within the same EGR window for LPG. Similarly, this effect was observed for CNG but to a lesser degree as bsNOx was reduced by approximately 70% at both CR. EGR was also found to be effective at mitigating heavy knock as it reduced the LPG knock intensity metric by 98% at CR 9:1, transitioning the engine from heavy knock without EGR to light knock at the EGR limit. For LPG at CR 8:1, this KI reduction was 84%. CNG, however, only began to experience incipient knock at CR 9:1, and as such, this EGR effect was not apparent. Finally, the combustion intensity metric (CIM) was successfully applied as a combustion control tool for LPG to perform controlled end-gas auto-ignition combustion and for performance enhancement. LPG operation demonstrated a 50% narrower region of control for the fraction of end-gas auto-ignition compared to CNG indicating a faster transition from normal combustion to an end-gas auto-ignition regime.

The findings suggest that determining an optimal EGR rate considering efficiency and relevant emissions is key to the overall performance of the LPG engine. They also illustrate the potential to apply the robust CIM tool to speed up the slower burn rates associated with higher EGR rates which may possibly extend the EGR limit and further increase efficiency. This chapter provides some clarity on research questions 1,2 and 4 and demonstrates the regions of superiority of the LPG fuel for further engine operation.

CHAPTER 4. THE IMPACT OF LPG COMPOSITION ON PERFORMANCE, EMISSIONS, AND COMBUSTION CHARACTERISTICS OF A PRE-MIXED SPARK-IGNITED CFR ENGINE[4]

4.1 Overview

After successfully setting up the CFR to run on LPG and demonstrating its advantages in terms of efficiency, emissions and EGR tolerance, several LPG blends that broadly represent the present LPG market were chosen to study the effect of LPG composition on the engine. The composition of LPG used as a transportation fuel varies according to season, country, properties of the supply crude oil/gas used, refining process and the balance of demand for the different refined products. In other words, there is no universal standard defining LPG composition for automotive applications. In Europe, LPG for the automotive market must comply with EN 589, which does not define the composition of the fuel, but puts limits on its properties [6]. The HD-5 specification exists in the US, which limits LPG compositions to > 90% Propane and < 5% Propylene. Between 2017 and 2018, Gomez et al. [77] documented the fuel quality and variability of LPG constituents across the continental United States. They found that LPG fuel quality from around the US was consistent in quality, and in most cases, well within the HD-5 specification limits [77]. Their results also showed LPG in the US typically contains higher amounts of ethane compared to other constituents (excluding propane). Campbell et al. [6] showed that the LPG in Europe mainly consisted of propane and n-butane [6].

[4] Chapter 4 extracted from published manuscript
[7] T. Fosudo, T. Kar, A. Marchese, B. Windom, D. Olsen. The Impact of LPG Composition on Performance, Emissions, and Combustion Characteristics of a Pre-mixed Spark-Ignited CFR Engine. SAE Technical Paper 2022-01-0476, 2022. doi:10.4271/2022-01-0476

Due to this variance in composition and the potential demonstrated in Chapter 3, it is a worthy venture to study the effects of LPG fuel composition on engine performance, emissions, and combustion behavior. Previous research works have only studied the effect of n-Butane and propane in the LPG composition on engine performance. However, the effects of unsaturated and lower hydrocarbons such as propylene and ethane, which are also present in common LPG blends, on the emission and performance characteristics of LPG engines remain to be properly studied. This work seeks to provide a more representative study of the influence of LPG composition on engine characteristics.

The chapter is extracted from a technical conference proceeding [7] presented at the SAE World Congress Experience (WCX) and begins with a quick overview. A brief section on the experimental methods and test matrices particular to the chapter follows, before a discussion of the results and a short conclusion brings the chapter to an end same as Chapter 3.

4.2 Experimental Methods

The engine used for this experimental study was the single cylinder, variable compression ratio, 4-stroke CFR engine. Three LPG blends identified as a representative US blend (%vol ethane = 6.5), a representative European blend (%vol n-butane = 18) and an HD-5 blend (%vol propylene = 2.5) were selected for this study. Also, chemically pure propane was included to provide a base of comparison with the other blends. The LPG blends were delivered in the liquid state in cylinders and the fuel in gaseous form was drawn from the top of the cylinders during engine operation. The compositions of the gas stream supplied from the top of the cylinders were analyzed as described in Section 3.2 and the fuel properties presented in Table 4.1 while the hydrocarbon constitution of the LPG blends is illustrated in Figure 4.1. The test matrix shown in Table 4.2 was designed to study the composition effects of each blend by employing a CR sweep, a load sweep, and an EGR

sweep while keeping other engine operating conditions constant. The CR was initiated from a point at which there was normal combustion for all blends i.e., without end-gas auto-ignition, and then swept by one-unit increments, through trace knock, and up to heavy knock for all blends. A baseline CR was then defined from the results of these tests. Spark timing was varied to maintain CA50 at ~ 9.5^0 aTDC for each test case (MBT for all cases was found to be between CA50 8.5-10^0 ATDC). Each test case was run at stoichiometric conditions and a constant speed of 900RPM, and all the experimental data taken at steady state engine operating conditions.

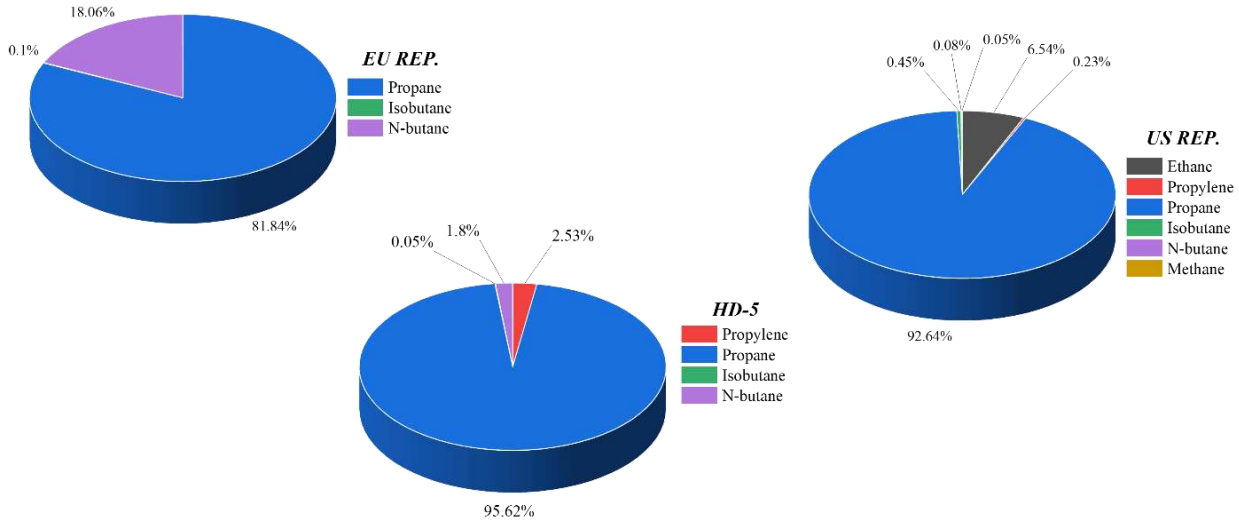

Figure 4.1. LPG blend composition showing other dominant constituents

In this chapter, the knock occurrence crank angle (KOCA) was an important metric for comparison between blends and it was calculated based on the third derivative of the average in-cylinder pressure trace, close to the peak knock region [78]. A central difference scheme numerical method was used, defined by Equation 14.

Table 4.1. Selected LPG blends composition details and their properties

LPG Blends	**Chemically Pure Propane**	**US Representative (US Rep.)**	**HD-5**	**European Representative (EU Rep.)**
Composition of gaseous sample (mol%)	Propane - 99.9	Propane - 92.6 Ethane - 6.5 Methane - 0.05 i-butane - 0.45 N-butane - 0.1 Propylene - 0.23	Propane - 95.6 Propylene - 2.5 N-butane - 1.8 i-butane - 0.1	Propane - 81.8 n-butane - 18.1 i-butane - 0.1
LHV (MJ/kg)	46.36	46.4	46.31	46.2
Laminar Flame Speed (cm/s) at STP	40.18	40.3	40.24	39.54
Energy density (kJ/m^3)	3500	3503	3499	3488
H:C ratio	2.67	2.68	2.65	2.63
Density(kg/m^3) @14.696psi, 60F	1.9	1.82	1.87	1.97
Stoichiometric Air-Fuel ratio	15.57	15.59	15.54	15.52

Table 4.2. The tested experimental conditions

LPG Blend	**Engine Operating Conditions**
EU Rep.	φ = 1, IMAP = 101.3kPa*, Speed = 900RPM, CA50 ~ 9.5 deg ATDC = MBT, Mixture Temperature = 60 deg C Oil Temperature = 55 - 60 deg C Coolant Temperature = 95 deg C Compression ratio = 7:1, 8:1, 9:1 and 10:1 IMEP (kPa) @ baseline CR 8:1 = 800, 900, 1000, 1100 EGR (%) @ baseline CR 8:1 and 800kPa = 0, 10, 15, 20, 30, 35
HD-5	
US Rep.	
Chemically Pure Propane	

$$P'(\theta) \sim [86 * (P_{i-4} - P_{i+4}) + 142 * (P_{i+3} - P_{i-3}) + \cdots$$

$$+193 * (P_{i+2} - P_{i-2}) + 126 * (P_{i+1} - P_{i-1})] \,/\, (1188 * \Delta\theta) \quad (14)$$

Where:

$P'(\theta)$ is the first derivative of the pressure with respect to the engine crank angle (CA)

P_{i+1} and P_{i-1} are the succeeding and preceding pressure values respectively.

$\Delta\theta$ is the engine CA step defined as 0.1CA in this work

This equation was applied three times to the pressure signal to achieve the third derivative. The successive application of Eq. 14 amplifies signal noise; therefore, a low pass filter was used on the second derivative before calculating the third derivative. This filter is given by Equation 15.

$$F(\theta) \sim [2 * (S_{i-4} + S_{i+4}) + 3 * (S_{i-3} + S_{i+3}) + 4 * (S_{i-2} + S_{i+2}) + 5 * (S_{i-1} + S_i + S_{i+1})] / 33 \quad (15)$$

Where:

S_{i+1} and S_{i-1} are the succeeding and preceding terms of the second derivative.

In general, knocking pressure peaks have significantly larger third derivatives than non-knocking pressure peaks and thus, the CA with the most negative third derivative corresponds to the KOCA of a cycle [78].

4.3 Results and Discussion

4.3.1 Combustion Characteristics

Key combustion metrics were calculated from the raw pressure data for each cycle and analyzed to describe the combustion events for all blends over the range of CR, loads and EGR rates. Figures 4.2 and 4.3 show the cycle-averaged in-cylinder pressure for the tested CR and loads respectively, with the cut-outs used for magnification. In Figure 4.2, normal combustion is observed for all blends at CR 7:1 with little difference in peak pressure. As CR is increased, end gas auto-ignition begins to occur more frequently and with greater intensity. This causes some variation in the peak

pressure for the tested LPG blends, particularly at CR 10. As shown in Figure 4.2, the peak in-cylinder pressures increased from ~3500kPa at CR 7:1 to ~5500kPa at CR 10:1 which agrees with the documented effect of CR. However, the fuel composition effect accounts for a meagre 2.4% difference between the peak of the HD-5 pressure trace and the peak of the chemically pure propane pressure trace at CR 10:1. Figure 4.2 also shows that the peak pressure location moves closer to TDC with increasing CR. This increases the work transfer to the piston and consequently, efficiency. While the fuel composition also impacts the peak pressure location as shown in the magnified portions of Figure 4.2, this effect is not very pronounced at each CR. This fuel composition effect on in-cylinder pressure is likely due to the reactivity of the fuel components (propylene in the HD-5 and n-butane in the EU Rep. blend). Similar trends were captured during the load sweep and are illustrated in Figure 4.3 with the HD-5 and EU Rep. blends indicating slightly higher peak in-cylinder pressures and LPP closer to TDC.

The AHRR is shown for all blends at the tested CR in Figure 4.4 and at the tested loads in Figure 4.5. With the increase of CR and load, the duration of heat release decreases and the magnitude of the AHRR increases. A faster AHRR shortens the combustion duration, allowing combustion phasing to be better optimized. For example, a higher CR results in a higher temperature at ignition, which increases the flame speed and in turn combustion rate. Figure 4.4 shows that there is no significant distinction between the AHRR of all blends at CR 7:1. However, with the increase of CR, there is a noticeable difference in the heat release rates among the LPG blends particularly at CR 10:1 (Figure 4.4d). The AHRR of the EU Rep. and the HD-5 blends are noticeably higher than those of the US Rep. and chemically pure propane blends at this CR. The presence of the more reactive n-butane in the EU Rep. blend and propylene in the HD-5 blend [10] is responsible for these trends. Pure propane has the lowest AHRR among all blends. While

the trends are similar to Figure 4.4 in terms of LPG blend order for the load sweep in Figure 4.5, the magnitudes of the AHRR are much higher compared to the CR sweep AHRR. Also, on closer inspection of Figures 4.4 and 4.5, there is a diminished reducing effect of increasing load on duration of heat release compared to the CR case.

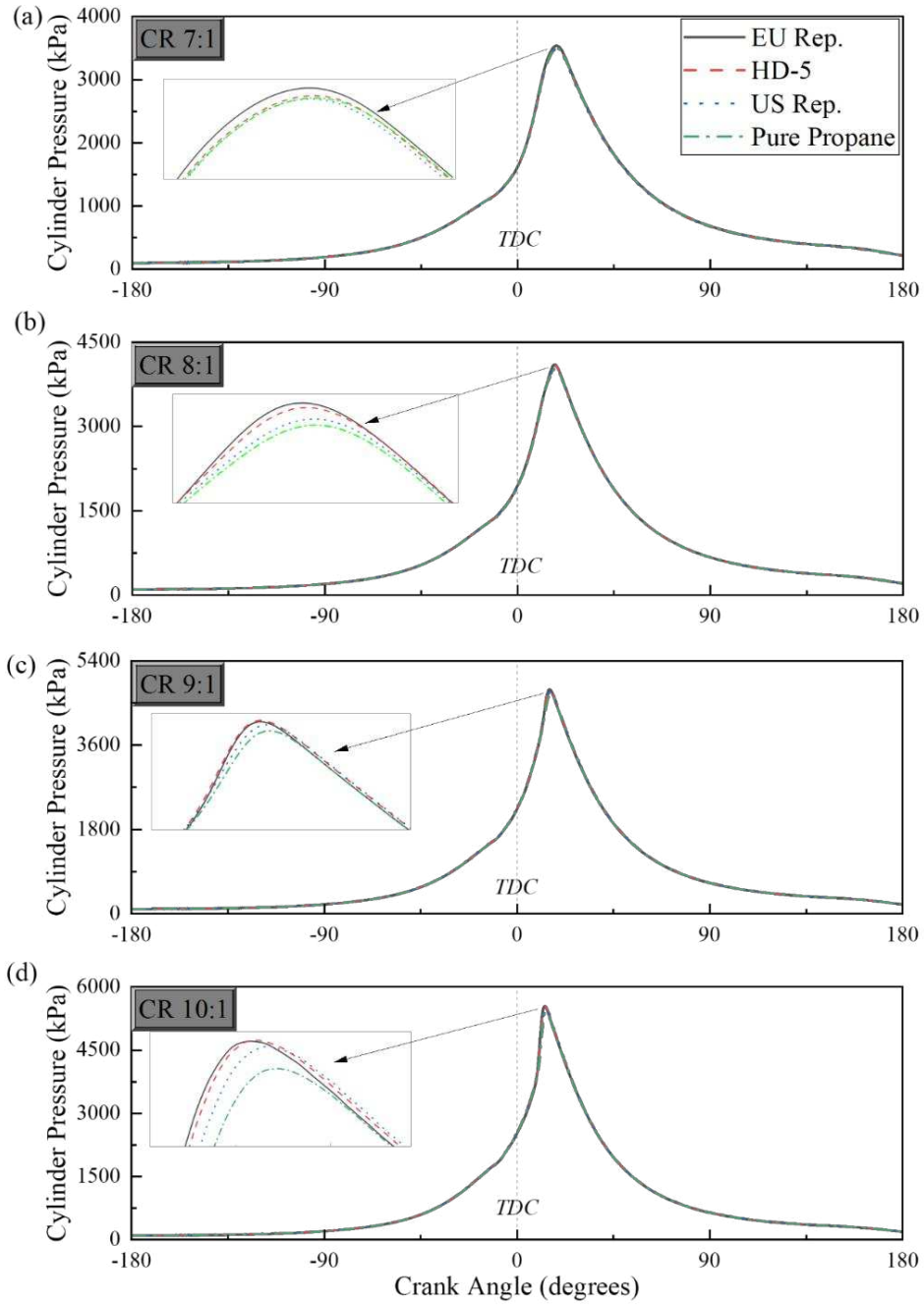

Figure 4.2. In-cylinder pressure traces for all blends at CR (a). 7:1, (b). 8:1, (c). 9:1 and (d). 10:1 for engine operating conditions: 900RPM, φ = 1, CA50~9.5 deg ATDC and coolant temperature = 95 deg C.

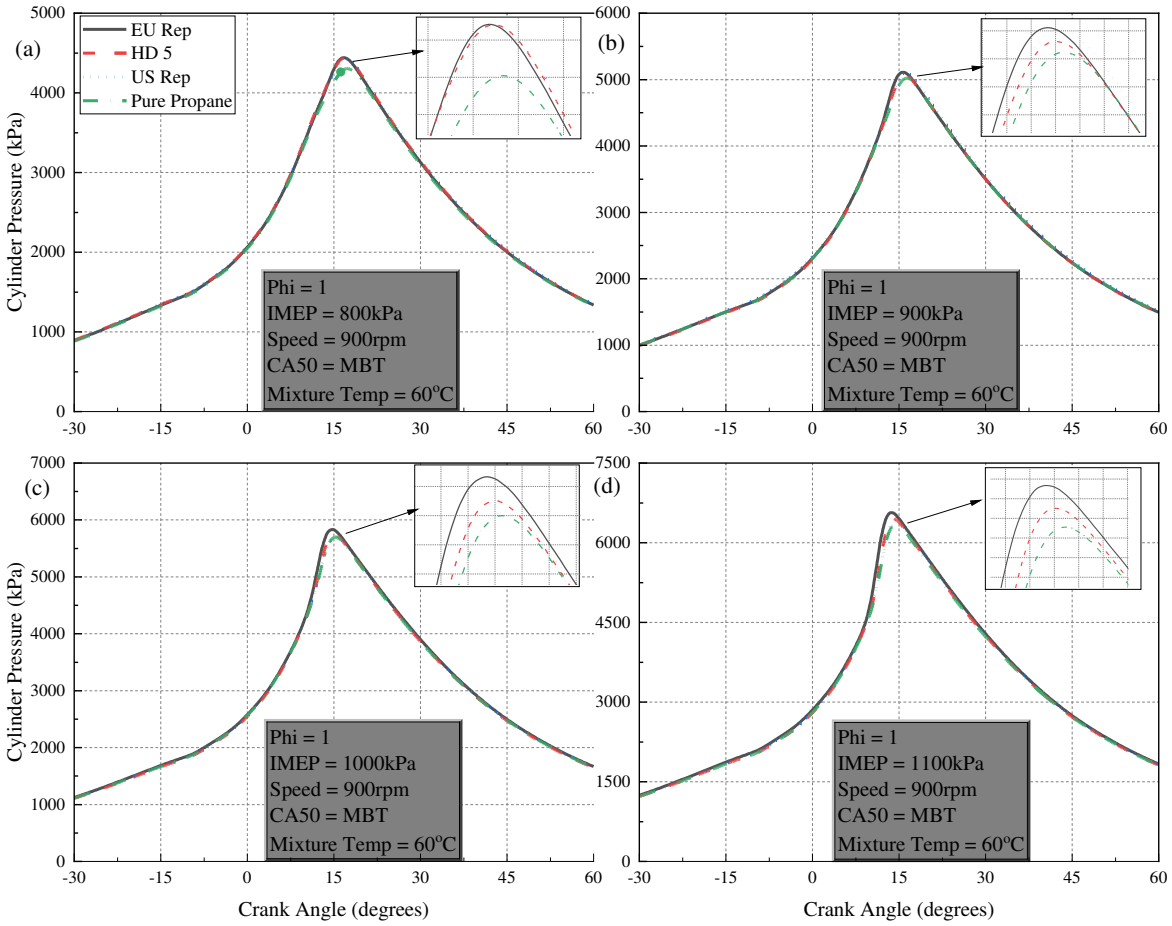

Figure 4.3. In-cylinder pressure traces for all blends at (a). 800kPa (b). 900kPa, (c). 1000kPa and (d). 1100kPa

EGR was introduced into the engine and swept from 0 to 35%, the in-cylinder pressure traces and AHRR for all the LPG blends at 0 and 25% are presented in Figure 4.6. As has been discussed earlier in this chapter, the blends demonstrated a meagre difference in terms of in-cylinder pressures and AHRR at 0% EGR with the EU Rep. and HD-5 indicating slightly higher values in Figure 4.6a. As EGR was introduced up until the 25% point in Figure 4.6b, the already slight differences grew began to disappear as heat release durations grew longer and the rate of pressure rise became gentler, albeit with similar peak AHRR and peak in-cylinder pressures to the 0% case.

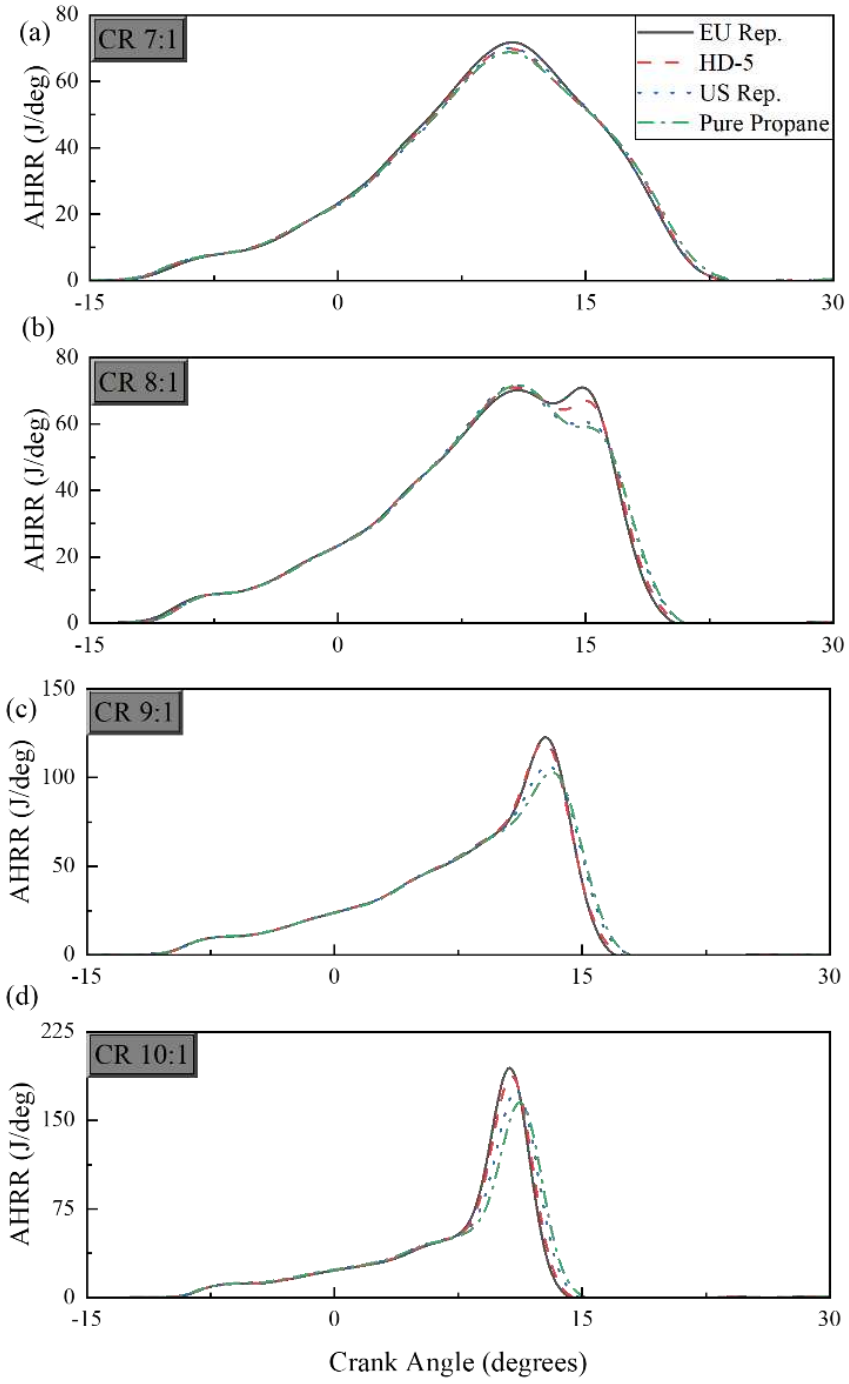

Figure 4.4. Apparent heat release rates (AHRR) for all blends at CR (a). 7:1, (b). 8:1, (c). 9:1 and (d) 10:1

Figures 4.7a and 4.7b show the combustion duration for the CR sweep in terms of 10-90% and 0-10% mass fraction burned (MFB) respectively while Figures 4.7c and 4.7d show the combustion duration for the load sweep in terms of 0-10% and 10-90% MFB respectively. From the figures

fuel composition plays a significant effect on engine combustion. Figure 4.7a and 4.7d shows that the rapid-burning time (i.e., crank angle duration for 10-90% MFB) follows the order, chemically pure propane > US Rep. > HD-5 > EU Rep., where chemically pure propane had the slowest burn duration and EU representative blend exhibited the fastest burn. This trend is influenced by the chemistry of the blends and combustion conditions. As earlier discussed, the more reactive compounds such as n-butane and propylene play a key role in the faster combustion times. Likewise, as CR is swept from 7:1 to 10:1, the 10-90% MFB duration reduces as flame propagation is increased with higher temperatures. This trend was also noticed in Figure 4.7d as the load was increased from 800kPa to 1100kPa, but to a lesser degree. The occurrence of end gas auto-ignition at higher CR and loads also plays an important role in the faster burn. Flame development time or ignition delay is generally defined as the crank angle duration from spark discharge to 10% MFB for SI engines. In contrast to rapid burning times, flame development time is almost constant across all blends at each CR and load (Figure 4.7b and 4.7c). However, there is a downward trend for 0-10% MFB duration with increasing CR exhibited in Figure 4.7b which is most likely governed by increasing in-cylinder temperatures.

Combustion durations trends are also shown for the EGR sweep in Figure 4.8. As EGR amounts are increased, the 0-10% and 10-90% MFB plots for all the blends almost exhibit a parabolic rise in durations. This is as a consequence of increased dilution of the in-cylinder charge which reduces in-cylinder temperatures, slows chemical reaction rate [31] and limits flame propagation causing slower and slower burns and even misfires in the extreme. Generally, the order described earlier for rapid-burn times (10-90% MFB) holds true, where chemically pure propane (slowest) > US Rep. > HD-5 > EU Rep. (fastest). However, this order is lost as combustion starts to transition from slow burn into partial burn and misfires at EGR rates greater than 25%.

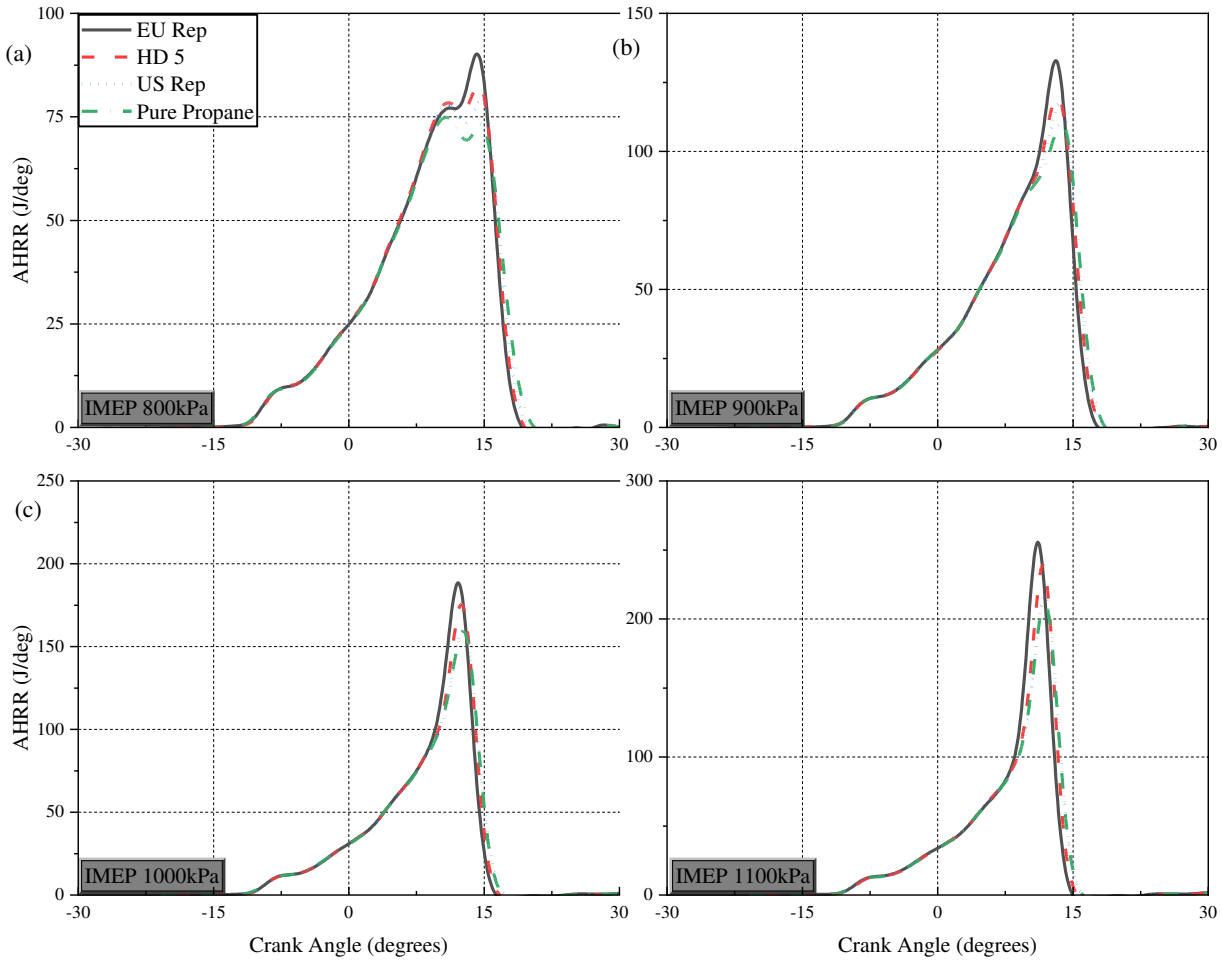

Figure 4.5. AHRR for all blends at (a). 800kPa, (b). 900kPa, (c). 1000kPa and (d) 1100kPa

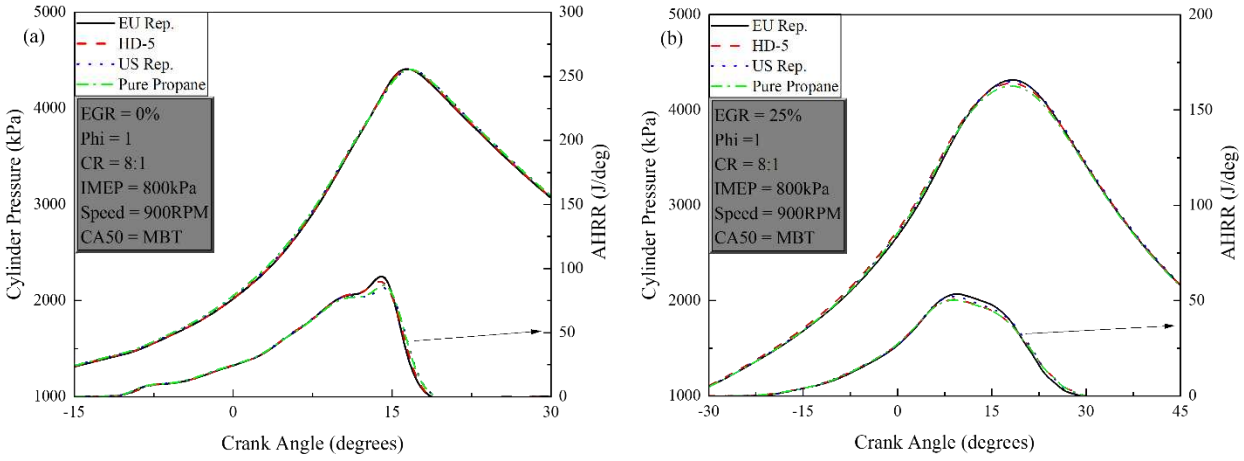

Figure 4.6. In-cylinder pressures and AHRR for all tested blends at (a) 0 and (b) 25%, EGR

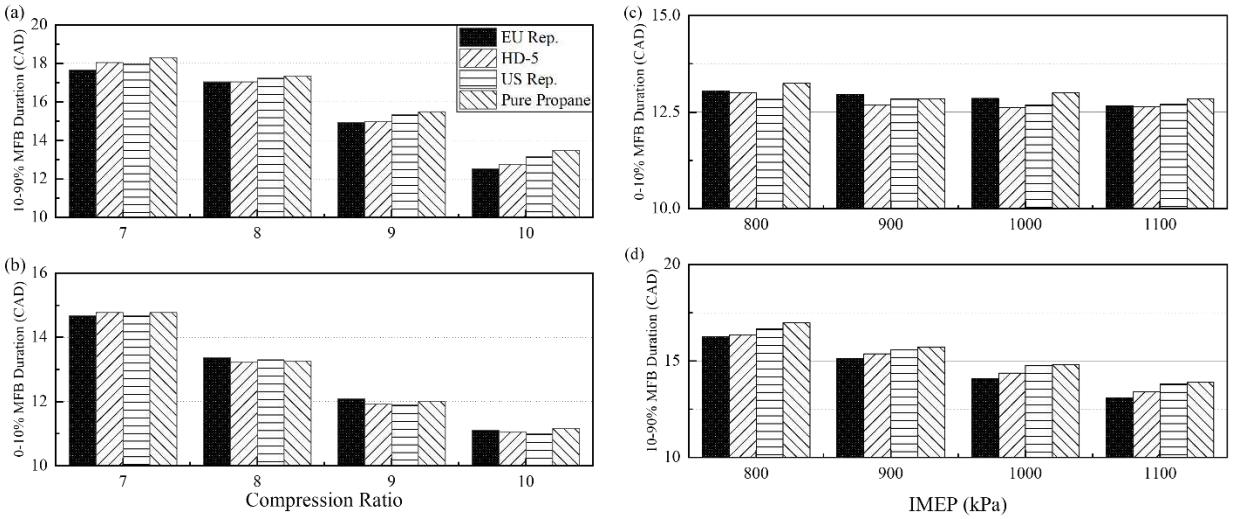

Figure 4.7. (a) 10-90% MFB duration for CR sweep (b) 0-10% MFB duration for CR sweep (c) 0-10% MFB duration for load sweep (d) 10-90% MFB duration for load sweep, for all blends on the CFR engine

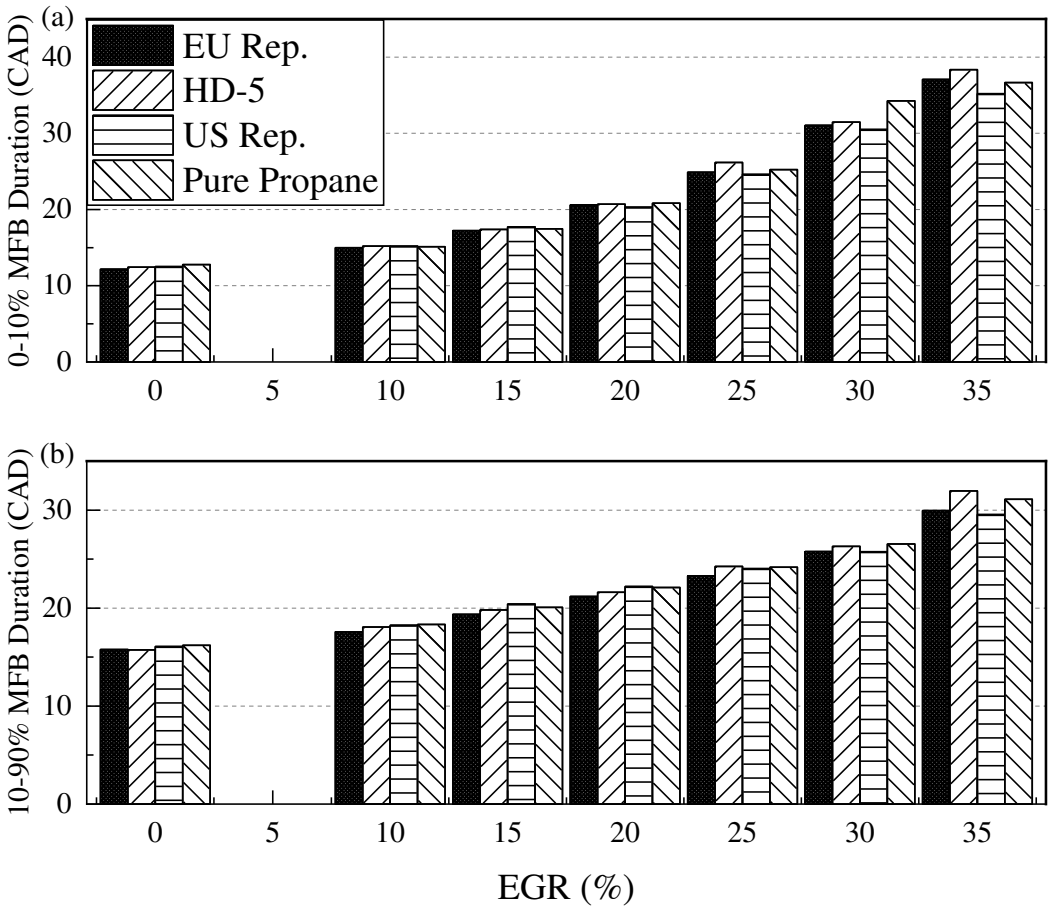

Figure 4.8. Blend (a) 0-10% MFB duration (b) 10-90% MFB duration, for the EGR sweep

Finally, the combustion subsection concludes with some discussion on knock, knocking intensities and knock occurrence location. In this work, a trace knock point $KI_{limit} \sim 5kPa^2$ was defined above which audible incipient knock began on the engine. In Figure 4.9a and b, at CR 7:1, KI for all the blends was below KI_{limit} and there was normal combustion. As CR was increased to 8:1, trace amounts of knock were noticed, particularly with HD-5 and EU Rep. As the CR increased to 9:1, the intensity of knock increased exponentially, and the fuel composition effect became more pronounced. The US Rep. blend and chemically pure propane also began to knock along with the other two blends. The ordering of the knock integral values among the blends was consistent with the reactivity of the components in the blends where n-butane > propylene > propane > ethane. Generally, increasing the length of the paraffin increases the knocking tendency of a hydrocarbon. However, propylene is an exception to the general rule of olefins as it knocks more readily than its corresponding paraffin, propane [10]. These effects coupled with the increased CR at 10:1 induced heavy knock and showed the most significant difference in KI observed among the blends in this work. The KI for the US Rep. and the chemically pure propane blends were considerably lower than that of the EU Rep. blend at CR 10:1. Similar trends were observed as engine load was increased from 800kPa to the engine limit at 1100kPa albeit with slightly reduced intensities and with all blends exhibiting some level of trace-light knock at 800kPa.

As knock intensities were more pronounced over the CR sweep, further analyses were conducted using Equation 14 and 15 to determine the relative location of knock occurrence between the blends. Figure 4.10 indicates that knock is occurring later (in CAD) for the chemically pure propane and then the US Rep. blend compared to the HD-5 and EU representative blends. The differences between blends become more apparent as the CR and the intensity of knock increases.

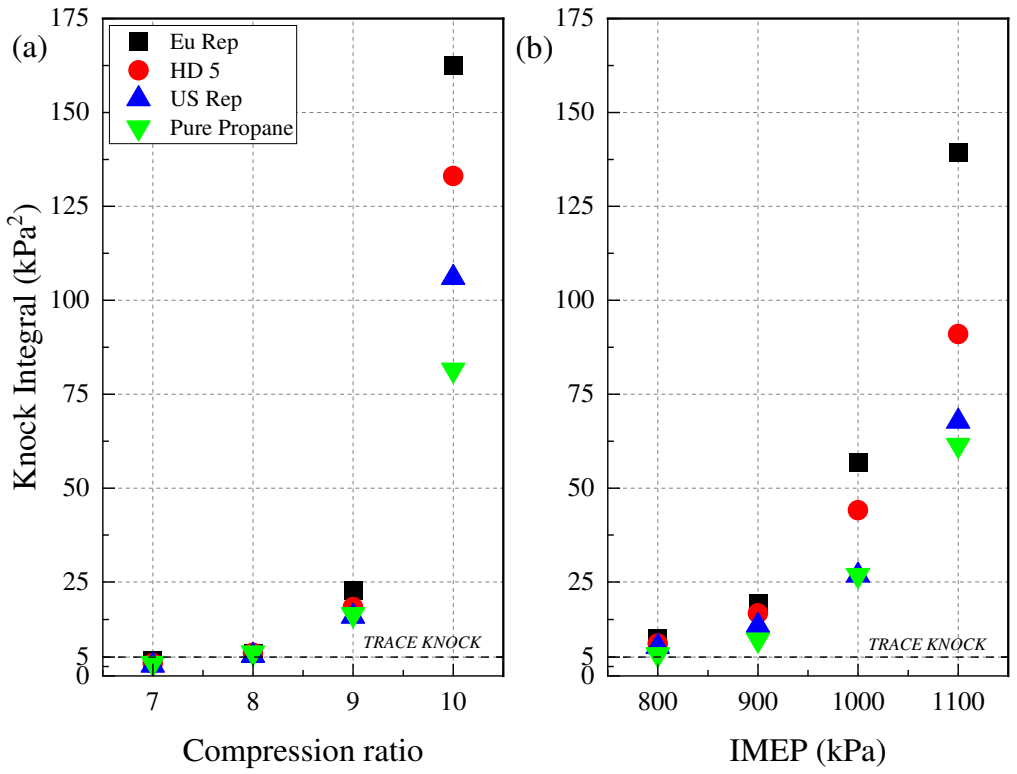

Figure 4.9: Plots of Knock Integral for all blends over the tested (a) Compression ratio (b) IMEP

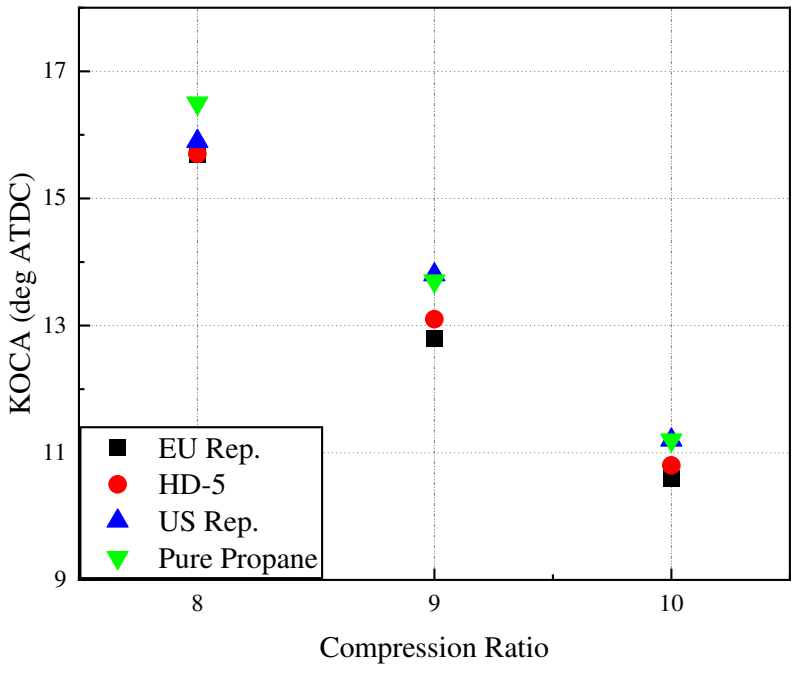

Figure 4.10. Knock Occurrence Crank Angle (KOCA), for all blends over the range of applicable CR

EGR had been shown to mitigate knock in Chapter 3 and in the literature [10, 24, 31], so it was considered for this study to determine if there were LPG composition effects on its mitigation properties. Figure 4.11a demonstrates this mitigation effect as the engine was transitioned from varying levels of trace-light knock for all the blends to non-knocking combustion by 10% EGR rate. To properly demonstrate the mitigation potential, the compression ratio was increased to 9:1 shown in Figure 4.11b and consequently the engine transitioned into medium knock for all blends with EU Rep. exhibiting the strongest knock intensities. Encouragingly, as EGR was introduced up to the 20% mark, the US Rep and Pure Propane had transitioned into non-knocking combustion while the HD-5 and EU Rep. were barely exhibiting trace knock which was then completely dissipated by the 30% mark. This points to a potential for greater knock mitigation levels with lesser knock resistant fuels like the EU Rep. and HD-5 blends. The KI began to trend upwards again after the minimum at 30% believed to be as a result of the unstable combustion and misfire at those extremely diluted high CR conditions.

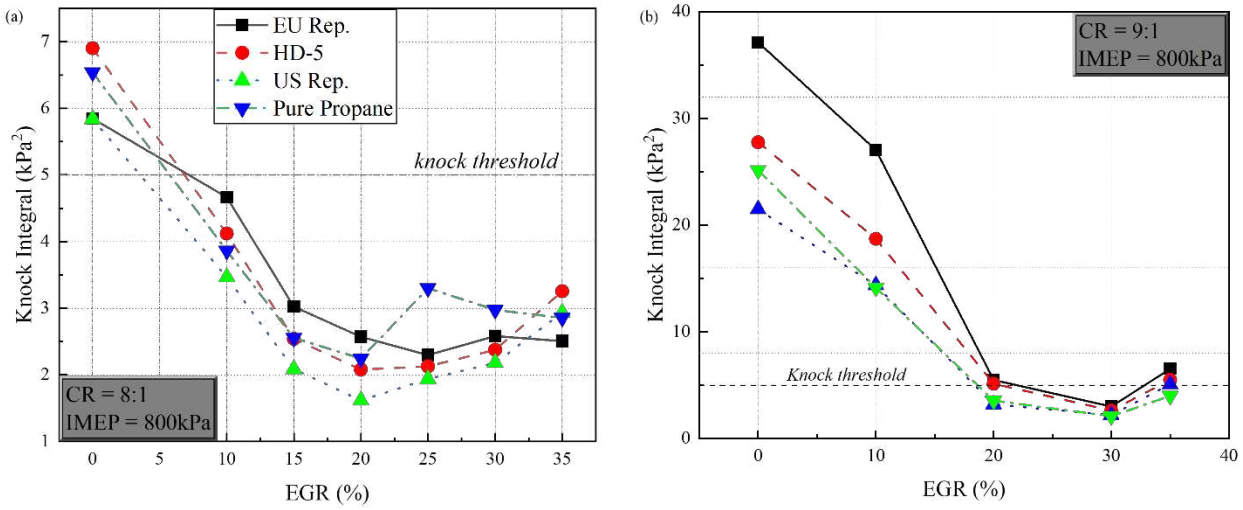

Figure 4.11. Knock intensity trends with increasing EGR rates for all blends at (a) 8:1 and (b) 9:1

4.3.2 Emission Characteristics

Figures 4.12, 4.13, and 4.14 show several engine-out emissions normalized by brake power for all the LPG blends over the CR, load and EGR sweeps. Several distinguishable trends are observed related to the chemistry of the fuel and their varying compositions.

Figure 4.12a shows brake specific oxides of nitrogen (bsNOx) emissions for the LPG blends over the tested CR range. From literature, NOx chemistry is governed primarily by the post combustion local in-cylinder temperatures and its emission increases with increased peak temperature. However, the expected increase in NOx due to higher peak temperature associated with increasing CR is less obvious in Figure 4.12a. This is likely due to the normalization with brake power which also increases with CR. In terms of LPG blend influence, the HD-5 blend produced the lowest average bsNOx over the CR range while the US Rep. blend exhibited the highest averaged value. Figure 4.12b shows the brake specific non-methane hydrocarbons (bsNMHC) over the range of CR for all LPG blends. NMHC are an important class of regulated emission compounds for SI LPG engines due to their reactivity on introduction to the atmosphere. The normalized NMHC emissions increased with increasing CR, which is likely due to the crevice volume filling [10]. As the CR increases, in-cylinder pressure also increases, which pushes more gases in the crevice volume compared to those at lower CR. A small variation in NMHC across the LPG blends may likely be linked to the presence of lower hydrocarbons relative to propane in the fuel composition. For example, the US Rep. blend, with 6.5vol% of ethane and the slightly higher H:C ratio shown in Table 4.1, had the lowest bsNMHC emission on average over the tested CR range. The combined effect of CR and fuel composition was also visible at CR 10:1 where EU Rep., the blend with the lowest H:C ratio, indicated the highest amount of normalized NMHC due to the significant presence of higher alkanes relative to propane (18.1mol% n-Butane), along with the increased

crevice volume filling effect. Conversely, the bsTHC and bsNOx presented in Figures 4.13a and 4.13b respectively did not indicate any significant sensitivity to engine load. A possible explanation for the bsTHC trend may be that the increase in HC with engine load documented in the literature [74] due to the increase in crevice volume filling with the now higher in-cylinder pressures was balanced by a higher oxidation rate of this crevice HC on reintroduction into the cylinder at the higher temperatures associated with the higher loads [79]. In terms of NOx however, the HD-5 blend still produced the lowest average bsNOx over the load range as was observed for the CR sweep in Figure 4.12a.

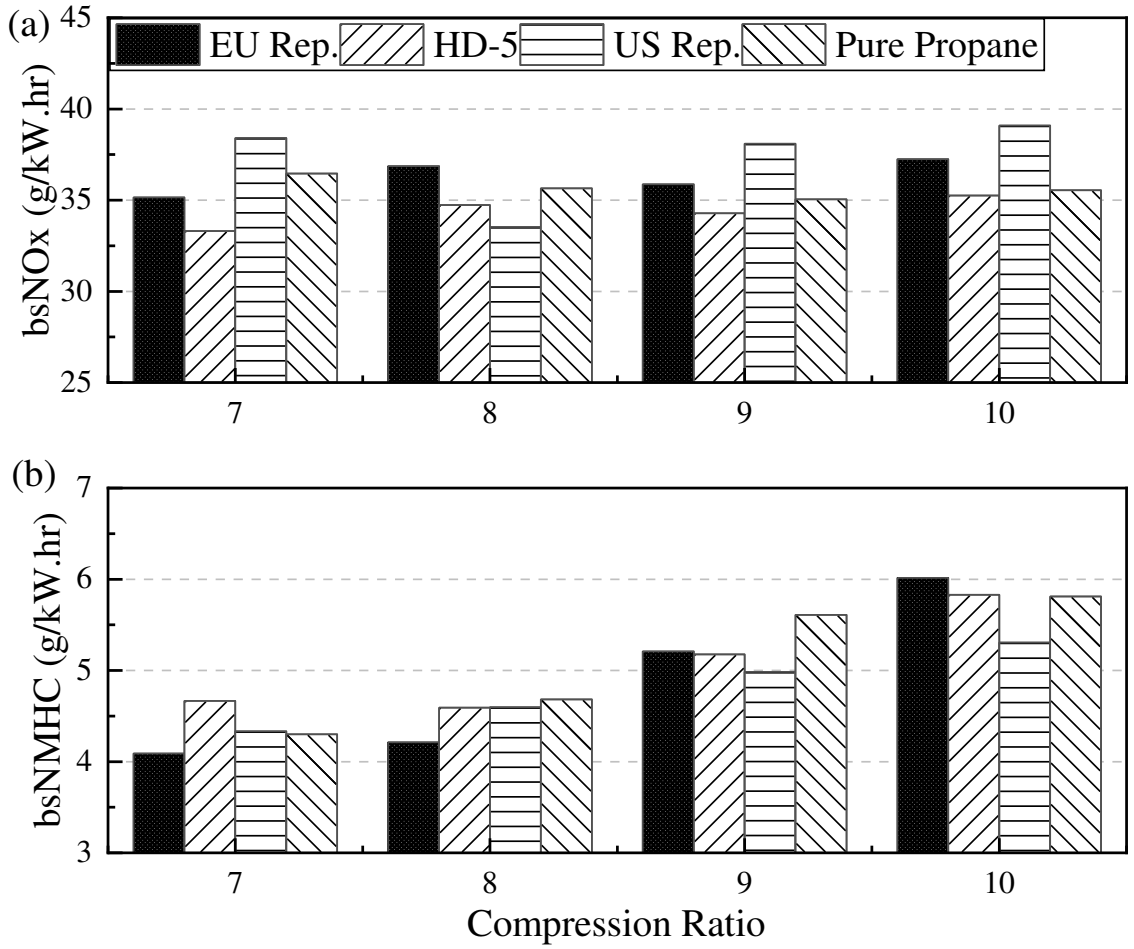

Figure 4.12. Brake specific engine out emissions: (a) NOx, (b) non-methane hydrocarbons (NMHC), for all LPG blends over the CR range at engine operating conditions: 900RPM, φ = 1, CA50~MBT.

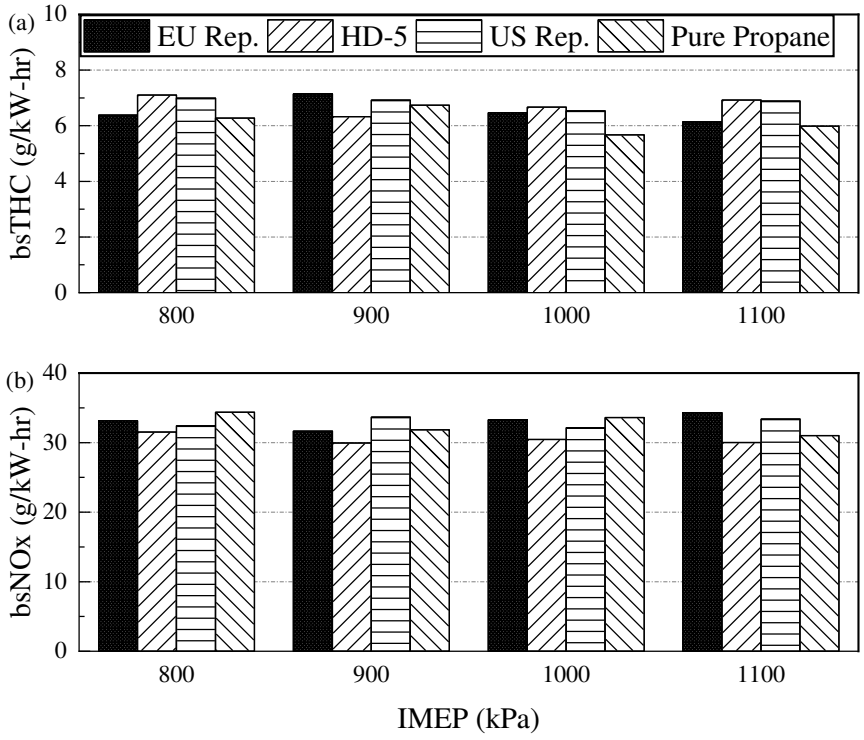

Figure 4.13. Brake specific engine out emissions: (a) THC (b) NOx, for all LPG blends at all tested loads

In Figure 4.14a, the bsNOx and bsTHC values are plotted as EGR was swept for all blends at CR 8:1 and 800kPa IMEP. The introduction of EGR had a mitigating effect on NOx and no demonstrable effect on THC up until an inflection point as previously identified in Chapter 3. Between 25 and 30% EGR rates, bsTHC indicated a sharp rise due to incomplete combustion caused by partial burn and misfire while bsNOx continued to trend downwards creating a trade-off scenario where even lower NOx emissions could be achieved, but at the expense of HC emissions. Among the blends, the bsTHC emissions were not too dissimilar, however, there was a blend effect on the bsNOx emissions with US Rep. producing the least NOx emissions at almost all conditions. Finally, the bsCO_2eq emissions introduced in section 3.3.2 are presented in Figure 4.14b for all the LPG blends over the tested EGR range. There was some blend effect on these GHG emissions as EU Rep. which had the lowest H:C ratio as a result of its significant higher-

alkane composition (shown in Table 4.1) generated the highest bsCO2eq emissions at every EGR rate. Conversely, the US Rep. blend which had the highest H:C ratio of 2.68 generated the lowest bsCO2eq emissions at all EGR rates except at 30% EGR which was a highly unstable engine operation condition. At non-EGR conditions (0% EGR) there was a much as a 4% difference in the GHG emissions between the EU Rep. and US Rep. blends.

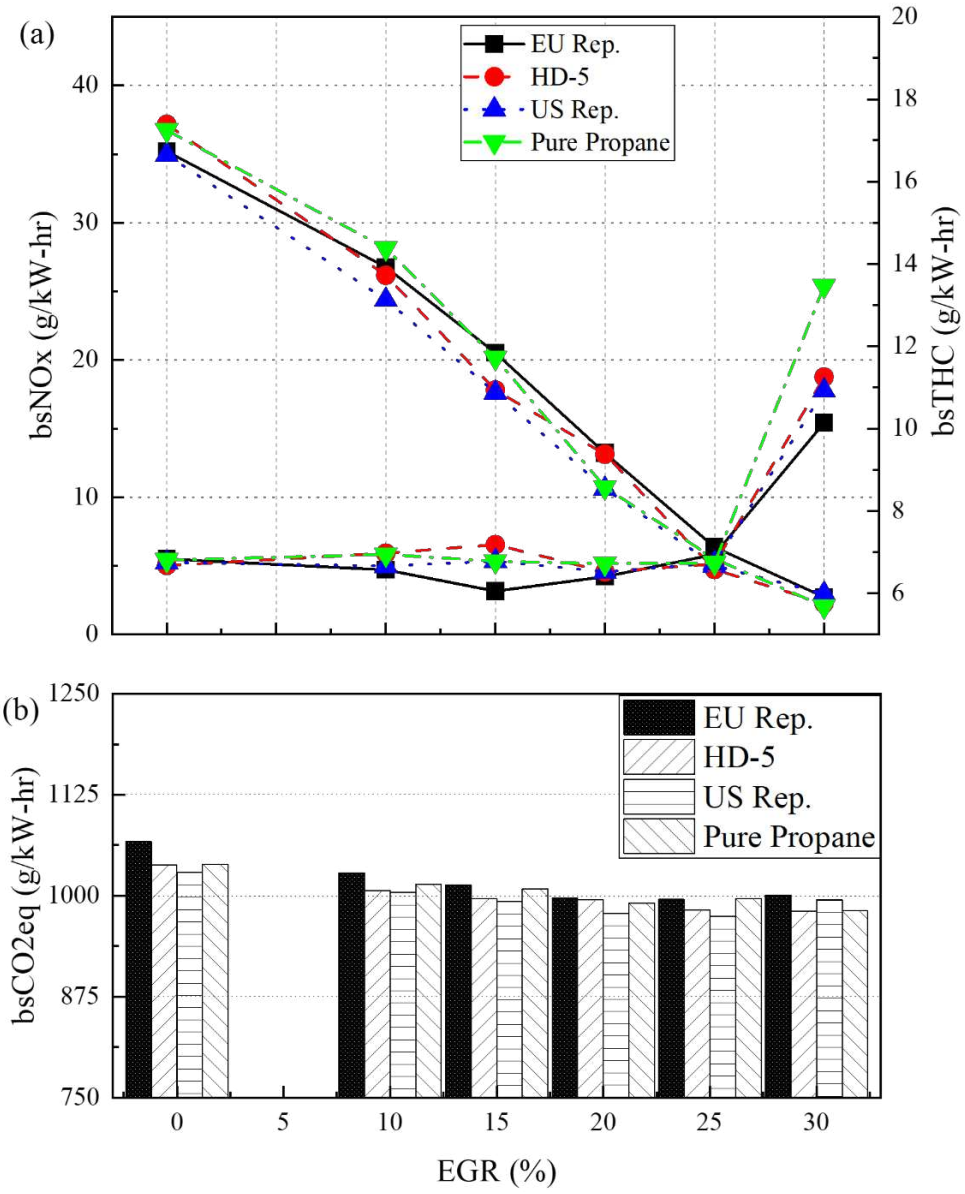

Figure 4.14: Variation of (a) bsNOx and THC (b) bsCO_2eq, at CR 8:1, IMEP 800kPa and for all blends, for the range of tested EGR rates.

4.3.3 Performance Characteristics

Figure 4.15 shows the brake power over the range of compression ratios and engine loads for the tested LPG blends. As shown, the differences in brake power between the blends are minimal especially for the load sweep in 4.15b. A similar trend was observed for both load and CR variations in a previous study that considered only propane and n-butane in the LPG fuel compositions [9]. In 4.15a, the differences are slightly more pronounced with the HD-5 and EU Rep. (at CR 7:1) producing marginally higher brake powers at all CR. As expected, brake power increased with compression ratio and load while the latter demonstrated a steeper rise in brake power over the tested range compared to compression ratio.

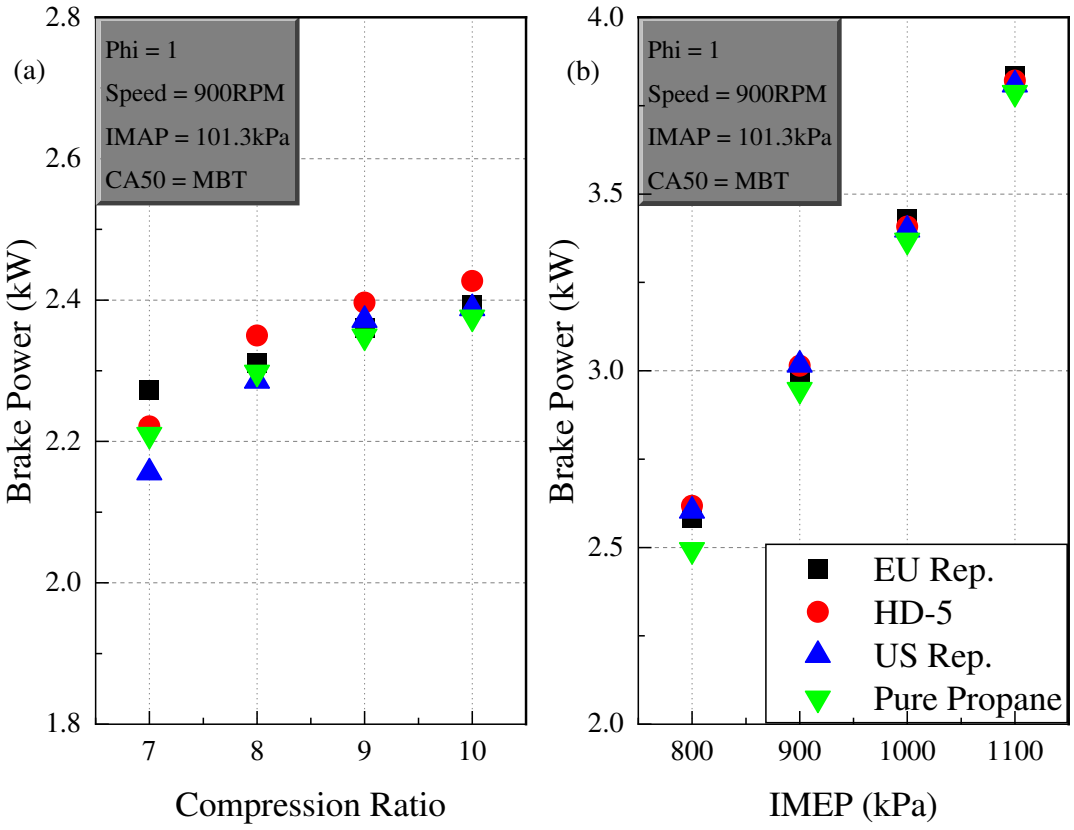

Figure 4.15. Brake power for all LPG blends over the range of tested (a) CR (b) Engine loads

Figure 4.16a and 4.16b show the brake thermal efficiency (BTE) for all tested LPG blends for the CR and load variations. Despite the stronger effect of load on brake power discussed earlier, both engine parameters (CR and load) had approximately equal effects on BTE. The BTE increased with increasing CR from an average of ~20.2% at CR 7:1 to ~22.3% at CR 10:1, which was likely due to improved cycle efficiency and reduced burn duration at higher CR illustrated in section 4.3.1. For the load sweep, BTE was increased from an average of ~22.1% at 800kPa to 24.4% at 1100kPa for all blends. This increasing BTE trend with increasing load was as a result of higher fuel quantity required to maintain stoichiometric conditions at the higher intake manifold pressures, in agreement with results shown by Kumar et al. [79]. Similar to the brake power, fuel composition exhibited a minimal effect on BTE for a given load and demonstrated a more recognizable yet still minimal effect on BTE for a given compression ratio. The brake power and BTE trend can be attributed to the combined effect of a fuel's energy density and flame speed at a given engine operating condition. The laminar flame speeds (LFS) of the blends were calculated using the NUIG 1.1 high temperature mechanism in CHEMKIN [80] at standard temperature and pressure. The energy density was calculated using the blend properties in Table 4.1 and the measured fuel mass during stoichiometric engine operation at CR 7:1. Despite the difference in the composition of LPG blends, there was no distinct difference in the calculated laminar flame speed and energy density values among the LPG blends (as presented earlier in Table 4.1). This is likely responsible for the similar fuel efficiency trends shown in Figure 4.16.

Finally, the BTE and COV of peak pressure for all the blends at CR 8:1 and 800kPa engine load are presented in Figure 4.17. Firstly, the EGR limit is defined as the EGR% at a threshold $COV_{peak\ pressure}$ of 10%. All the tested blends indicated similar trends and demonstrated an EGR limit between 26 and 27%. After this point combustion became unstable and misfire was more likely to

happen as the mixture became too diluted and heat release and combustion durations, discussed in section 4.3.1, became longer to the detriment of engine stability and efficiency. This engine instability possibly explains the spike in bsTHC shown in Figure 4.14a earlier. Secondly, the BTE values are also plotted in Figure 4.17. As EGR was introduced, the blend efficiencies started to converge, which indicated that there was also no significant fuel composition effect on performance with EGR. Maximum efficiencies were observed for all blends between 20 and 25% EGR rate with the HD-5 and US Rep. blends both achieving an overall maximum BTE of 23.2% among all the blends. Thirdly, all the tested LPG blends experienced a sharp drop in BTE beyond 30% EGR as a sizeable portion of the charge was not being combusted in the cylinder as shown in the bsTHC values in Figure 4.14a. In conclusion, these EGR results indicate that there is a window before and after the determined EGR limit where engine operation may be most beneficial in terms of BTE, but considering the bsTHC-bsNOx emissions trade-off, knock mitigation requirements and hardware limitations, an optimal EGR rate may exist just before this EGR limit.

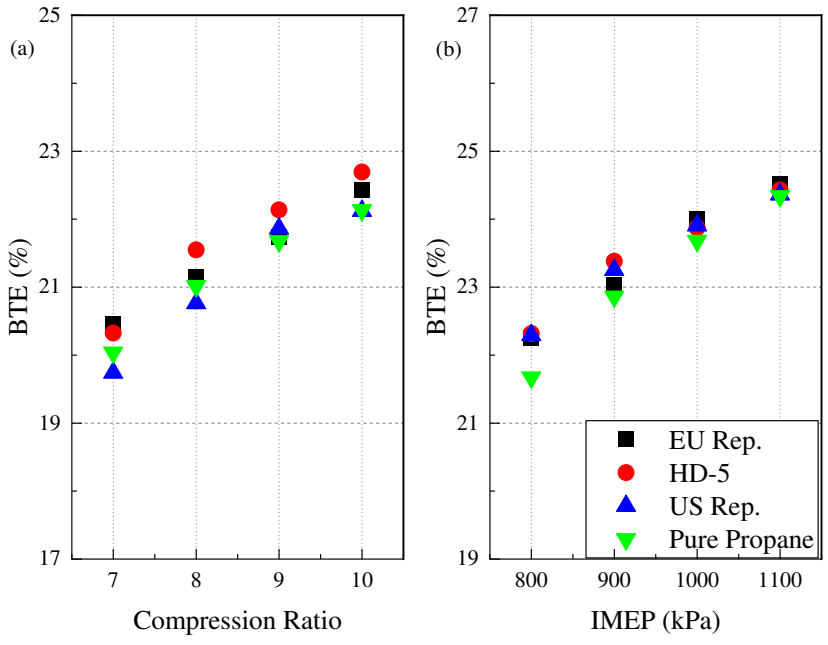

Figure 4.16. BTE for all LPG blends over the range of tested (a) CR (b) Engine loads

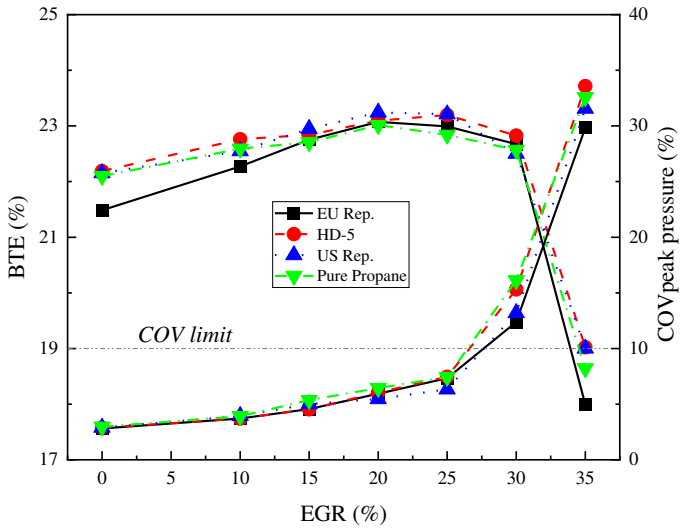

Figure 4.17: BTE and $COV_{peak\ pressure}$ (%) vs EGR (%) at CR 8:1, IMEP 800kPa and for all tested blends

4.4 Conclusions

This chapter concludes experiments conducted on the single cylinder CFR engine. The experiments involved varying key engine parameters such as the compression ratio, engine load and EGR for representative LPG blends. The experimental results showed that:

The BTE of the CFR engine increased as CR, load, and EGR was increased, with minimal difference between the BTE of the blends at any given CR, load, and EGR rate. However, there were notable fuel composition effects on brake specific emissions. The HD-5 blend exhibited the lowest amounts of brake specific NOx emissions while the US Rep. blend had the lowest average brake specific emissions for bsNMHC averaged over the CR range. The HD-5 blend also produced the lowest average bsNOx over the load range. With EGR, the US Rep. blend generated the lowest GHG emissions in terms of $bsCO_2eq$ amongst the blends, achieving a 4% relatively lower $bsCO_2eq$ value than the EU Rep. blend at 0% EGR.

The most visible fuel composition effect was observed in their combustion characteristics. In-cylinder pressure and AHRR were similar across blends at CR 7:1. As CR and load were increased,

observed peak pressure and AHRR trends for the tested LPG blends were: $P_{EU\ rep} > P_{HD\text{-}5} > P_{US\ rep} > P_{pure\ propane}$ and $AHRR_{EU\ rep} > AHRR_{HD\text{-}5} > AHRR_{US\ rep} > AHRR_{pure\ propane,}$ respectively. The rapid burn combustion duration showed the same trend as $\theta_{EU\ rep} > \theta_{HD\text{-}5} > \theta_{US\ rep} > \theta_{pure\ propane}$ in order of increasing duration. Flame development time remained roughly constant for all blends while increasing the CR and load reduced the rapid burn time for all blends. The described order for rapid-burn times (10-90% MFB) was observed with EGR same as with CR and load, however, as EGR rates were increased beyond 25% and as combustion quality degraded from partial burn to misfires, this order was lost.

The order of reactivity for the tested LPG blends as a result of their variable composition was found to be EU Rep. > HD-5 > US Rep. > Pure Propane. The EU Rep. and HD-5 blends showed knock propensities much higher than the US Rep. and chemically pure propane, which was further increased at higher CR and loads. For resistance to knock, the results indicated the trend as Pure Propane > US Rep. > HD-5 > EU Rep. As a result of their lesser resistance to knock, the EU Rep and HD-5 blends demonstrated higher need for EGR knock mitigation at CR 9:1 and EGR was shown to adequately transition the engine operation on these two fuels from medium knock to incipient knock to non-knocking combustion within their EGR limits.

The findings suggest that variable blend composition is not a significant determinant of engine performance. The results showed that perhaps the most critical consideration when considering LPG blend composition would likely be the varying levels of knock intensity and how to design controls to accommodate this effect. This minimal effect of blend composition on performance informed the selection of the liquid LPG source for the remainder of the research work on the heavy-duty engine. This chapter provides some clarity on research questions 1 and 4.

CHAPTER 5. EXPERIMENTAL INVESTIGATION OF THE COMBUSTION, EMISSIONS, AND PERFORMANCE CHARACTERISTICS OF A HEAVY-DUTY LPG ENGINE USING DIRECT AND PORT-FUEL INJECTION STRATEGIES[5]

5.1 Overview

The preceding two chapters have focused on developing an understanding of the combustion, emissions and performance of LPG in response to certain important variables including compression ratio, fuel composition, EGR, and the CIM. The results from these chapters were employed in developing and validating computational models while operating the engine with to load, knock and EGR limits provided an appreciation for the possible constraints and limits that would be encountered in designing the required hardware for the next phase of the research. The next phase of the research was conducted on the heavy-duty engine which was run at 1200RPM for the best torque performance. This chapter is focused on the set-up and initial operation of the heavy-duty Cummins X15 engine on LPG using the designed fuel delivery systems discussed in section 2.3.

The literature highlights the popularity of engine studies conducted with manifold or port injected LPG in light and medium duty applications, due in part to their simplicity and mixing benefits [35, 37, 38, 81, 82] with obvious gaps however in heavy-duty studies. Similarly, the direct injection of LPG, especially in the liquid phase, represents huge potential and evokes a different set of challenges but has been studied but to an even lesser degree, especially in heavy-duty applications.

[5] Chapter 5 extracted from a manuscript submitted for journal publication and a published manuscript
- Fosudo, T., Windom B., Olsen D. Experimental Evaluation of Direct and Port-Fuel Injection Strategies on a Heavy-Duty LPG Engine. 2024.
[60] Fosudo, T., Kar, T., Windom, B., Schlagel, J. et al. (2023). Performance, Combustion and Emissions Evaluation of Liquid Phase Port-Injected LPG on a Single Cylinder Heavy-Duty Spark Ignited Engine. SAE Technical Paper 2023-01-0245.
doi:10.4271/2023-01- 0245

For example, the direct injection of LPG presents strategic advantages especially in terms of reducing short-circuiting losses, increasing volumetric efficiency [83] and atomization mixing, and more research is needed into its application and hardware design for heavy-duty engines. This chapter is based on a research article that addresses that need and presents the operation of a heavy-duty LPG engine on liquid PFI and DI.

This experimental study begins with the use of an off-the-shelf port fuel injector currently in use on an LPG engine on the market, the Roush Cleantech Ford 6.8L-V10, then, it describes the engine operation with a Delphi gasoline direct injector modified for use on this heavy-duty platform [56]. The influence of injection strategy at different start of injection timings, equivalence ratios, combustion phasing, and engine load conditions were studied. The chapter presents the combustion, emissions and performance characteristics for the different engine and injection configurations. The results indicated consistent liquid LPG injection with the designed fueling system, excellent control of the air-fuel ratio and the combustion in the engine, an optimal combustion phasing for engine operation on liquid LPG, and the potential for increasing the brake thermal efficiency while reducing fuel consumption and emissions.

The chapter is extracted from a journal article submitted to the SAE Journal of Engines and a technical conference proceeding [60] presented at the SAE World Congress Experience (WCX) and begins with a quick overview. A brief section on the experimental methods and test matrices particular to the chapter follows, before a discussion of the results and a short conclusion brings the chapter to an end.

5.2 Experimental Methods

The key components used for this study were the single cylinder heavy-duty research engine, injectors, and baseline 9.3:1 piston described in detail in Section 2.2 and the LPG fuel delivery systems described in Section 2.3. The preliminary set of tests for this study was the baseline evaluation which commenced with the start of injection (SOI) tests. These tests were done to evaluate the effect of closed (after IVC) and open valve (after IVO) port injection on performance, emissions, and combustion, and to select the optimal SOI for the rest of the baseline study. Afterwards, a spark timing sweep was carried out to establish the optimal combustion phasing, described as the MBT. Then, IMAP was increased from the naturally aspirated condition until a knock-limited load was achieved. Finally, the effect of equivalence ratio was explored from lean to rich engine operation regimes. The relative valve open and close locations and how they interact with the SOI tests are shown in Figure 5.1. It must be pointed out that the PFI configuration in this chapter was slightly upstream of the intake ports and an optimized PFI system with dual-injection and valve targeting shown also in Section 2.2.3 was designed to improve the port injection strategy for the final phase of this research.

The baseline study was built upon by running experiments with direct injected liquid LPG on the heavy-duty platform using the modified Delphi GDI. Liquid LPG was injected at 170bar, and the results compared with the PFI case (~16bar). Like the baseline evaluation, an SOI sweep was performed. Initial observations indicated that early SOI at 360 deg BTDC (EVC was 362 deg bTDC) and late SOI at 150 deg bTDC (IVC was 155 deg bTDC) could offer some insight into the competing effects of maximized mixing time without short-circuiting of fuel and maximized charge mass in the cylinder respectively. So, following the SOI tests an ignition timing sweep was done to determine the MBT in DI mode at both representative SOIs. A load sweep was then

conducted with CA50 held constant at 9 deg aTDC similar to the PFI case. Finally, equivalence ratio was swept on the heavy-duty spark ignited engine platform at both representative SOIs.

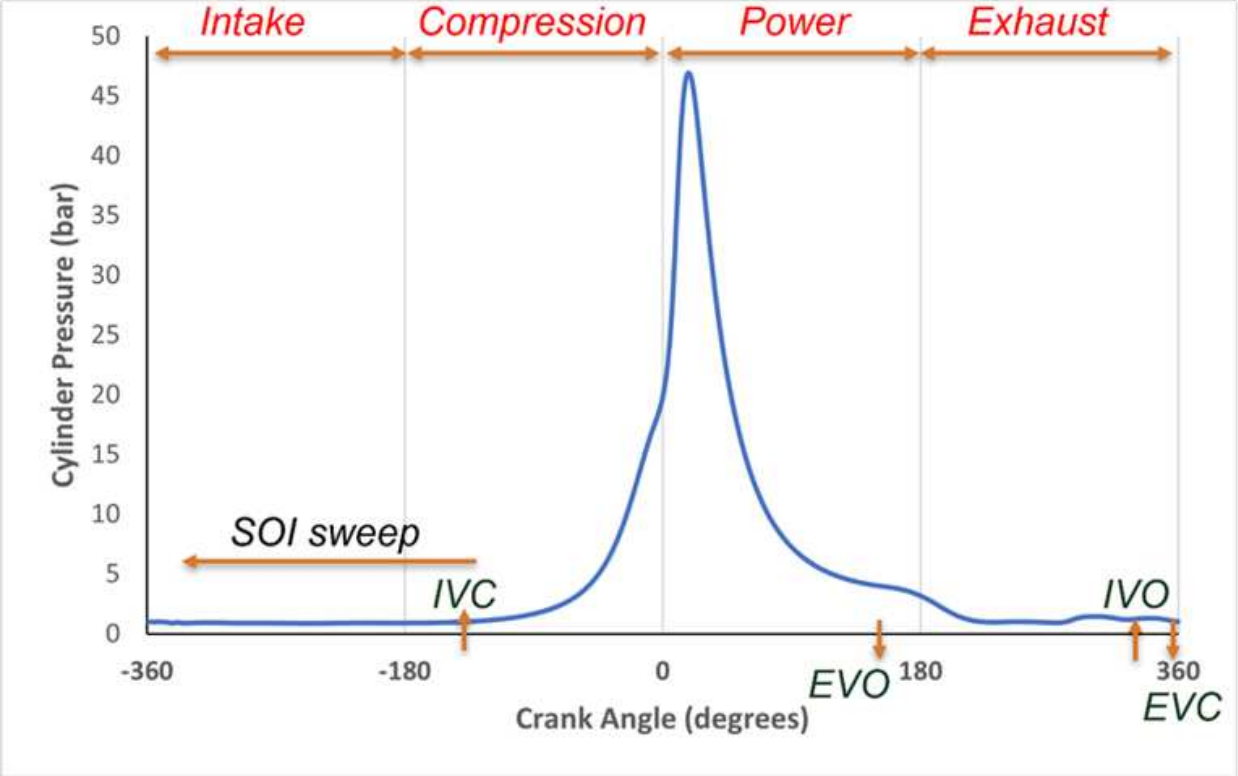

Figure 5.1. Representative in-cylinder pressure trace showing valve closing and opening locations

Considering the conclusions from Chapter 4 on the meagre effect of the LPG fuel composition on engine performance, LPG tanks were filled at a local gas station daily before the tests in this study and the composition of the fuel was measured using a gas chromatograph during engine operation. The composition was very constant across the test days and the average composition, and the fuel properties are shown in Table 5.1. The tested experimental conditions are also presented in Table 5.2.

Table 5.1. The LPG fuel properties

Composition (%vol)	
Propane	98.473
Ethane	0.95
I-butane	0.49
N-butane	0.07
Propylene	0.01
Nitrogen	0.007
Properties	
LHV (MJ/kg)	46.36
H:C ratio	2.67
Stoichiometric AFR	15.57
Density (kg/m3)	493

5.3 Results and Discussion

5.3.1 Performance Characteristics

The BTE and COVimep for the SOI tests are shown in Figure 5.2 below. First, we take a look at the COV for the baseline PFI case. The limit of COVimep was determined in this research to be 3%, below which combustion and engine operation can be said to be stable. All tested start of injection timings in the baseline evaluation were below this COV limit, indicating that PFI operation was insensitive to start of injection in terms of engine stability. This was likely a result of rapid atomization of the LPG causing sufficient mixing with the air entering the combustion chamber at both open and close valve timings. Similar results were shown by Lee et al. [84] for stoichiometric conditions. This behavior with SOI for the baseline PFI configuration was carried on to the BTE results as the thermal efficiencies were similar across all SOI timings. The reverse

was the case however for the DI configuration as there was a distinct relationship between the SOI and both the BTE and the COVimep. The engine was most stable and most efficient at the earliest SOI timing, 360 deg bTDC, believed to be a result of the maximized mixing time which promoted homogeneity of the charge in the combustion chamber and aided combustion completeness. Other research works have found this relationship with mixing and engine stability and efficiency to hold true with DI LPG [85].

Table 5.2. The test matrix

<table>
<tr><th>Operating Conditions</th><th>Compression Ratio</th><th>Start of Injection (deg bTDC)</th><th>Ignition Timing (deg bTDC)</th><th>Phi</th><th>IMAP (kPa)</th></tr>
<tr><td colspan="6">Port-Fuel Injection at ~1.6MPa</td></tr>
<tr><td>Start of Injection</td><td rowspan="4">9.3</td><td>120, 150, 330, 360</td><td>14*</td><td rowspan="2">1</td><td rowspan="3">100</td></tr>
<tr><td>Ignition Timing</td><td rowspan="3">120</td><td>6 - 24</td></tr>
<tr><td>Equivalence Ratio</td><td>MBT**</td><td>0.83 – 1.25</td></tr>
<tr><td>IMAP</td><td></td><td>1</td><td>100 - 140</td></tr>
<tr><td colspan="6">Direct Injection at ~17.2MPa</td></tr>
<tr><td>Start of Injection</td><td rowspan="4">9.3</td><td>120, 150, 330, 360</td><td>MBT</td><td>1</td><td rowspan="3">100</td></tr>
<tr><td>Ignition Timing</td><td>150 (Late DI)</td><td>6 – 24***</td></tr>
<tr><td>Equivalence Ratio</td><td rowspan="2">360 (Early DI)</td><td>MBT</td><td>0.83 – 1.25</td></tr>
<tr><td>IMAP</td><td></td><td>1</td><td>100 - 140</td></tr>
</table>

A spark timing of 14 deg bTDC was set for the baseline PFI test corresponding to a CA50 of 11 deg aTDC, **An average representative CA50 ~9.5deg aTDC was determined for the rest of the engine tests for uniformity, ***The Late DI ignition timing tests were conducted from 6 – 20 deg bTDC.

However, Figure 5.2 suggests that there is more than maximized mixing time to enabling engine stability as the really retarded SOI timing, 150 deg bTDC, demonstrated stable engine operation while a much earlier SOI timing 330 deg bTDC and the most retarded SOI timing were highly unstable engine conditions. A possible explanation is that in-cylinder motion like tumble, spray pattern, valve and piston position also play important roles in determining local equivalence ratio conditions especially around the spark plug at spark which can promote, or hinder engine stability as seen in numerical studies [45 – 47, 86]. Still, despite the fluctuation in COV with SOI, the BTE trend was steadier, decreasing with retarded SOI timings. This likely meant that mixing time and charge homogeneity were the most significant determinants of engine efficiency. Overall, these results imply that optimizing the start or end of injection is a critical step in DI operation with LPG. Given these initial results, SOI timings 150 deg bTDC and 360 deg bTDC were then selected in DI mode for the rest of this study to provide insight into the competing effects of maximized mixing time without short-circuiting of fuel (360 deg bTDC – after EVC) and maximized charge mass in the cylinder (150 deg bTDC – after IVC). For the rest of the baseline PFI evaluation, 120 deg bTDC was selected as the SOI timing based off slight overall advantages in terms of emissions, combustion, and performance.

Next, the maximum brake torque timing (MBT) defined as the ideal combustion phasing where the work done by the combusting gas is minimized during compression and maximized during the expansion stroke was determined by sweeping the spark timing from a retarded timing of 6 deg bTDC to more advanced timings for both the DI and PFI configurations. Brake torque, shown in Figure 5.3, was influenced by advancing the spark timing until this MBT was achieved at spark timing 16 deg bTDC corresponding to a CA50 of 9 deg aTDC for the PFI configuration. At this operating condition, the BTE was found to be 34%. This BTE was then designated as the baseline

efficiency of the heavy-duty LPG engine for reference purposes. Polynomial curves were fitted to the individual points in Figure 5.3 and while the actual spark timings differed, the MBT in terms of CA50 for all configurations was found to consistently be between ~6.5 and ~8.5 deg aTDC on the curves. Previous studies by Sierens [87] determined this optimal combustion phasing to be between 7 and 8 deg aTDC, while Heywood [10] indicated that this value is typically at about 10 deg aTDC. An average representative CA50 of ~9.5 deg aTDC was selected for uniformity for the rest of the tests. Comparing the injection strategies, the early DI strategy generated the most torque on the engine, followed by the PFI while the late DI strategy performed the worst. At naturally aspirated conditions and 1200RPM, the early DI strategy improved brake torque over the baseline by around 3%, producing 187Nm. These results show that while PFI may present superior mixing conditions, the potential benefits of DI including charge cooling, prevention of short-circuiting, increased volumetric efficiency added to the maximized mixing time at the early SOI timing combine to make DI a more superior strategy in this engine configuration.

Following this, equivalence ratio was swept on the engine for all three injection configurations and the BTE presented in Figure 5.4. Once again, the early DI strategy dominated the performance across all tested equivalence ratios, responsible for an engine high BTE of 37% with the current piston and LPG fueling, a 3% absolute increment on the baseline BTE. The order was once again Early DI > Baseline PFI > Late DI, indicating that the early DI benefits mentioned earlier possibly dominate even at lean and rich conditions. For all configurations, the lean conditions were more efficient than the rich operation. This increased efficiency accounted for a ~22% relative improvement in BTE for the PFI, and a ~15% and ~24% relative BTE improvement between the leanest (ϕ = 0.83) and richest (ϕ = 1.25) operating conditions for the late and early DI strategies respectively. Several studies have also observed this trend of increasing efficiency with reducing

equivalence ratio [10, 36, 40]. The BTE at lean conditions is higher due to the combustion products being at lower temperatures causing lower heat transfer and therefore, more expansion work to be extracted by the piston, while at the rich conditions the combustion inefficiencies from an overly rich mixture dominate [10] and this severely diminishes the BTE at these conditions.

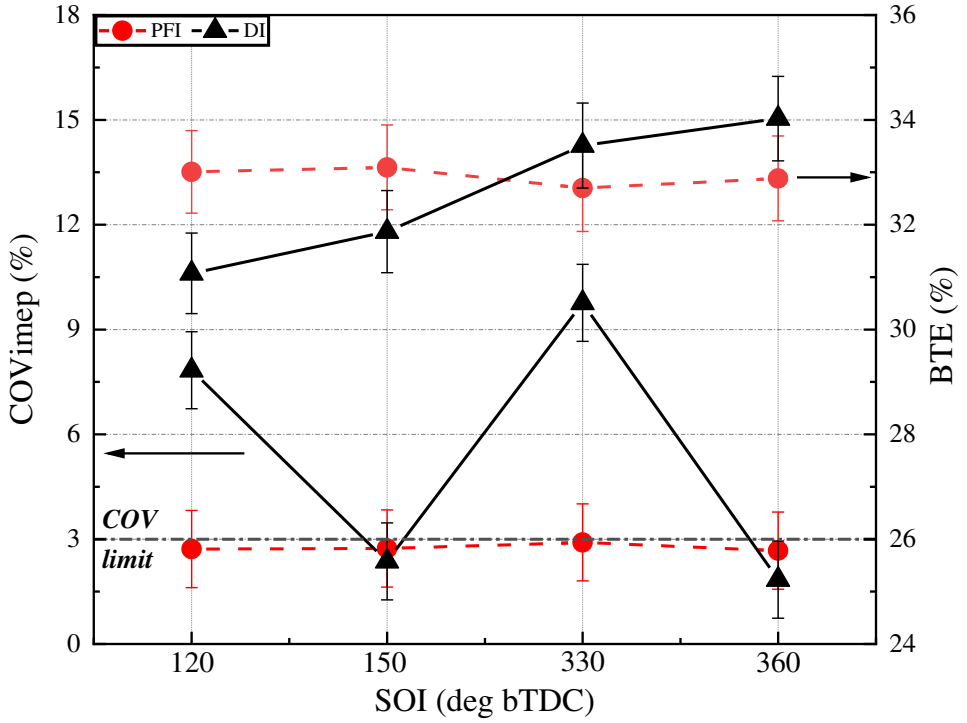

Figure 5.2. BTE (%) and COVimep (%) for the PFI and DI configurations as a function of SOI

Finally, the performance metrics for the engine load sweep are presented in Figure 5.4 for the three engine configurations. With the CA50 kept constant at around MBT, the IMAP was increased from naturally aspirated conditions and the brake torque increased accordingly: a result of the increasing fuel and air quantity in the combustion chamber. The IMAP was swept up to 140kPa, the point at which the engine had begun to experience at least incipient knock in all three configurations. The plots illustrate once again the superiority of the early DI strategy at all tested loads. The early DI

configuration produced an engine high brake torque in this baseline piston configuration of 258Nm, a 7% improvement in torque over the late DI configuration at the same condition.

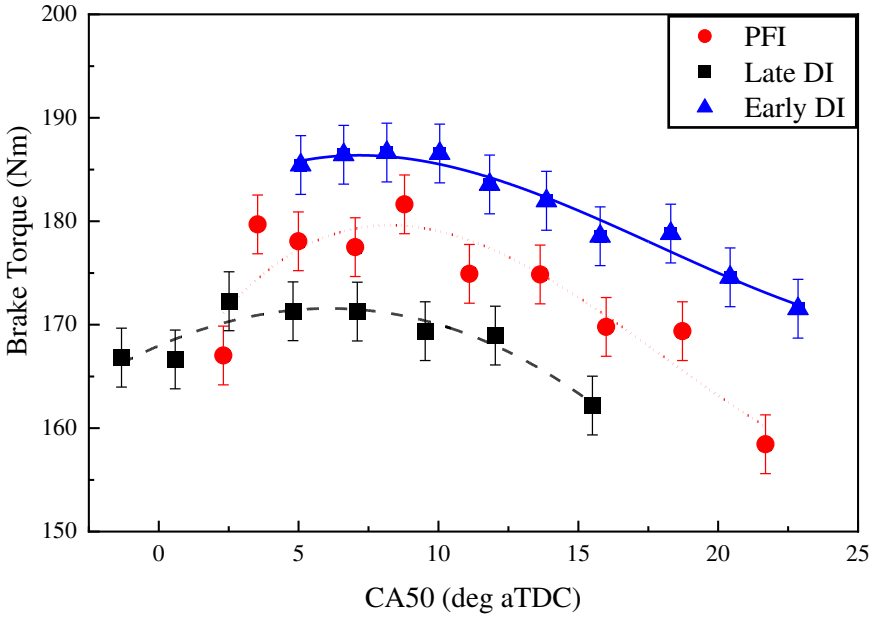

Figure 5.3. Demonstration of maximum brake torque timing vs CA50 for the three tested configurations

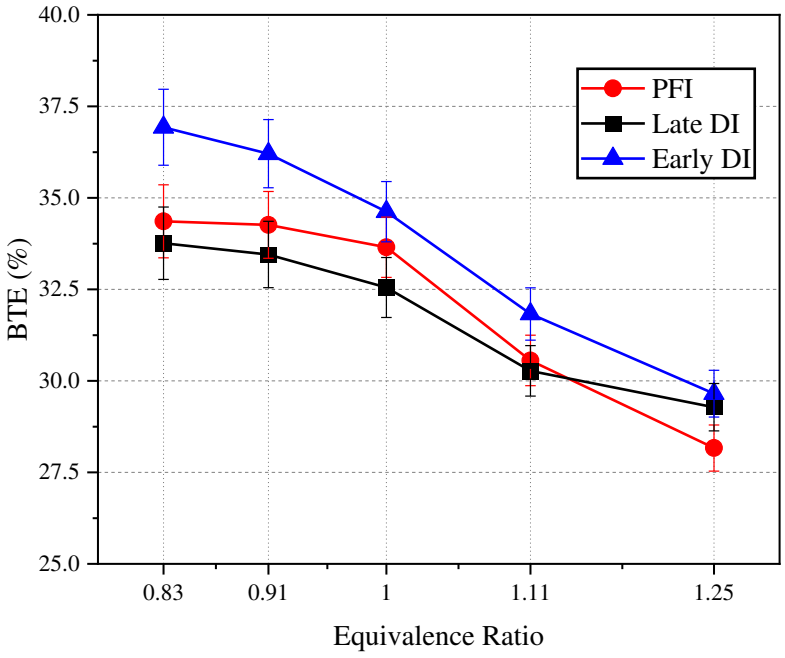

Figure 5.4. BTE (%) vs Equivalence ratio for three tested injection configurations

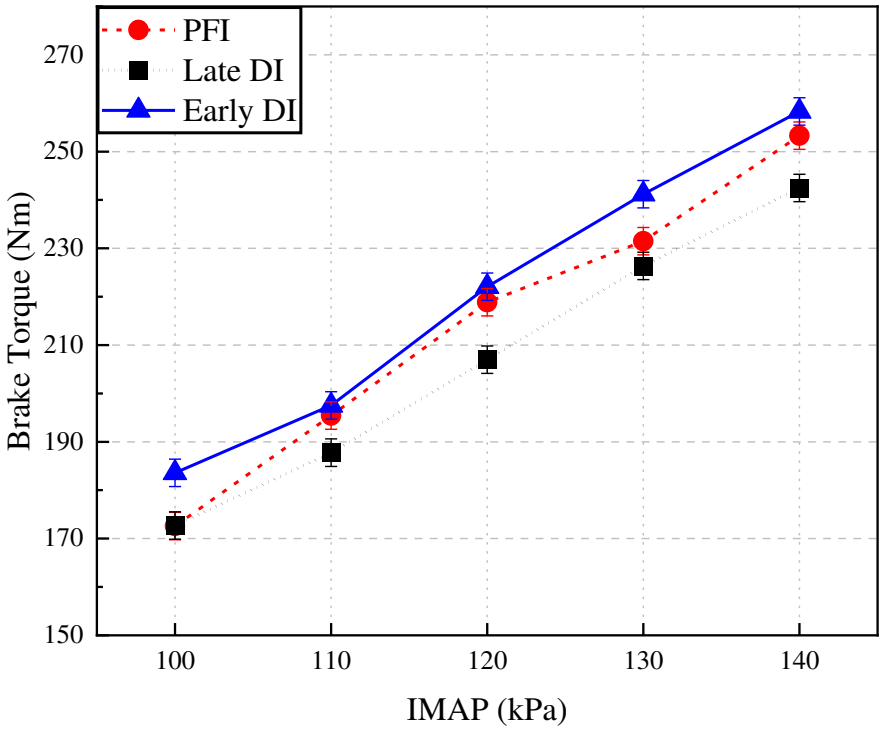

Figure 5.5. Brake Torque (Nm) vs IMAP (kPa) for three tested injection configurations

5.3.2 Combustion Characteristics

The in-cylinder pressure traces and AHRR curves for the PFI and DI configuration as SOI was varied on the engine are plotted in Figure 5.6. For the baseline PFI evaluation, the curves are more closely packed, especially the AHRR curves, indicating that the effect of SOI was minimal on the engine pressure history. Conversely, in DI configuration a substantial effect of SOI was observed on the in-cylinder pressure trace and AHRR curves. The earliest SOI, 360 deg bTDC exhibited the highest peak in-cylinder pressure followed closely by a late SOI, 150 deg bTDC. Interestingly, retarding the SOI by just 30 degrees from both points resulted in significant reductions in in-cylinder peak pressures and AHRR. For example, despite being an early injection time SOI 330 deg bTDC indicated the lowest pressures and heat release rates among the tested SOI on the engine. SOI 150 deg bTDC indicated the shortest heat release duration and largest peak believed to be a

consequence of the maximized charge mass in the cylinder as all the charge air is inducted into the cylinder and the intake valves closed before fuel injection begins.

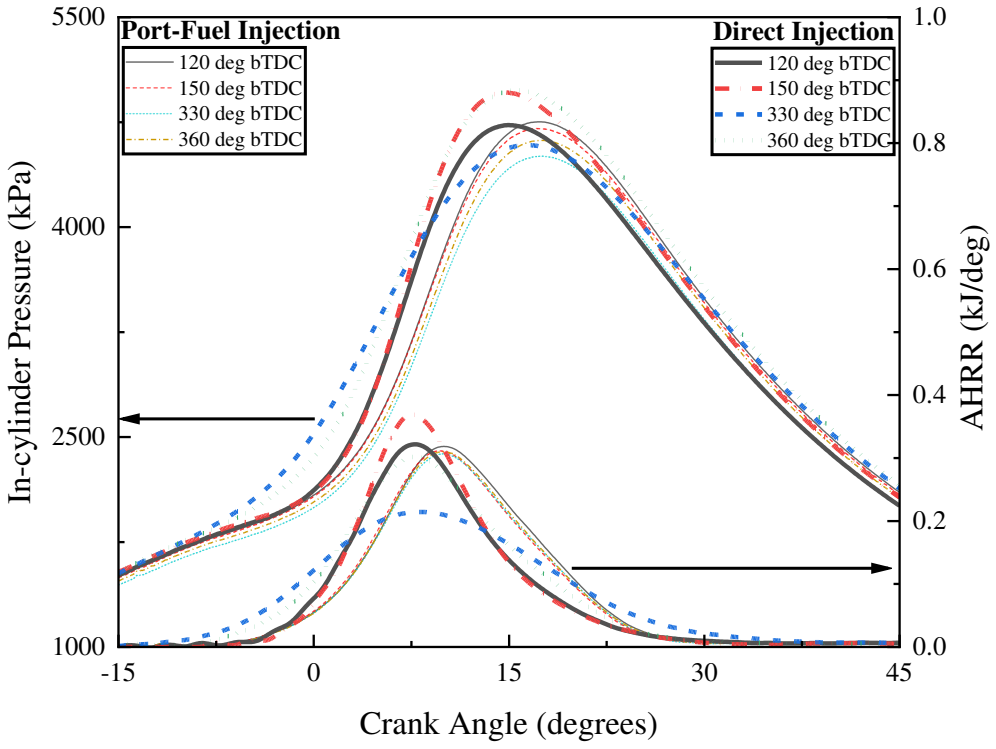

Figure 5.6. The in-cylinder pressure (kPa) and AHRR (kJ/deg) for the baseline PFI and DI SOI sweep

Next, the combustion metrics for the ignition timing sweep were compared for all three configurations in terms of knock intensity measured by the knock ripple sum (KRS) described in Section 2.5.1 and COVimep. The KRS threshold, above which the engine experienced incipient knock was determined to be 4.2%, while the COVimep limit for engine stability was 3% as previously discussed in Section 5.3.1. Figure 5.7a indicates that the engine did not experience any knock at all tested ignition timings using the early DI strategy. This was most likely due to the charge cooling as the liquid LPG has a high tendency to flash boil after injection [84, 88, 89] absorbing latent heat from its surroundings. Another possible reason was the improved homogeneity of the mixture in the combustion chamber due to the maximal mixing time which

promotes a more uniform combustion thus preventing end-gas auto-ignition initiated by rich pockets of charge. The PFI KRS trends were similar to the early DI trends most likely due to the charge homogeneity. Intuitively, the late DI mode was expected to improve this charge cooling phenomenon due to reduced residence time of the charge before combustion, however, mixing preparation times were also reduced believed to result in pockets of high local equivalence ratio mixtures in the cylinder which was then believed to promote end-gas autoignition and knock shown in Figure 5.7a. Computational studies by Churchill et al. [90] on the heavy-duty engine show the tendency for rich pockets of end-gas to form for late DI SOI timings. Similar trends to the KRS ones were also observed in terms of COVimep in Figure 5.7b where the early DI and baseline PFI tracked each other as COVimep increased with retarded ignition timings. Kim et al. [85] demonstrated this relationship of COVimep with ignition timing in their work on an LPG engine [85]. The COVimep for the late DI mode exhibited a less predictable relationship with ignition timing and crossed the COVimep limit at a much more advanced CA50 compared to the baseline PFI and early DI modes.

The in-cylinder pressure traces and AHRR curves for the most efficient (leanest, $\phi = 0.83$) tested conditions are presented for each injection strategy in Figure 5.8. The notable details were that the late DI mode exhibited the shortest heat release duration and largest peak rate of heat release due to its maximized charge mass amount in the cylinder whilst the early DI mode produced the largest peak in-cylinder pressures. The early DI strategy increased peak pressures by 5% and 6%, respectively, compared to the late DI and baseline PFI configuration. A final key take-away from the equivalence ratio sweep on the heavy-duty engine was that the early DI strategy was the only configuration with stable engine operation (denoted by COVimep < 3%) at the leanest tested

condition, $\phi = 0.83$, indicating the potential for further extension of the lean limit with LPG using early DI strategies compared to the other two modes.

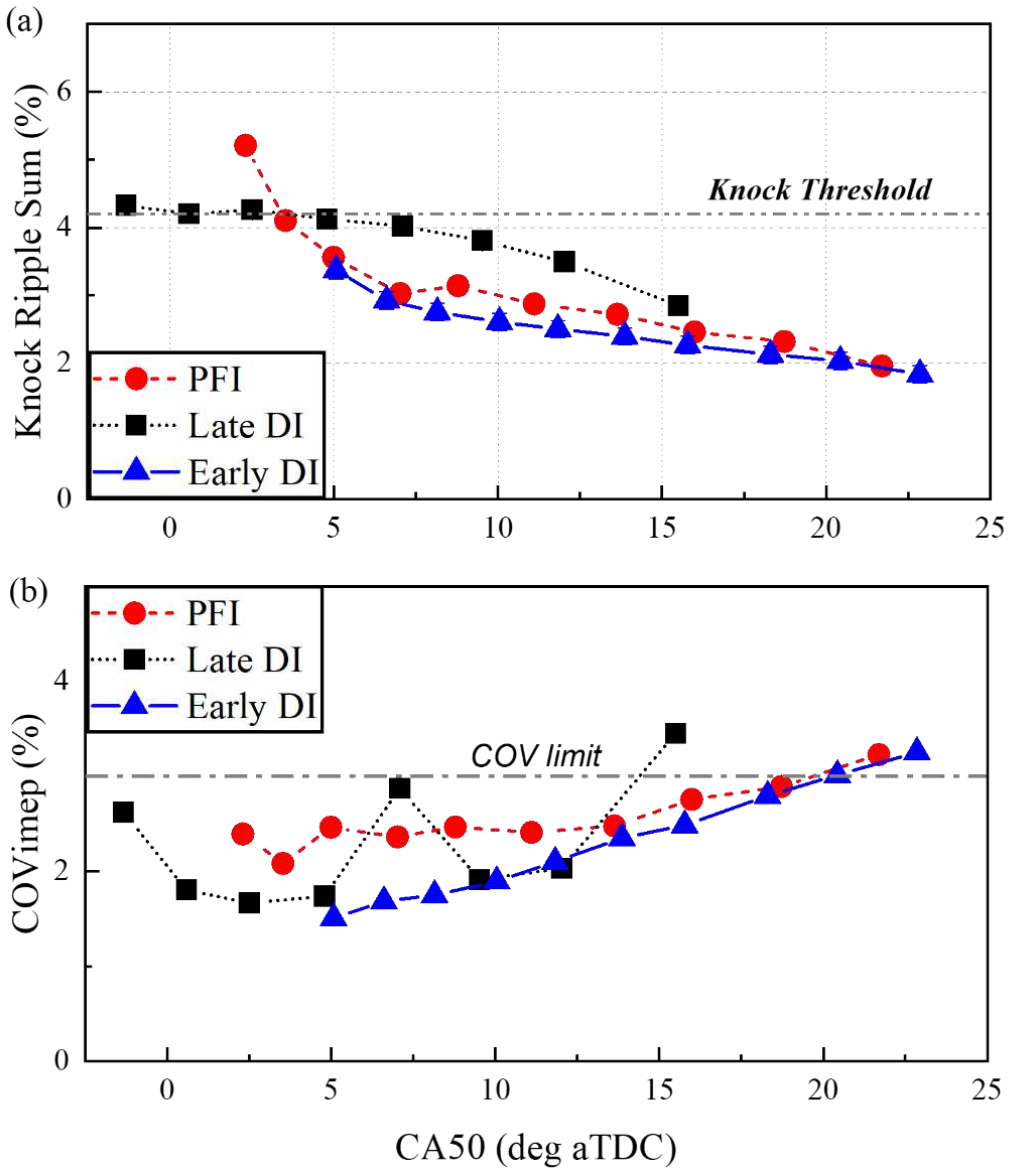

Figure 5.7. Combustion metrics in terms of (a) Knock ripple sum (%) (b) COVimep (%), vs CA50 (deg aTDC) for the ignition timing sweep on the engine

The subsection on combustion characteristics concludes with the knock trends for all three configurations as IMAP was varied. As depicted in Figure 5.9, the early DI strategy demonstrated the most resistance to knock due to a combination of the charge cooling effect discussed earlier which reduces the in-cylinder charge and combustion temperature as well as the end-gas

temperature, and the well-mixed fuel and air mixture as a result of the increased mixing time promoting a uniform combustion in the engine. The PFI strategy followed closely for the same reasons, demonstrating incipient knock at the same IMAP (but lower engine BMEP) as the early DI case. On the other hand, the late DI strategy indicated a more rapid transition into knock despite the improved charge cooling tendencies of the DI spray especially at retarded SOI timings. A possible explanation is that as fuel and air quantities increase at higher loads, the reduced mixture preparation time associated with the late DI configuration gets even more inadequate, worsening the stratification of the charge in the combustion chamber. This potentially increases the occurrence of rich pockets of end-gas ready to auto-ignite.

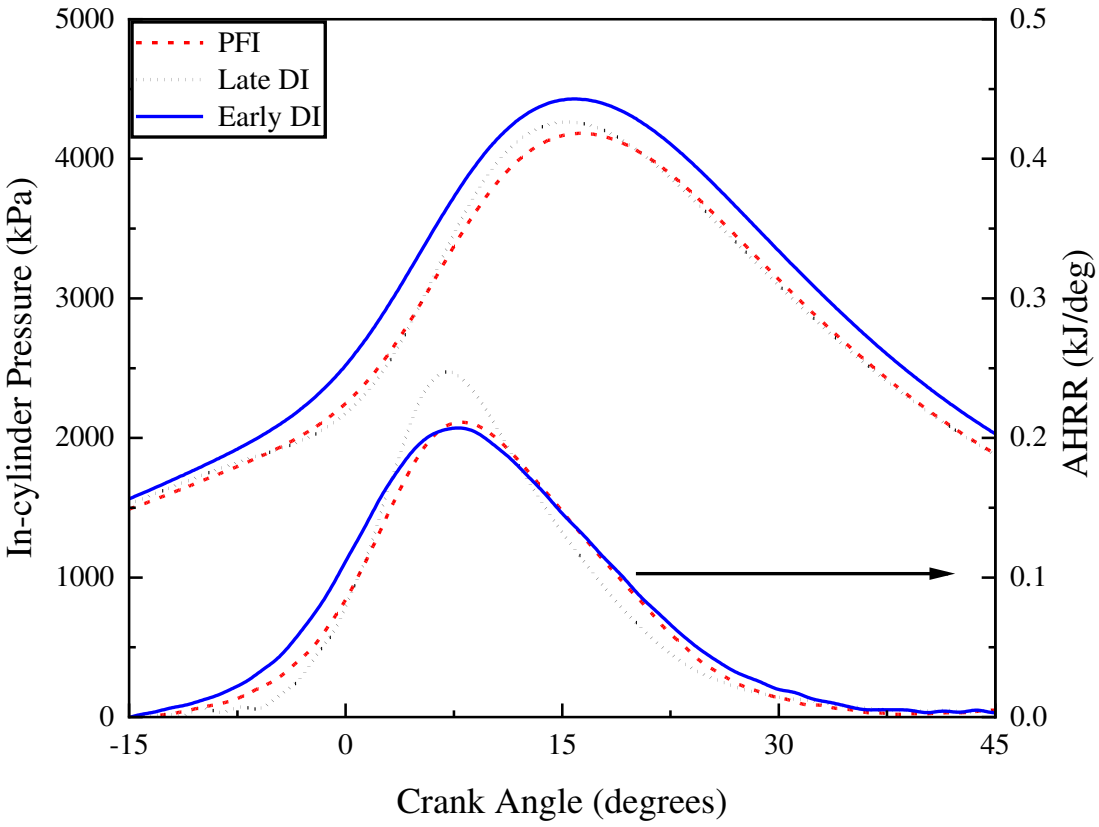

Figure 5.8. The in-cylinder pressure (kPa) and AHRR (kJ/deg) for the leanest (ϕ = 0.83), most efficient tested condition on the engine for all three configurations.

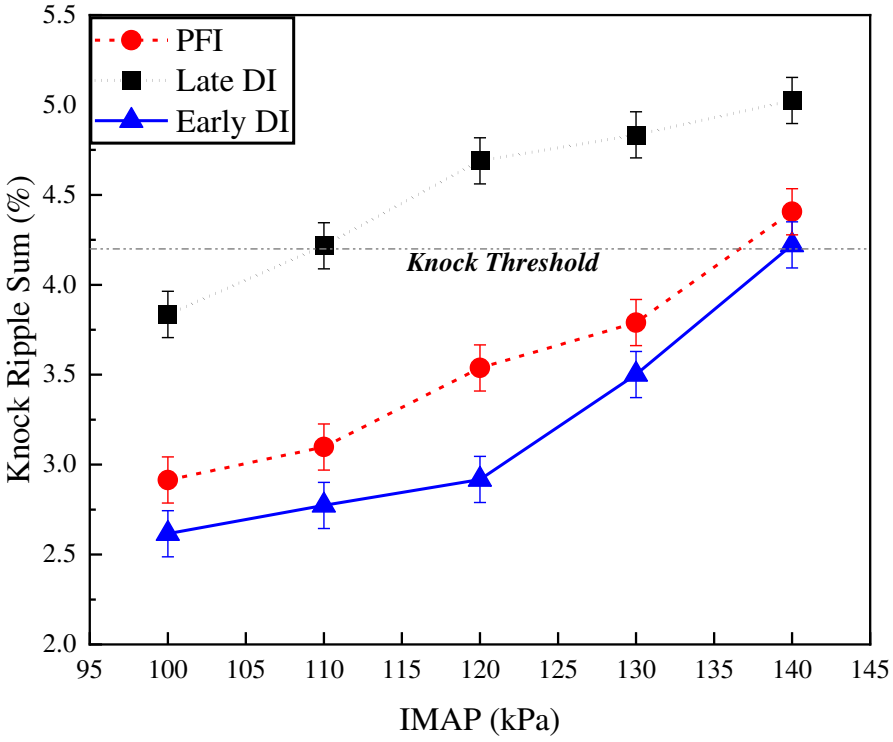

Figure 5.9. Knock ripple sum (%) vs IMAP (kPa) for all three tested injection configurations

5.3.3 Emission Characteristics

The emission in terms of bsNOx, bsTHC, and bsCO for the SOI and ignition timing sweeps on the heavy-duty LPG engine are captured in Figure 5.10. The bsNOx shown in Figure 5.10a, demonstrates the charge cooling advantage of DI over the PFI strategy as discussed in section 5.3.2. NOx formation is governed by peak in-cylinder temperatures and available oxygen concentration [10, 91]. Therefore, as the experiments were conducted at the same average equivalence ratios, the charge cooling effect of the direct injected LPG was likely to be the dominant factor in mitigating the engine NOx since it effectively lowers combustion and in-cylinder temperatures. The late DI strategies had the advantage here, achieving over 33% reduction in bsNOx at SOI 150 deg bTDC when compared to the PFI configuration which had similar bsNOx outputs at all tested SOI timings.

In terms of bsTHC shown in Figure 5.10b, however, the PFI mode had the upper hand with around 1g/kW-hr of bsTHC at all close and open SOI timings. McGee et al. [92] showed not too dissimilar results in their close and open valve comparisons with port targeting, at similar temperatures (90^{o}C) and lower intake pressure [92]. For the DI modes, the SOI 360 and 150 deg bTDC recorded similar bsTHC values to the PFI configuration. Generally, HC emissions are from trapped crevice volume gas and incomplete combustion, thus the COVimep shown in Figure 5.2 and discussed in section 5.3.1 provides some explanation for these bsTHC behaviors. At conditions where the COVimep was below the 3% limit and combustion was stable, the bsTHC values were similar across configurations, however, at 120 and 330 deg bTDC SOI timings which displayed unstable combustion, the bsTHC values were at least doubled, to even as much as 2.7g/kW-hr, due to the resulting partial burns and misfire. In Figure 5.10c, the PFI mode again exhibited an insensitivity of brake specific emissions to SOI with the bsCO emissions remaining approximately equal as a result of the properly mixed charge at all SOI timings. CO emissions are affected mostly by equivalence ratios and combustion completeness, and this effect can be seen clearly with the DI mode. As SOI was retarded, mixture preparation time is reduced, and charge stratification becomes more likely [93]. This effect was noticeable as bsCO emissions increased by over 50% from 21.2g/kW-hr at 360 deg bTDC to 32.3g/kW-hr at 150 deg bTDC.

In Figure 5.10d, the charge cooling advantage of the late DI strategy is further demonstrated as the bsNOx emissions are presented for the ignition timing sweep. The plot demonstrates an increasing relationship of bsNOx with advanced ignition timings [81, 87]. This was due to increased in-cylinder temperatures as ignition timing was advanced and combustion moved towards TDC, increasing pressures and temperatures. However, the biggest difference was observed at the most retarded ignition timing where the late DI strategy generated 12.2g/kW-hr of bsNOx, 39% lower

than the bsNOx for the PFI mode at the same condition. Advancing the ignition timing was also observed to increase bsTHC in Figure 5.10e, possibly due to higher in-cylinder pressures forcing more of the charge into the crevice volumes whilst also allowing shorter time for the fuel vaporization and mixture preparation [85]. Retarded timings also produce higher late-cycle in-cylinder temperatures which aids the oxidation of the reintroduced fuel-air mixture. Previous studies have also observed this trend for PFI [81] and DI [85]. Finally, the bsCO emissions for the ignition timing sweep are presented in Figure 5.10f. The standout trends are that the bsCO emissions for both DI modes increased with advanced ignition timing while the PFI bsCO remained fairly stable across all tested ignition timings and that the late DI mode produced significantly higher bsCO emissions than any other configuration. The late DI mode produced 35g/kW-hr of bsCO emissions at ignition timing 20 deg bTDC, the highest produced during the ignition timing experiments, which was 55% higher than the lowest bsCO achieved during the experiments with the PFI strategy. Kim et al. [85] also showed this increasing effect of spark advance on DI bsCO emissions in their studies [85].

Finally, the chapter concludes with a discussion on the emissions characteristics of the three injection configurations as equivalence ratio and IMAP were varied. The bsNOx was shown in Figure 5.11a to increase with decreasing equivalence ratio. This trend can be described by the competing effects of available oxygen and in-cylinder temperatures. At rich conditions, there is not enough available oxygen for the formation of NOx despite the high in-cylinder temperatures, hence the lower values of bsNOx made lower still by the normalization with larger brake power numbers. At the lean conditions temperatures are low enough to discourage NOx formation but the available oxygen from the abundant air encourages the formation of NOx. For the PFI strategy the bsNOx peaked at $\phi = 0.91$ and began to drop at 0.83, in this regard the reduced in-cylinder

temperatures had now begun to dominate the NOx chemistry. This almost bell shape relationship with reducing equivalence ratio can be found in the literature [36, 84, 94]. For the DI configurations, similar trends were observed however the theoretical point at which the NOx peaks and begins to reduce was not captured within the experimental conditions. The full trend was captured by Ho Choi et al. [95] in their DI experiments on a heavy-duty engine showing the DI NOx peak at around $\phi = 0.83$. The PFI mode demonstrated an advantage over the DI modes with lower bsNOx at the rich conditions, however, the late DI strategy described an even more significant reduction in bsNOx at stoichiometric and lean conditions.

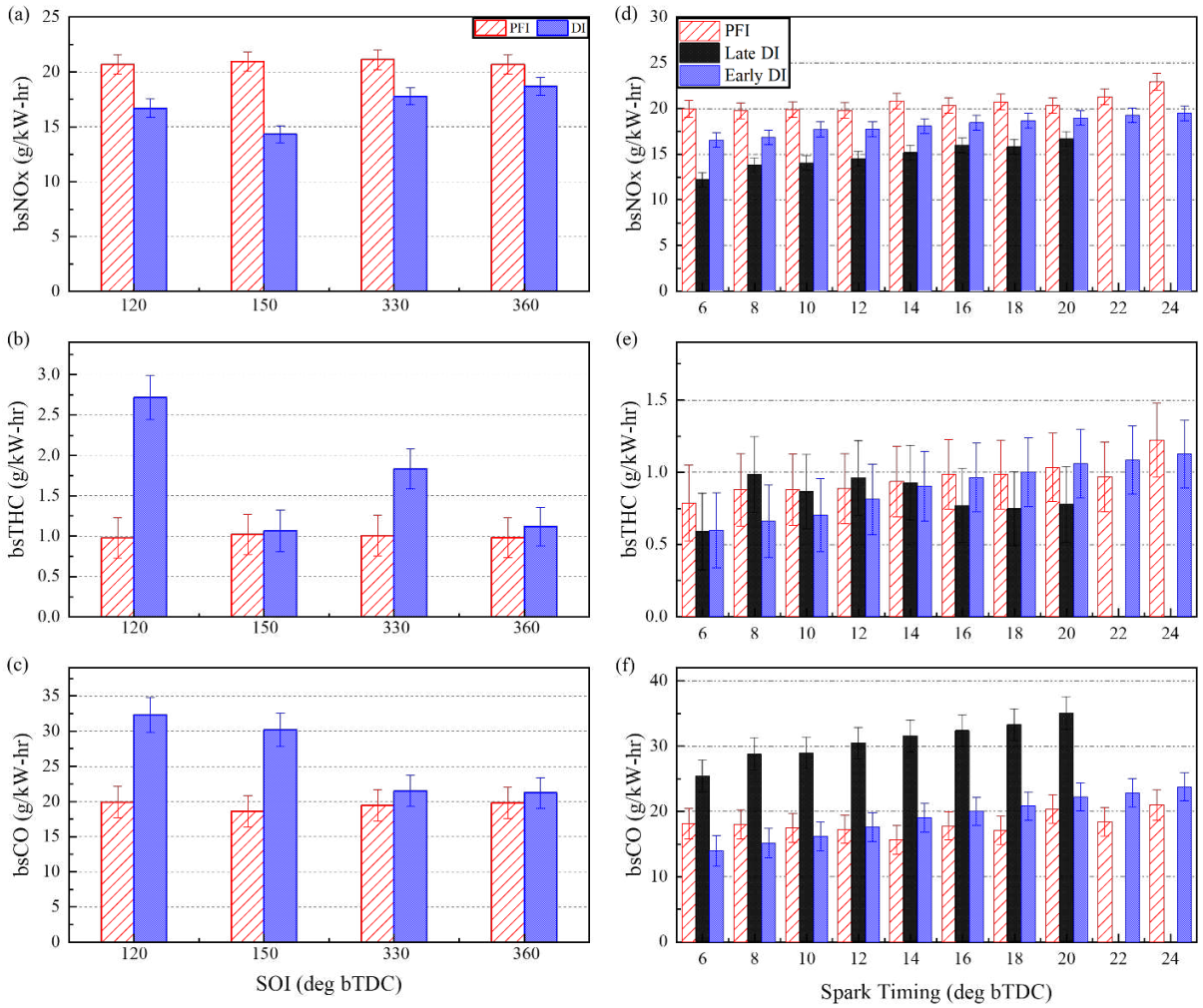

Figure 5.10. Brake specific emissions in g/kW-hr in terms of (a) NOx (b) THC (c) CO vs SOI (deg bTDC) and (d) NOx (e) THC (f) CO vs Ignition timing (deg bTDC) for all tested injection configurations

Next, the bsTHC emissions are presented in Figure 5.11b. There was a slight drop in these emissions as equivalence ratio increased from ϕ = 0.83 due to combustion becoming more stable and complete, and then a significant rise at richer conditions. Other researchers have described the same results in their experiments, with bsTHC reducing as equivalence ratio was increased to stoichiometric conditions and then increasing again with further increase in equivalence ratios [36, 94]. On average, the bsTHC values were in the order late DI > early DI > baseline PFI. A possible explanation for this trend is that the PFI with its superior mixture preparation time experienced a more uniform combustion (COVimep of 0.8 at ϕ = 1.25) with the higher fuel quantity required at rich conditions causing only a modest increase in the bsTHC emissions from 0.82g/kW-hr at ϕ = 0.83 to 1.9g/kW-hr ϕ = 1.25. At the extreme, the late DI mode indicated relatively poorer combustion stability (COVimep of 1.8 at ϕ = 1.25) and possibly experienced a more substantial crevice volume filling effect due to the higher fuel quantity required at the rich condition ϕ = 1.25 causing an increase in bsTHC emissions from 1.94g/kW-hr at ϕ = 0.83 to 5.11g/kW-hr ϕ = 1.25. In Figure 5.11c, the bsCO trends for the three injection modes are shown as a function of equivalence ratios. At rich conditions, there is insufficient oxygen for complete oxidation and as such the bsCO was exponentially higher compared to the really low values at lean conditions where a 99% and 98% reduction in bsCO was recorded for the PFI and the early DI strategies respectively. Similar trends have been recorded in the literature [10, 36, 40, 94, 95]. The late DI indicated significantly higher bsCO emissions than the early DI and PFI modes at lean to stoichiometric conditions.

To conclude this section, the brake specific emissions as IMAP was varied are presented in Figure 5.11d to 5.11f. In Figure 5.11d, the bsNOx emissions for the PFI and early DI modes remain fairly consistent across the load sweep, however, the late DI bsNOx demonstrated an increasing trend

with IMAP. This was believed to be a consequence of the increasing intensity of end-gas auto-ignition with IMAP shown earlier in Figure 5.9 causing an increase in in-cylinder temperatures thus aiding the formation of NOx. Despite this trend, the late DI configuration maintained the lowest bsNOx values over the entire IMAP sweep as a result of its superior charge cooling effect as the LPG spray immediately vaporizes and collapses upon entering the combustion chamber reducing the in-cylinder temperatures and causing a reduction in the NOx generated.

The bsTHC in Figure 5.11e decreased for the modes with adequate mixing (baseline PFI and early DI), as the load was increased, from 0.91g/kW-hr to 0.63g/kW-hr for the baseline PFI and from 0.56g/kW-hr to 0.31g/kW-hr for the early DI mode. This bsTHC relationship with load has been observed in previous studies [37, 94, 96]. Although, the crevice volume filling is expected to have a more pronounced effect on the bsTHC at the increased in-cylinder pressures for higher engine loads, it is more likely that the competing effects of a more superior, complete combustion due to higher in-cylinder temperatures [96] and the normalization with larger brake powers at the higher intake pressures combine to drive the bsTHC trend downwards. The reverse relationship was the case for the late DI mode as bsTHC increased with intake pressure on the engine. The COVimep was found to be greater than 3% for this configuration as intake pressure was increased to 110kPa and beyond and this unstable combustion was likely responsible for the uptick in bsTHC emissions. Still, the absence of short-circuited fuel in the DI strategies likely played a key role in achieving lower bsTHC emissions than the PFI mode. The bsCO emissions for the DI configurations in Figure 5.11f trended downwards with increasing intake pressure as described by Woo et al. [94], while the baseline PFI bsCO emissions did not describe any distinctive pattern with intake pressures. Singh et al. [96] suggests that the higher combustion temperatures resulting

from the increased injected fuel amount per cycle at higher loads enables a more homogeneous in-cylinder charge burn, causing a reduction in CO emissions [96].

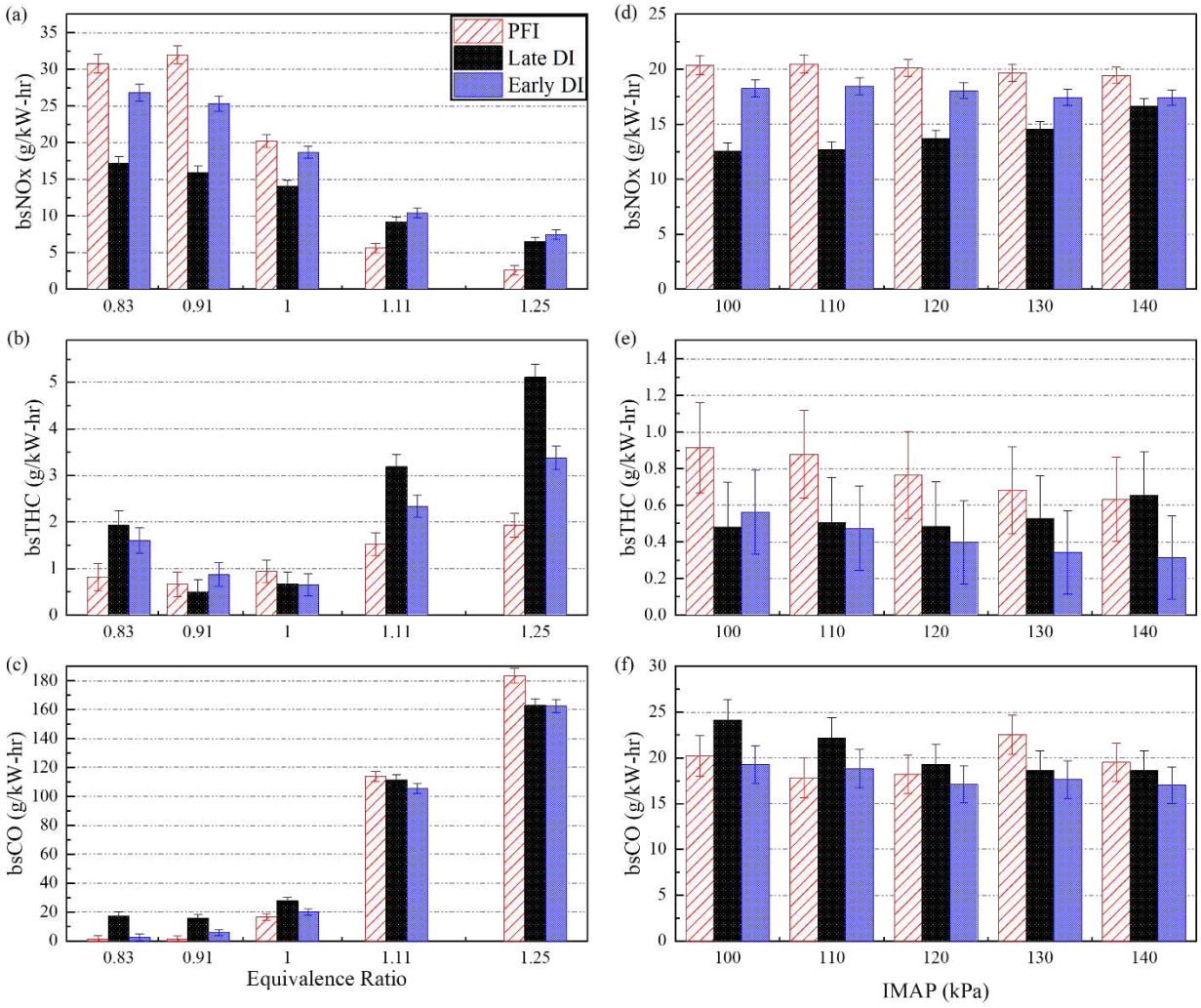

Figure 5.11. Brake specific emissions in g/kW-hr in terms of (a) NOx (b) THC (c) CO vs Equivalence ratio and (d) NOx (e) THC (f) CO vs IMAP (kPa) for all tested injection configurations

5.4 Conclusions

This chapter presented the baseline evaluation of the performance, combustion, and emissions characteristics of a heavy-duty LPG engine using port-fuel injection so as to establish a benchmark comparable to existing LPG engines. Then, a Delphi GDI with nozzle number, size, and pattern modified for high flow LPG operation on this engine was installed and the engine operated in DI

mode. Three injection strategies namely, baseline PFI, early DI, and late DI were investigated, and the results showed that:

Mixing and mixture preparation time, maximized at the baseline PFI and early DI strategies were shown to be the key determinants of the performance of the engine with liquid LPG. For example, the early DI improved engine brake torque by 7% compared to the late DI mode at high loads (1300kPa BMEP corresponding to intake pressures of 140kPa). The baseline PFI configuration also outperformed the late DI mode at almost all tested operating conditions in terms of BTE and brake torque accounting for a 1.1% absolute increment in BTE over the late DI case at the same stoichiometric, naturally aspirated conditions.

SOI had a significant effect on the performance, emissions, and combustion characteristics in DI configuration only. Notably, BTE was increased by ~10% as SOI was advanced from close valve timing 120 deg bTDC to open valve timing 360 deg bTDC while bsCO and bsTHC were reduced by 34% and 59% respectively from 32.3g/kW-hr to 21.2g/kW-hr and from 2.7g/kW-hr to 1.1g/kW-hr as SOI timings were advanced from 120 deg bTDC to 360 deg bTDC. The SOI results also demonstrated the importance of other factors apart from mixing time such as tumble, LPG spray pattern, engine valve and piston position in ensuring engine stability as SOI 330 deg bTDC was significantly more unstable than the late SOI timing 150 deg bTDC despite its superior mixture preparation time. PFI operation on the other hand displayed an insensitivity to SOI timings, maintaining COVimep < 3% at all tested SOI points. This trend was also evident in the PFI emissions as the brake specific NOx, THC and CO showed little variation with SOI.

The charge cooling effect of the vaporized liquid LPG spray was a key feature of the DI configuration but was most evident in the late DI strategy where this cooling effect was maximized. This effect was responsible for a >33% reduction in bsNOx for the late DI configuration compared

to the baseline PFI mode at the same 150 deg bTDC SOI. In another scenario, the late DI configuration achieved a 39% reduction in bsNOx (12.2g/kW-hr) compared to the baseline PFI (19.95g/kW-hr) and a 26% reduction in bsNOx when compared to the early DI mode at the most retarded ignition timing condition evaluated.

In terms of emissions, the DI strategies were able to avoid short-circuiting of the fuel, which was evident in the bsTHC emissions at stoichiometric, naturally aspirated conditions. The DI modes reduced the bsTHC emissions by 47% for the late DI and 38% for the early DI mode compared to the baseline PFI mode. The baseline PFI strategy did however show overall advantages in terms of bsCO emissions, most notably at similar lean conditions and when compared to the late DI strategies. For example, at the leanest evaluated condition, $\phi = 0.83$, the PFI configuration achieved 93% and 52% lower bsCO emissions when compared to the late DI mode and the early DI mode respectively.

Of the two tested DI configurations, the early DI timings indicated superiority in key areas, with a combination of favorable charge cooling and extended mixture preparation time, along with the similar short-circuiting benefits, the early DI was responsible for extending the knock limit and allowing more advanced CA50 operation and higher engine loads, extending the lean operation by supporting stable operation of the engine at leaner conditions and demonstrating tangible bsCO benefits compared to the late DI strategy. The late DI strategy showed combustion advantages in terms of shorter heat release durations translating to faster burn durations, but this was mostly due to stratification of the in-cylinder charge with rich pockets at the walls and crevices which then had unfavorable effects on the knock tendencies, bsCO emissions, and stability of the engine.

Finally, the designed PFI and DI system consistently delivered liquid LPG at the required injection pressures, 1.6MPa and 17.2MPa respectively. This set-up guaranteed excellent control of the

combustion and air-fuel ratio during the heavy-duty experiments. The baseline efficiency to be used as a reference for the rest of the study was determined to be 34%, achieved with PFI and compression ratio 9.3:1, at 1200RPM, MBT, and naturally aspirated (101.3kPa) stoichiometric conditions.

The results from this chapter demonstrate the 34% baseline BTE on the engine and necessitate an improvement in the BTE of at least 10% in order to achieve the goal of matching the diesel efficiency on the engine. The results also show the importance of designing an injection strategy tailored to the properties of the LPG fuel for optimal combustion, performance, and emissions behavior. Two possible strategies are the stratified direct injection strategy with early injection at low cylinder pressure which show higher penetration lengths [97] and improved mixing and then a late injection to take advantage of the charge cooling effect of the spray, or a mixed DI/Optimized PFI strategy that takes advantage of the PFI mixing benefits and the DI charge cooling, volumetric efficiency, and eliminated short-circuiting benefits, especially at higher loads. Finally, the findings suggest that the key to achieving the 10% improvement in BTE would be to drastically improve the injector flow and thereby shorten injection duration so as to further harness the benefits of mixing and potentially, switch to late DI timings to enable maximized trapped and higher levels of charge cooling. This chapter provides some clarity on research questions 2 and 3.

CHAPTER 6. OPTIMIZATION OF THE HEAVY-DUTY ENGINE TO ACHIEVE DIESEL EFFICIENCY AND LOW EMISSIONS WITH DI/PFI, CONTROLLED END GAS AUTO IGNITION AND EGR

6.1 Overview

The chapter presents the results of the final phase of investigations conducted on the engine. The results described herein are the culmination of the three preceding chapters and draw on their conclusions in pursuit of the overarching goal of achieving near diesel efficiency with LPG on the heavy-duty Cummins 1SX15L engine. The engine was run with several different combinations of key variables and hardware configurations including but not limited to different ignition sources, pistons, engine loads (in terms of BMEP), combustion phasing, exhaust gas recirculation rates etc. The developed computational models played a critical role especially in the design of the pistons and injection strategies, but those discussions are out of the scope of this dissertation.

The outcomes from Chapter 5 highlighted the potential associated with improving injector flow and distribution which would consequently reduce injection duration and maximize mixture preparation time. Efforts were made on three fronts in this regard, the first was to attempt to increase the flow rate of the baseline Delphi 5-hole injector while optimizing the nozzle pattern for even more superior mixture distribution. This was done using the CFD models to optimize mixture homogeneity at engine relevant conditions and the models showed promising results for a second generation 3-hole Delphi design that improved flow rate and mixture distribution. The second direction was to modify an off-the shelf short-body injector with almost double the flow rate of the baseline Delphi injector albeit with unmodified nozzle patterns. This high-flow injector required extensive modification for operation on the heavy-duty engine especially considering the off-center installation location of the direct injectors on this engine. The third was to optimize the

PFI strategy in terms of location and flow by designing a double-injector intake valve targeting system that would be capable of higher loads and take advantage of the charge cooling properties of the LPG spray.

Compression ratio and piston design also took center stage in this chapter as the innovative optimization of piston/compression ratio design has been shown to be one of the biggest determinants of engine efficiency [10, 11, 29, 72, 98 – 100]. The final piston, the high squish 14:1 piston, was developed using the CFD models for high load and efficiency and to extend the knock limit on the engine. Finally, three different ignition hardware were tested on the engine in a bid to extend the EGR tolerance and the knock limit and improve combustion stability and efficiency. Other works have studied the effect of ignition source location [40, 101] and type [101, 102] for fuels such as natural gas and LPG, in diluted and stoichiometric conditions. In this work, the ignition hardware is top mounted and centrally located.

The investigations following the baseline 9.3:1 studies conducted in Chapter 5 began with the installation of the 11.9:1 piston on the engine. This piston, originally designed for natural gas operation on the Cummins ISX15L engine, presented a pathway to improved efficiency, better understanding of the engine behavior with LPG, and further tuning of the developed computational models. EGR was introduced at this stage to develop an understanding of engine dilution tolerance limits and characteristics and also to provide baseline EGR data for the CFD model. The baseline Delphi 5-hole and optimized PFI configurations were then compared at this compression ratio as were the 3-prong Altronic and Woodward FTI prechamber spark plugs. The CFD optimized piston was then installed on the engine and all three ignition sources tested on the engine as well as all three injection configurations, the baseline 5-hole Delphi DI, the high-flow DI and the optimized

double-injector PFI systems. Engine load, SOI, combustion phasing, and EGR rates were all varied at these configurations.

The results showed that the required 10% increment in BTE over the baseline efficiency to match the 44% diesel efficiency target was achieved with both the high-flow DI and optimized PFI configurations using the Woodward FTI spark plug. In finer details, EGR played a critical role in this regard by extending the knock limit of the engine thus allowing more advanced combustion phasing especially at higher loads, which led to these high efficiencies. The chapter begins with a brief section on the experimental methods and test matrices. Then, a section on the response surface method optimization using a full factorial design of experiments and finally, a discussion of the results and short conclusion brings the chapter to an end.

6.2 Experimental Methods

The engine was operated in different configurations as discussed in section 6.1 and as shown in Table 6.1. The operation of the engine with the baseline 5-hole Delphi injector at compression ratio 9.3 has been discussed in extensive details in Chapter 5. The 11.9 ‘natural gas’ piston was then installed on the engine and operated with the three injection configurations described in section 6.1. The results from these set of experiments guided the design of the optimization experiments and the final approach to the target efficiency. The 3-prong Altronic spark plug from the baseline configuration was initially used at this 11.9 compression ratio configuration before the Woodward FTI prechamber spark plug was introduced to determine the potential combustion benefits with a different, more advanced ignition concept.

Table 6.1. The complete engine configurations

Set-up Type	Compression Ratio			Ignition source			Injection strategy		
Set-up No.	High Squish 14:1 piston	11.9 'natural gas' piston	Baseline 9.3 piston	Woodward FTI Pre-chamber spark plug	3-prong spark plug	J-Gap spark plug	Optimized double injector PFI	High-flow 6-hole DI	5-hole modified DI
1	x			x			x		
2	x			x				x	
3	x			x					x
4	x				x			x	
5	x					x		x	
6		x		x			x		
7		x		x					x
8		x			x		x		
9		x			x			x	
10		x			x				x
11			x		x				x

Following this, the piston was swapped for the CFD optimized high squish 14:1 piston on the engine. Again, investigations began with the baseline 5-hole Delphi injector, this time with the Woodward FTI prechamber spark plug. The engine was then switched to the high-flow DI configuration at which all three ignition sources were investigated. Finally, the engine cylinder head was swapped to the PFI configuration to allow for the testing of the optimized PFI mode with

the 14:1 piston and the Woodward FTI Prechamber spark plug. The LPG fuel delivery system described in sections 2.3.1 and 2.3.2 were used as required depending on the injection configuration. LPG bought daily at the same local gas station was used for all of the heavy-duty engine tests and the GC reports from measurements of the fuel composition showed a consistent > 98% propane content for all the tested LPG fuels used in the heavy-duty engine study. A list of engine variables and their ranges of operation across all configurations as well as engine constant operating parameters across the test days can be found in Table 6.2.

Table 6.2. Engine variables and constants

Variable	**Range**
Start of Injection	120 – 360 deg bTDC
CA50	5 – 22 deg aTDC
EGR	0 – 31%
BMEP	900 – 2100 kPa
Constants	**Set point**
Speed	1200RPM
Phi	1
Coolant Temperature	85 deg C
Mixture Temperature	38 deg C
Injection Pressure – Delphi 5-hole DI	17.2MPa
Injection Pressure – High-flow DI	13MPa
Injection Pressure – Optimized PFI	1.6MPa
LPG Composition / average LHV	>98% propane (HD-5) / ~46.34MJ/kg

6.3 Response Surface Method Optimization

Given the large number of variables that influence engine efficiency, a response surface method (RSM) technique was applied to optimize the efficiency of the heavy-duty LPG engine. The method involved a 2^k full factorial with center points design of experiments on the engine using the k = 5 variables and procedure shown in Table 6.3. In this case, the experiments were non-randomized and without replication except for the center point which had multiple replicates to provide an estimate of the error and to check the time trends. The five variables were chosen based on experience with the engine and previous engine data and results. The variables were BMEP, SOI, EGR, Injection pressure and the CIM. The factor (variables) effects and their interactions, which typically account for the response surface curvature [103] were studied and a steepest ascent/descent technique (a gradient search method) was used to optimize the desired parameter [104]. The objective function was to minimize BSFC (desired parameter), which translates to an increase in BTE. 32 corner points were tested on the engine in the full factorial 2^5 design. The factor levels spacings were chosen to be as aggressive as possible due to the unreplicated factorial design [103] of the experiments while also ensuring that the engine operated within its limits by leveraging the experience of previous engine results, for example, in picking a center point that allowed engine operation within the limits of engine stability and practical EGR rate increments given hardware limitations.

The half-cube plot in Figure 6.1 provides a visual representation of the experimental design where the "+" and "-" denote the high and low levels of a factor, respectively. The method involved two stages, experiments representing the 32 corner points which were combinations of the high and low factor levels of the five variables were run on the engine as well as several replicate runs of the center point (eight in this case). The responses (BSFC) from these 32 operating conditions

formed the data that was used to quantify factor effects, statistically relevant factor interactions, and ultimately, generate a steepest descent vector of the five variables that would trend the response in the desired direction (reducing BSFC). The second stage involved following the vector into the optimization space, testing the engine operating conditions along the vector until an inflection point (optimum point) was reached in terms of the response (BSFC). This point then served as the new center point for the next iteration of the optimization routine.

Table 6.3. Response surface method design template – Method of steepest descent

Objective Function: The Goal is to minimize BSFC					
Procedure					
1.	Select center point parameters				
2.	Select appropriate increments				
3.	Take data to complete cube				
4.	Follow optimization vector until objective function reaches minimum				
5.	Repeat process				
Parameters	BMEP (MPa)	SOI (deg bTDC)	EGR (%)	Injection Pressure (MPa)	CIM (%)
Value at center point	1.2	315	10	16	20
Increment (+/-)	0.2	15	5	2	5

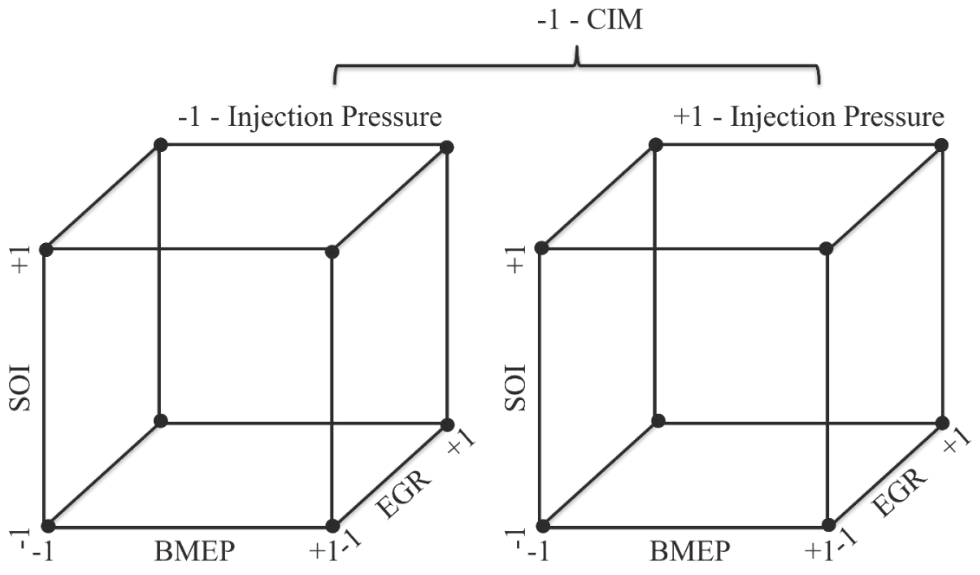

Figure 6.1. Half-cube plot of the five variables

The RSM optimization in this work was carried out in three phases. The first phase was with the 5-hole Delphi injector, the second phase was with the XDI high-flow injector, and the third phase was with the optimized PFI configuration which had only 4 variables due to the narrow window between the pressure required to maintain liquid LPG in the fuel delivery system and the injection pressure. The vector of operating conditions for the three phases as well as the factor effects of the five variables from phase 1 and the four variables from phase 3 are shown in Figure 6.2. The key takeaway from phase 1 was that the direction of increasing efficiency for injection pressure was to reduce it. This was counterintuitive given the desire to reduce injection duration by increasing injection pressure, however, a possible explanation for this trend was that at higher injection pressures, the momentum of the fuel spray forces it to sit at the bottom of the piston bowl preventing beneficial mixing with the charge air. There was also the increased possibility of liner impingement and crevice volume filling at these higher injection pressures. This trend of optimizing efficiency with decreasing injection pressure was also observed in phase 2 with the high-flow direct injector configuration. Given that the optimization vector of phase 1 indicated

that the direction of increasing efficiency was towards lower BMEPs, conflicting with the required project goals for high loads/peak torque efficiency and observing the limitations of the 5-hole Delphi injector in terms of flow rate and injection durations especially at high-loads, a subjective center point was chosen for the start of phase 2 and the injector changed to the high-flow XDI injector. The 32 corner points and replicated center points were tested once more and the vector of operating conditions followed until the inflection point. Due to the similarity of the high-flow XDI and the optimized PFI configurations in terms of performance as well as time limitations on the test cell, phase 3 was done in the optimized PFI configuration with four variables and $2^4 = 16$ corner points. This cut engine operating time and resources in half and still demonstrated the required optimization of the engine efficiency.

Optimization Vector – PHASE 1

Tested	BMEP	SOI	EGR	Injection Pressure	CIM	BSFC	
	12	315	10	160	20	207.5351	
1	12	319	11	157	22	203.8841	
2	11	323	13	154	24	198.0146	
	11	327	14	150	26		New center
3	10	331	16	147	28	196.1474	
	10	335	17	144	30		
4	9	339	19	141	32	193.2097	

Optimization Vector – PHASE 2

BMEP	SOI	EGR	Injection Pressure	CIM	BSFC	
11	327	14	150	26	194.7706	
11	331	17	149	28		
10	334	20	147	31	190.8722	
10	338	24	146	33	188.3637	new center
9	341	27	144	36	189.0592	
9	345	30	143	38		
8	348	33	142	40		

Optimization Vector – PHASE 3

BMEP	SOI	EGR	CIM	BSFC
10	338	24	33	184.5491
12	340	26	34	182.5843
14	343	28	35	182.1193
16	345	30	36	180.7142
18	347	**32**	37	
20	349	33	38	
22	352	35	39	

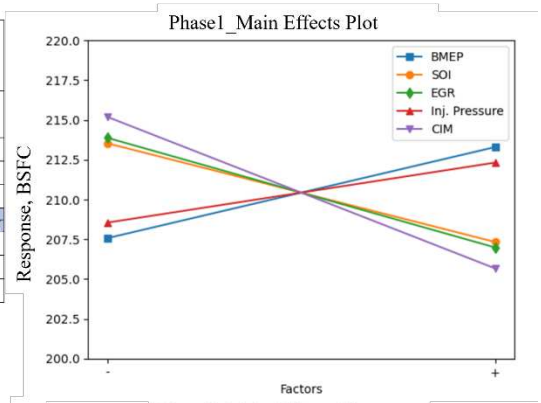

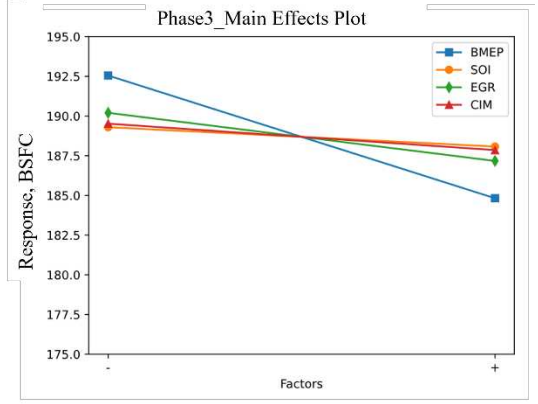

Figure 6.2. Optimization vectors for the three phases and the factor effects plot for phase 1 and 3

Figure 6.3 illustrates the successful application of the optimization technique, as BTE was increased by >16% from ~37% at the beginning of phase 1 to near-diesel efficiencies at ~43% at the end of phase 3. The EGR rate at the end of phase 3 had approached and exceeded the EGR limit meaning that the engine would have begun to experience severe misfires and unstable combustion if the vector was followed any further in that direction. Thus, the EGR rate would need to be dropped as an operating variable and a 2^3 full or fractional factorial design of experiments run for phase 4. However, the CIM tool was shown to be susceptible to engine noise specifically from the spark plug and this discouraged the continuation of the RSM optimization technique after the successful demonstration of its potential in order to protect the engine from damage at the higher loads the engine was now being operated at. Importantly, the RSM results pointed to the need to reduce injection pressure for optimized engine performance in the direct injection configurations, and this was critical in the achievement of the 44% target efficiency with the high-flow DI configuration as demonstrated in the one-factor-at-a-time design of experiments results discussed in the next section. All three phases of the RSM engine operation were conducted at 1200RPM, $\phi = 1$, and MAT = 38 deg C with the pre-chamber spark plug and the 14:1 high-squish piston on the heavy-duty liquid LPG engine.

6.4 Results and Discussion

6.4.1 Compression Ratio Optimization

The results from the compression ratio optimization investigations are discussed in this section. Start of injection and combustion phasing in terms of CA50 were varied on the engine at all tested compression ratios. The 3-D plots in Figure 6.4 demonstrate the relationship between compression ratio and key engine combustion, performance and emission metrics. Figure 6.4a indicates that combustion is mostly stable (COVimep < 3%) in the early start of injection timings for all CR

configurations due to the maximized mixture preparation time as explained in the section 5.3.1. There were islands of relative stability encountered at a few late SOI timings, while the region between 240 and 300 deg bTDC suffered from higher combustion instability than some later SOI timings pointing to the possible influence of other in-cylinder factors such as piston and valve position, combustion chamber design and spray dynamics on combustion stability. For example, the high squish 14:1 piston did not indicate any late SOI region of combustion stability with as high as 40% COVimep at the most retarded SOI timing. Figure 6.4b showed that the direction of improving efficiency is at higher compression ratios as backed by the literature [10, 11] and earlier SOI timings as previously demonstrated in section 5.3. For example, the 14:1 piston improved BTE by ~13% relative to the baseline 9.3:1 piston at 360 deg bTDC. Figure 6.4c described very interesting results for the bsNOx emissions as the maximum region was found at earlier SOI timings due to the reduced effect of the LPG spray charge cooling but not exactly at the earliest SOI times which would have the most reduced charge cooling effect. The minima also found as expected at retarded SOI timings due to the increased effect of the LPG spray vaporization cooling the charge and reducing combustion temperatures but not exactly at the most retarded SOI times. Even more interesting was the observed trend of CR 14:1 piston producing the lowest bsNOx while the CR 11:9 piston generated the highest bsNOx emissions. This was believed to be as a result of the superior design of the CR 14:1 piston specifically for LPG combustion and for better thermal management as despite the higher in-cylinder pressures and consequently temperatures the piston was exposed to, the CR 14:1 piston indicated similar exhaust gas temperatures (not shown) as the CR 11.9 piston at all tested CA50s. This led to comparatively better bsNOx emissions at this high compression ratio. Finally, the bsTHC emissions are presented in Figure 6.4d. The bsTHC plot demonstrates a distinct dependence on the COVimep as the regions of severe combustion

instability (retarded SOI timings, high 14:1 compression ratio) were also the regions of high THC emissions. The misfires and partial burns associated with the retarded injection timings were most likely responsible for this trend. Another possible contributor was the design of the 14:1 piston. The high squish design likely forces more charge into the crevice regions especially at the late SOI timings which is then reintroduced into the cylinder. The fraction of this charge which has now been reintroduced into the cylinder that escapes the late-cycle low temperature oxidation then proceeds into the exhaust stream as HC emissions.

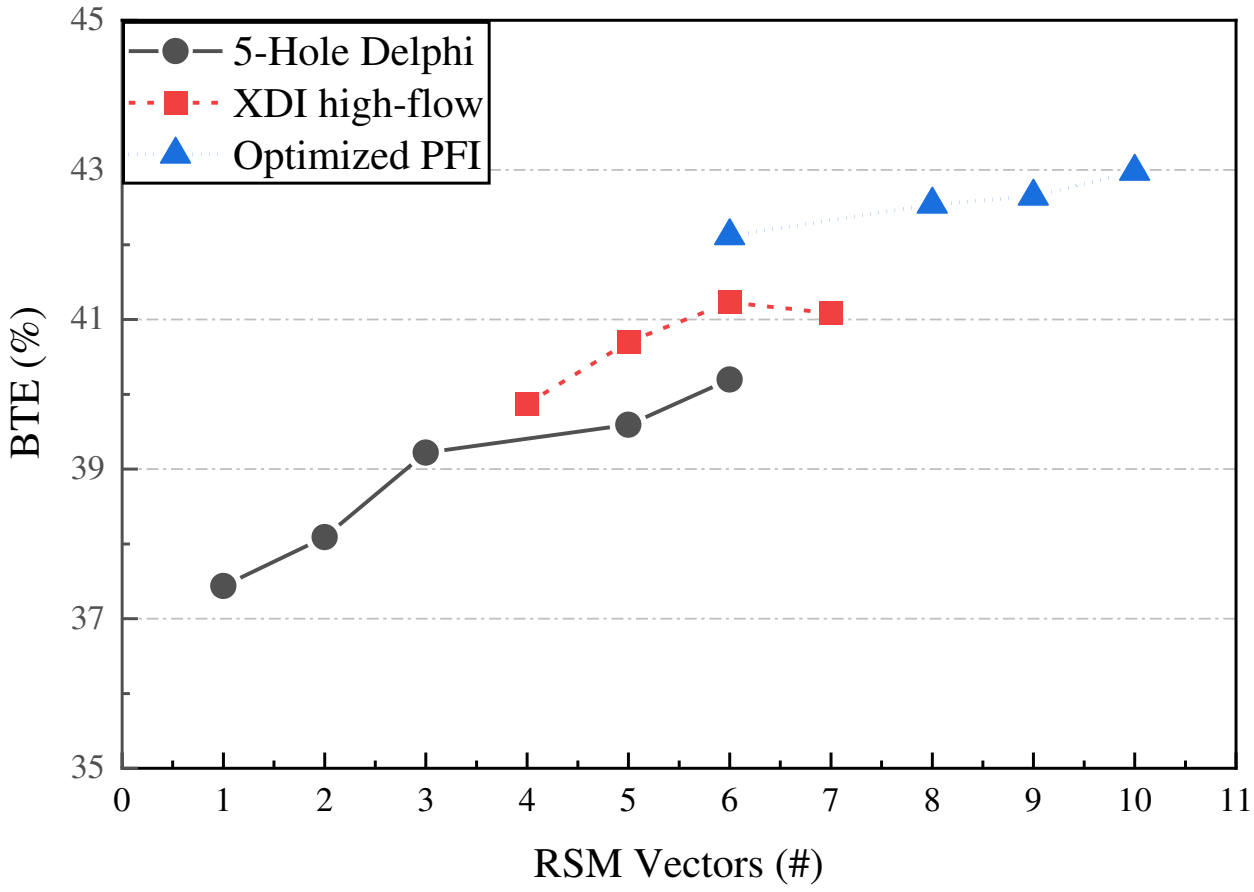

Figure 6.3. Response surface method efficiency optimization

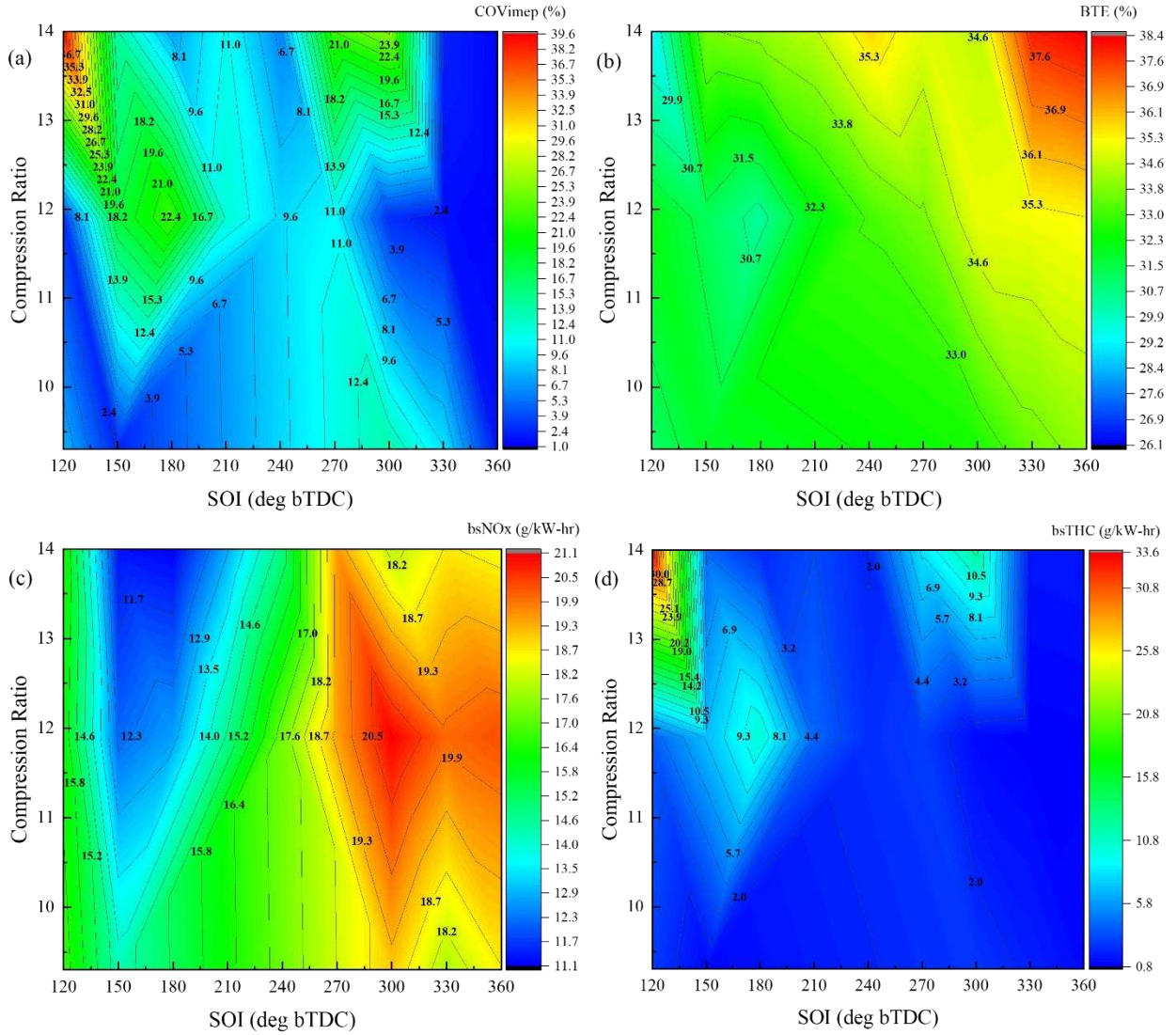

Figure 6.4. 3-D plots showing the relationship between compression ratio and (a) COVimep (%) (b) BTE (%) (c) bsNOx (g/kW-hr) (d) bsTHC (g/kW-hr) and SOI (deg bTDC) with the 5-hole DI configuration.

Upon conclusion of the SOI tests, the combustion phasing was advanced for all tested pistons from a retarded CA50 timing to the MBT combustion phasing. If the spark cannot be advanced until MBT before the occurrence of knock, the engine is said to demonstrate knock limited spark advance or be knock limited. The limits on the left of the 3-D plots in Figure 6.5 are the knock limits on the engine as compression ratio was increased, implying that the engine will transition into uncontrollable, abnormal combustion if the spark was advanced into that region. While there was some play left in this knock region for further slight advances of combustion phasing, these

tests were limited to safe intensities of medium knock as the knock limit. To further demonstrate the relationship of compression ratio with knock and combustion phasing, the knock ripple sum (KRS) is plotted in Figure 6.5a. As the center of combustion is advanced towards TDC leading to higher peak pressures and temperatures, the KRS increases. A similar effect was observed as compression ratio was increased up from 9.3 to 14 with a maximum KRS at CA50 10 deg aTDC for the CR 14:1 piston. A subjective KRS threshold of 4.2% was determined as the value above which the engine began to exhibit incipient knock in this study. The 4.3% line on Figure 6.5a shows that the higher compression ratios would require significant combustion phasing retardation to completely avoid knock with the LPG fuel on the heavy-duty engine. Next, the MBT timing was determined from the brake torque trends in Figure 6.5b. The MBT timing points to the combustion phasing where the combination of work done on the gas by the piston and work done by the gas produce the highest torque for a particular engine configuration. The lower compression ratios (9.3:1 and 11.9:1) showed that maxima somewhere between CA50 7 and 9, but then the engine began to exhibit knock limited spark advance as compression ratio was increased further as can be observed from the change of slope on the left limit of the 3-D curve. Nevertheless, CR 14:1 achieved the highest brake torque and BTE with the compression ratio configurations with 193.7Nm, ~4% higher than the peak torque at CR 9.3:1, and 39.1% BTE. The bsNOx trends in Figure 6.5c demonstrate similar patterns to those discussed earlier in Figure 6.4c in terms of their relationship with compression ratio. Combustion phasing had the effect of increasing bsNOx as phasing was advanced owing to the higher in-cylinder pressures as combustion is moved closer to TDC and the consequently higher temperatures which then promote the NOx formation chemistry. Figure 6.5d presents the relationship between bsTHC, combustion phasing and compression ratio. As combustion phasing is retarded, the engine experiences higher late cycle temperatures which

then improves the low temperature oxidation of the reintroduced charge from the crevices. This effectively reduces the bsTHC emissions as is shown in Figure 6.5d. On the other hand, as compression ratio is increased the in-cylinder peak pressures are also increased (demonstrated in the next figure), this increased pressure forces more charge into the crevices. This, along with the possibility of the high squish design forcing more charge into the crevices, was likely responsible for the increase in the peak bsTHC, from 1.13g/kW-hr at the baseline 9.3:1 compression ratio to 1.37g/kW-hr at the high squish CR 14:1 compression ratio configuration at the most advanced CA50 tested for each CR.

Finally, the in-cylinder pressures and apparent heat release rate curves are shown in Figure 6.6 for the three compression ratio configurations and the same engine operating condition. The CR 14:1 piston exhibited the highest peak pressures as mentioned earlier and the steepest rate of pressure rise amongst the three tested configurations. The CR 14:1 piston also indicated the highest peak rate of heat release and the shortest heat release duration of the three pistons. A significant observation in this plot is the presence of the distinctive shoulder on the AHRR curve for the CR 14:1 piston which pointed to the presence of a secondary combustion event or some end-gas auto ignition at this operating condition on the engine. Considering all factors, the CR 14:1 was shown to be a successful design and was moved forward for the BTE optimization tests.

6.4.2 Ignition Source Comparison

At the intermediate 11.9 ‘natural gas’ piston configuration, the ignition source was changed from the baseline 3-prong spark plug to the Woodward FTI prechamber spark plug. For both ignition sources, engine load in terms of BMEP was increased from 900kPa to 1800kPa, however, this BMEP increase was made possible with the introduction of EGR which allowed combustion phasing to be advanced by mitigating the much higher knock intensities at the high load and high

compression ratio conditions. This enabled the efficiency benefits of increasing engine load to become apparent on the engine. An important threshold in these BMEP+EGR combinations was the EGR limit defined in this chapter as the peak EGR (EGR_{peak}) which was the point at which the combustion stability metric, the $COV_{peak\ pressure}$ was maximized at ≤10%. At all conditions, this still correlated to a COV_{imep} < 3% which is the key determinant of combustion and engine stability in this work. An in-depth discussion on EGR, its effect on NOx and knock and the inflection point at which peak efficiency is achieved in correlation to the $COV_{peak\ pressure}$ as EGR is introduced has been presented in section 3.3.3 and chapter 4. The set of experiments described in the section were conducted to demonstrate the ability of the heavy-duty LPG engine to achieve higher engine loads and develop an understanding of EGR and the EGR_{peak} behavior on the heavy-duty LPG engine as well as determine any possible benefits of operating the LPG engine with a different ignition source than the baseline 3-prong spark plug. To do this, the combustion phasing advance upper limit was set manually by a KRS limit of 15% at which point the engine experienced light knock. Then EGR was added slowly at the desired engine load until EGR_{peak}. At this point, KRS was 10 < KRS <15%, BMEP was the desired value and EGR was at EGR_{peak} while other engine constants presented in Table 6.2 remained constant. This point differed significantly for the 3-prong and FTI prechamber configurations and the combustion characteristics are shown in Figure 6.7. Firstly, in terms of EGR both ignition sources tolerated different amounts of EGR at each BMEP with the 3-prong allowing 20%, 16%, 17% and 15% respectively as load was increased from 900 to 1200 to 1500 to 1800kPa while the FTI prechamber spark plug allowed 22%, 18.5%, 19%, 15% respectively at the same engine loads. Several studies have shown how the prechamber ignition concept can shorten main chamber heat release duration and improve combustion stability and efficiency for high octane number fuels including propane and natural gas [102, 105, 106]. Benajes

et al. particularly showed how passive prechamber design can affect EGR dilution tolerance with their prechamber design 2 concept falling way short of the design 1 in terms of EGR tolerance [106]. For the passive prechamber system used in study, the shorter heat release duration was likely responsible for the increase in EGR tolerance which then allowed combustion phasing to be slightly more advanced relative to the 3-prong spark plug as can be seen in the closer-to-TDC peak pressures in Figure 6.7. The combination of the slight advance in combustion phasing and higher EGR_{peak} consequently guaranteed higher efficiencies for the prechamber spark plug. However, as BMEP was increased up to 1800kPa, the combustion phasing had to be retarded to maintain the KRS at 15%, this hurt the efficiency as the highest efficiencies were recorded at 1500kPa BMEP for both tested ignition configurations.

Next, the ignition configurations were tested at the CFD optimized 14:1 compression ratio piston and the high-flow DI configuration. Figure 6.8 shows the comparison between the 3-prong spark plug and the prechamber spark plug at 1600kPa BMEP and EGR_{peak} as combustion phasing was advanced. The BTE was observed to be higher with the prechamber spark plug at all tested CA50 as presented in Figure 6.8a accounting for as much as a 1.2% absolute increase in BTE at the most advanced CA50 12.5 deg aTDC when compared to the 3-prong spark plug. The direct reason for this was the higher EGR_{peak} values once again demonstrated by the prechamber spark plug (~29%) compared to the ~26% EGR_{peak} for the 3-prong configuration. At stoichiometric conditions, this 3% increase in EGR reduces the in-cylinder temperatures further reducing heat losses and improves the gas exchange efficiency thus increasing efficiency. The operation of the passive prechamber spark plug involves forcing in-cylinder charge into the prechamber at high velocities, especially towards the end of the compression stroke, where mixing then happens rapidly. This mixture is then ignited and the combustion pressure differential between the prechamber and the

main chamber forces flame jets to exit the prechamber, increasing the flame surface area that can now ignite the extremely EGR-diluted mixtures in the main chamber and maintain short enough combustion durations that guarantee stable combustion. Figure 6.8b is also a direct consequence of the difference in EGR tolerance. Due to the 3% difference in EGR_{peak}, there was improved knock mitigation at all tested CA50s pointing to the possibility of further advancing the combustion phasing with the prechamber configuration and achieving even higher brake thermal efficiencies. At the most advanced CA50 tested of 12.5 deg aTDC, the 3-prong configuration had begun to exhibit medium knock while the prechamber configuration which exhibited a 47% reduction in knocking intensities at the same CA50 was only experiencing light knock. As combustion phasing was retarded in both Figures 6.8a and b, BTE and KRS reduced. This relationship between knock, efficiency and combustion phasing has been shown to be one of the key design limitations for spark ignited engines. The bsNOx emissions are plotted in Figure 6.8c for both configurations. Another direct consequence of the improved prechamber spark plug EGR tolerance was the higher level of mitigation of NOx emissions at the lower in-cylinder temperatures which effectively hampers the NOx formation chemistry. For both configurations, as combustion phasing was retarded in-cylinder pressures and temperatures are reduced which also effectively reduces engine out NOx. Finally, the bsTHC emissions are shown in Figure 6.8d. The passive prechamber ignition system can be seen to generate slightly higher HC emissions with the biggest difference at CA50 15 deg aTDC where it indicated ~9% higher bsTHC than the 3.01g/kW-hr measured for the 3-prong spark plug. The reason for this was believed to be three-fold. First, the higher EGR_{peak} was believed to contribute to more partial burns for the prechamber configuration. This effect was also responsible for the increase in bsTHC at retarded combustion phasing. Second, the lower temperatures associated with the higher EGR_{peak} for the prechamber configuration also could

reduce late cycle temperatures which are critical for the oxidation of crevice volume HCs reintroduced into the combustion chamber. Third, the prechamber concept was passive and unscavenged and as such any HC left after the flame jets exit the prechamber could contribute to the total engine-out HC.

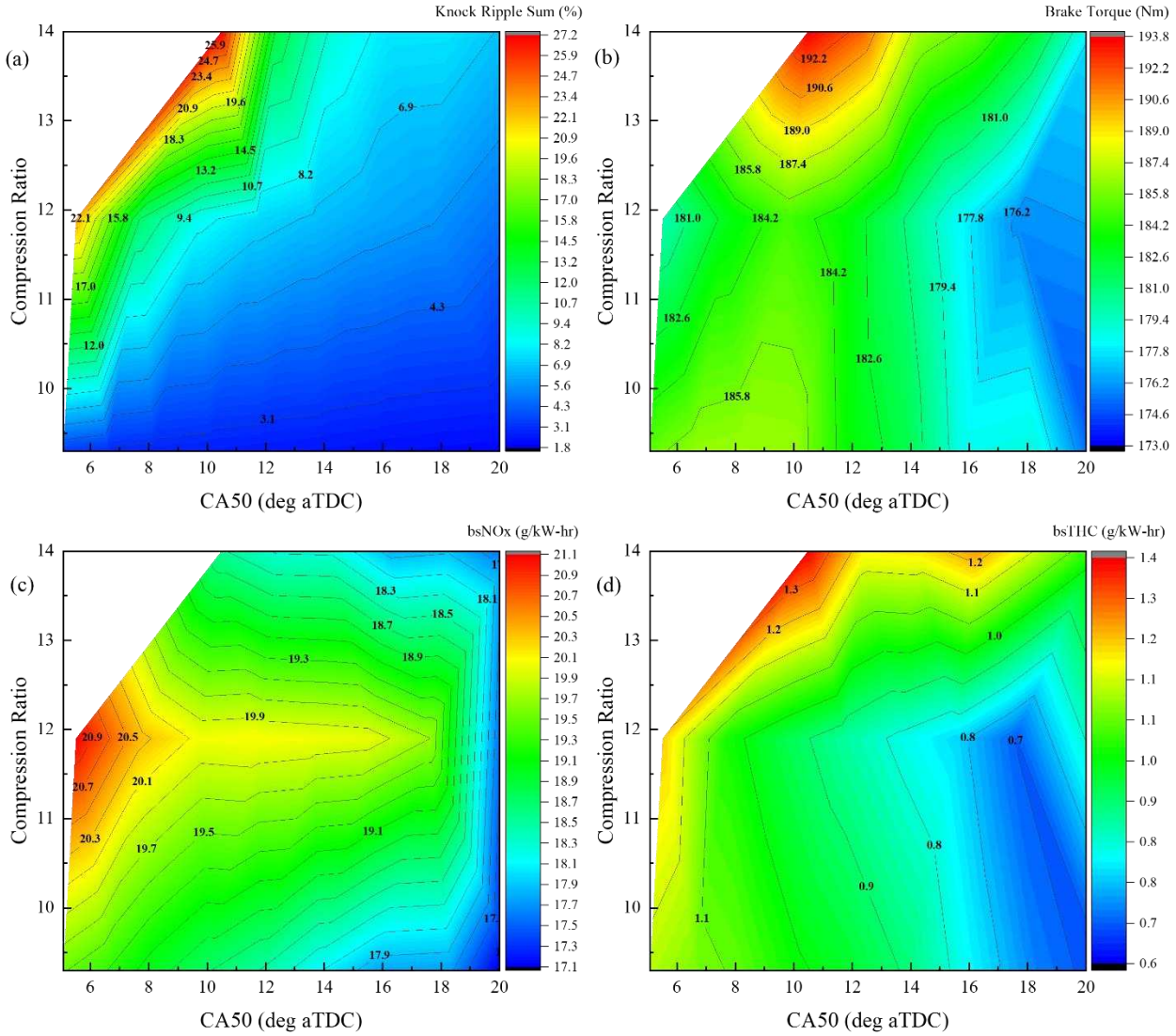

Figure 6.5. 3-D plots showing the relationship between combustion phasing and (a) KRS (%) (b) Brake Torque (Nm) (c) bsNOx (g/kW-hr) (d) bsTHC (g/kW-hr) and CR with the 5-hole DI configuration.

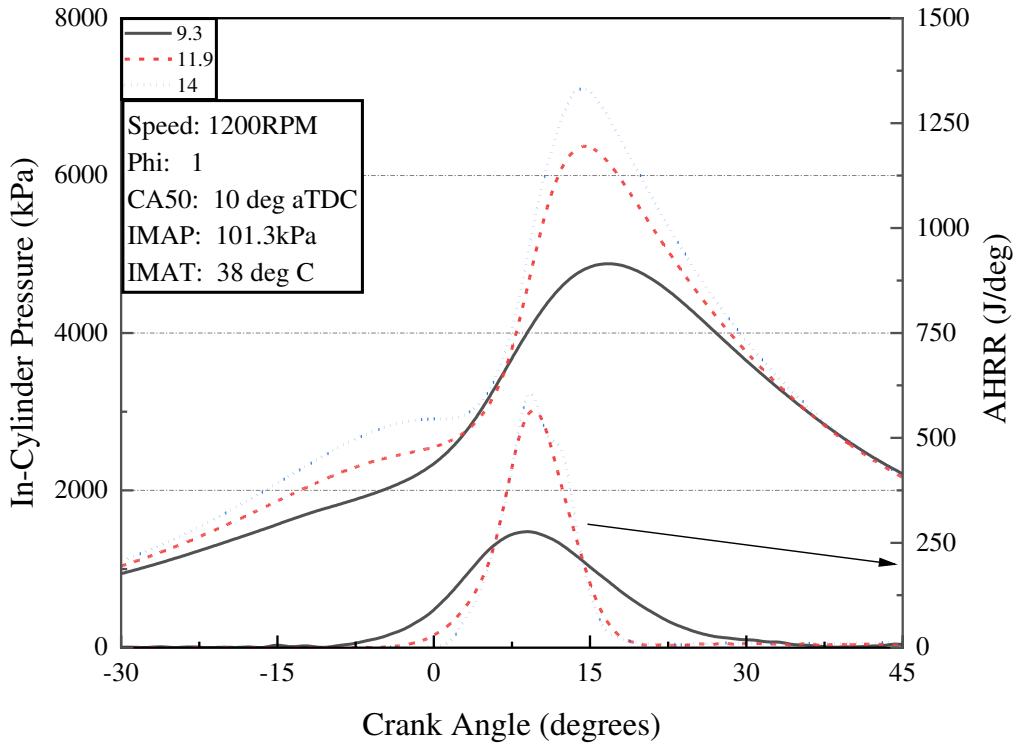

Figure 6.6. Combustion characteristics for the three compression ratio configurations on the engine

To conclude the section on the ignition source comparison, a regular J-gap spark plug was tested on the engine using the high flow DI and high squish 14:1 piston configuration. The J-gap spark plug exhibited pre-ignition and run-away uncontrollable knock as shown in the bottom right of Figure 6.9a. Figure 6.9a is a snapshot of the LECM interface during engine operation with the J-gap at CA50 20 deg aTDC, 1200RPM, MAT 38 deg C, naturally aspirated (101.3kPa), stoichiometric conditions. It is unclear why this happened, but a possible explanation was that the aggressive design of the 14:1 piston which was intended to maximize efficiency caused a knock event of substantial magnitude that deformed the J-gap electrode and caused instabilities in its operation. This was backed up upon uninstalling the J-gap from the engine, it was observed that the gap had been closed after only an hour of engine operation.

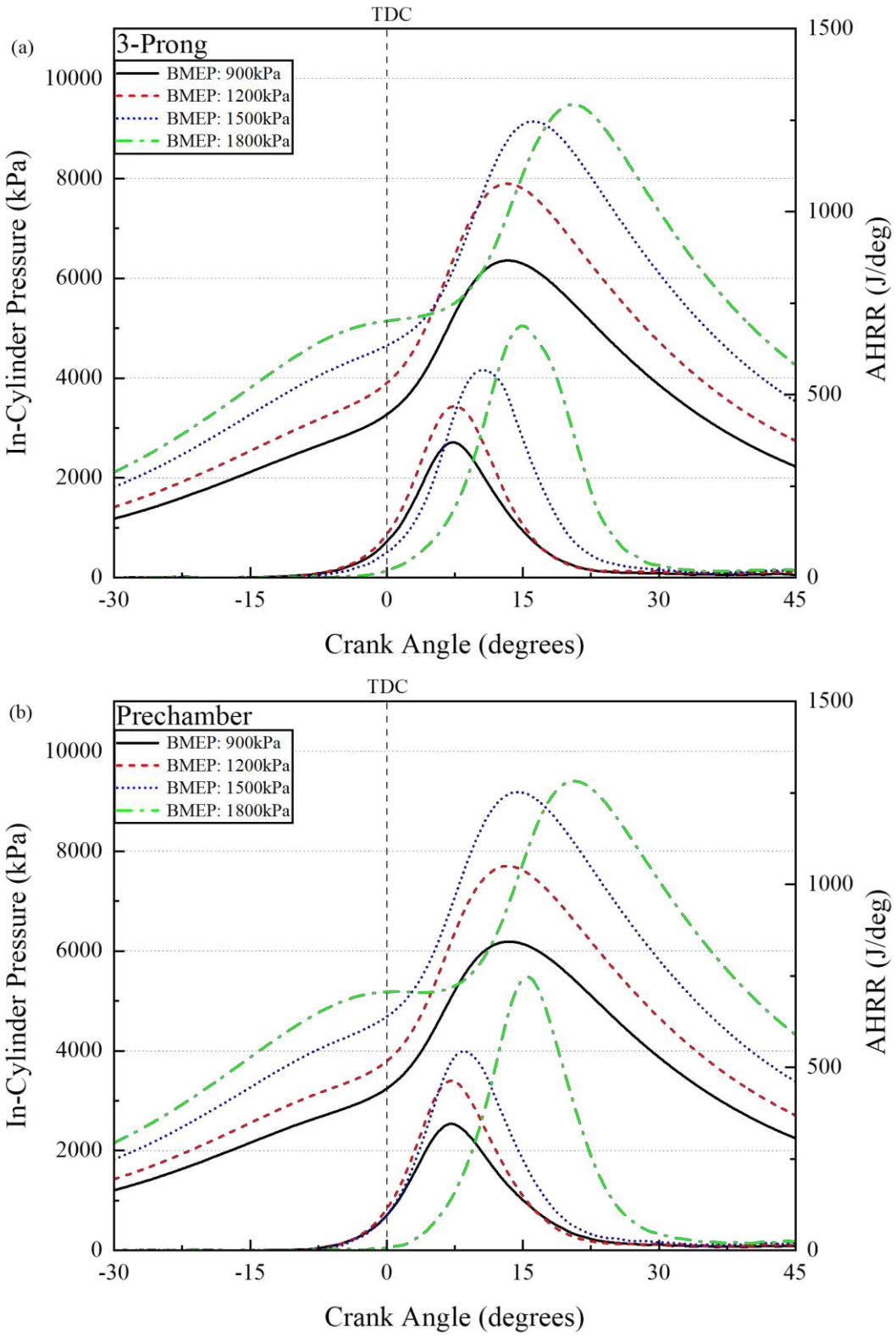

Figure 6.7. Combustion characteristics for the (a) 3-prong (b) Prechamber, ignition configuration on the heavy-duty LPG engine for the BMEP sweep with EGR_{peak} amount introduced at KRS 15% for the 5-hole Delphi DI configuration

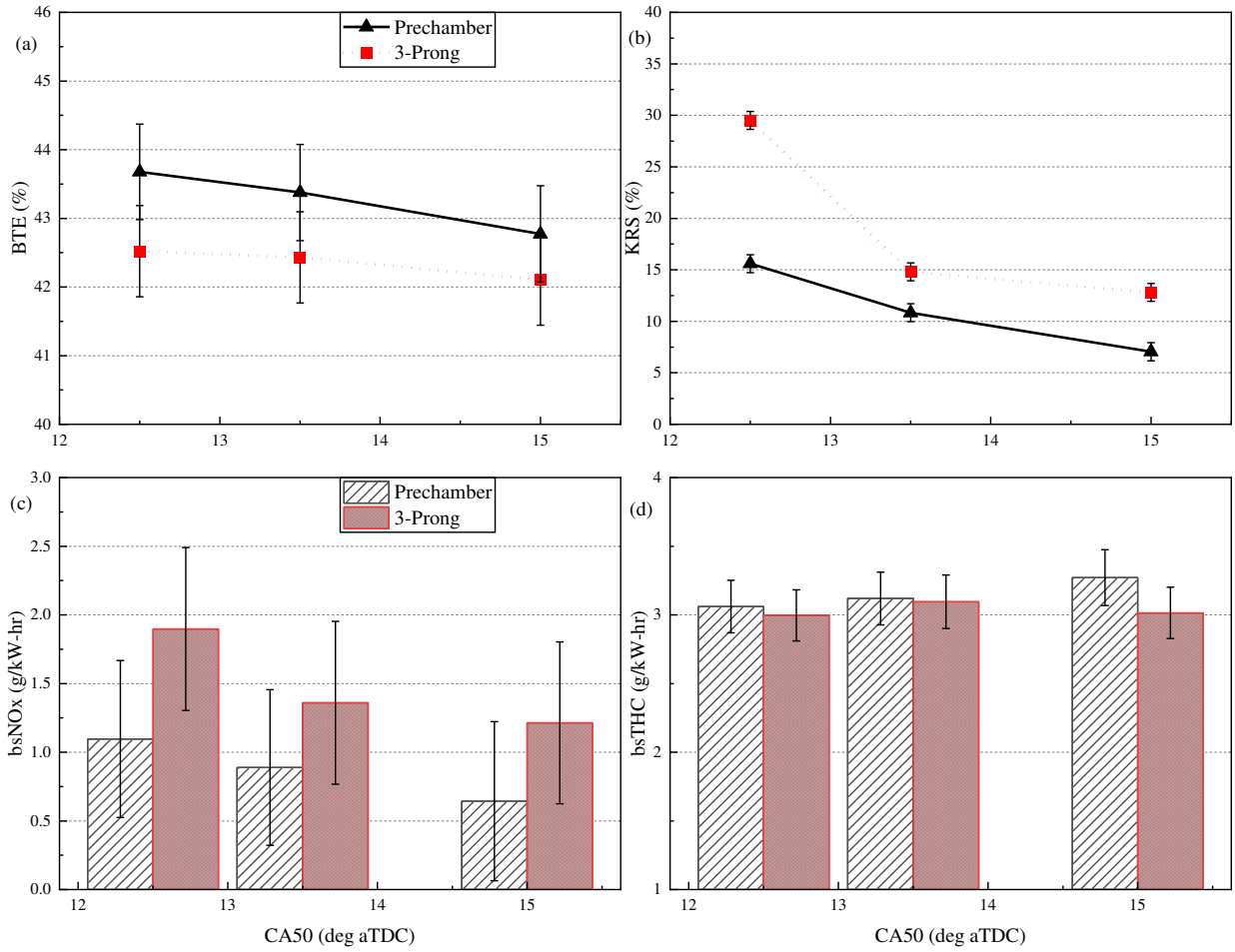

Figure 6.8. Plots of (a) BTE (%) (b) KRS (%) (c) bsNOx (g/kW-hr) (d) bsTHC (g/kW-hr) vs CA50 (deg aTDC) at 1600kPa BMEP + EGR_{peak} for the 3-prong Altronic and Woodward FTI prechamber spark plugs using the high flow DI and high squish 14:1 piston engine configuration.

For this reason, the J-gap tests were not extensive and were conducted solely at naturally aspirated conditions at the baseline BMEP of ~900kPa. This is an advantage of the advanced, robust ignition systems as they were perfectly capable of operating safely at low loads and then delivering near-diesel efficiencies for the heavy-duty LPG engine at advanced combustion scenarios such as the high boost, high EGR, high compression ratio configurations presented. Despite this, the trends in Figure 6.9b show some promise for the regular J-gap configuration with comparable efficiencies to the prechamber configuration at all tested CA50s. A possible reason for this is found in the literature [10], as the combustion gases and flame jets exit the prechamber channels, there is some

heat transfer to the walls and passageways that could effectively reduce the overall efficiency of the engine, just enough to match the regular J-gap performance at low loads in this case despite the prechamber spark plug's superior performance in advanced combustion scenarios. However, the $COV_{peak\ pressure}$ trends demonstrated this operational instability already discussed for the J-gap configuration.

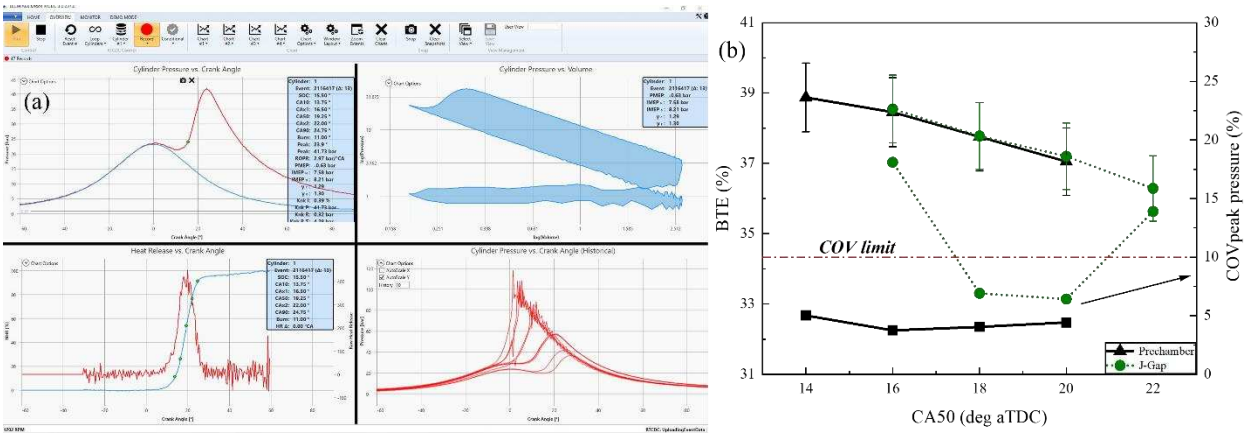

Figure 6.9. (a) Snapshot of the LECM interface during engine operation showing the in-cylinder pressure and heat release trends. (b) BTE (%) and $COV_{peak\ pressure}$ (%) vs CA50 (deg aTDC) for the J-gap and Prechamber sparkplug at naturally aspirated, stoichiometric conditions (high-flow DI, 14:1 piston)

6.4.3 Injection Configuration

With an understanding of the ignition source and compression ratio configuration effects, this final results section focuses on the injection configurations tested on the heavy-duty LPG engine to achieve target 44% brake thermal efficiency. Figure 6.10a shows the COV_{imep} for the three tested injection configurations; the 5-hole Delphi DI, the high-flow DI and the Optimized PFI. All configurations exhibited combustion stability at early SOI timings 360 and 330 deg bTDC as a result of the maximized mixture preparation time as discussed in chapter 5 and section 6.3.1. As SOI was retarded, the DI modes illustrated interesting trends with extremely unstable combustion at SOI 270 and 300 deg bTDC. This has also been discussed earlier in section 6.3.1 and chapter 5 as a possible contribution of other factors apart from mixture preparation time to combustion

stability. The stability of the high-flow and 5-hole Delphi DI configurations began to diverge as SOI continued to be retarded and the high-flow DI started to tend towards combustion stability again suggesting that at this engine configuration, the influence of mixing time overshadowed the effect of better mixture distribution which the 5-hole injector was designed to do. The biggest takeaway, however, was that the optimized PFI was insensitive to SOI timing and remained stable at all injection timings due to its location outside of the cylinder which naturally allowed sufficient mixing time. This stability trend for the optimized PFI was transferred to the BTE results shown in Figure 6.10b, however, the maximum efficiency was once again indicated at the earliest SOI timing, 360 deg bTDC for all injection configurations. The BTE curve could almost be read to be the inverse of the COV curve for all the three injection configurations with the optimized PFI configuration being the clear winner. For context, just after exhaust valve closing (SOI 360 deg bTDC), the optimized PFI was responsible for a ~2% and 3% relative improvement in BTE over the high-flow and 5-hole DI respectively. However, just after intake valve closing (SOI 150 deg bTDC) the relative improvement is more substantial with ~6% and ~16% respectively. The brake specific NOx and THC emissions are illustrated in Figure 6.10c and d respectively. The DI configurations consistently demonstrated lower NOx emissions when compared to the optimized PFI mode a trend which had been linked to the charge cooling properties of the vaporized LPG which would be more effective in DI mode and especially at retarded SOI timings. For the bsTHC emissions, the values were not too dissimilar between all three modes at the stable early SOI timings 330 and 360 deg bTDC but as combustion stability and misfire occurred more frequently for the DI modes, the bsTHC increased significantly peaking at 270 deg bTDC for the high-flow DI configuration and at the super unstable 120 deg bTDC for the 5-hole DI mode. Apart from the severely unstable regions at 270 and 300 deg bTDC, the high-flow DI and optimized PFI posted

comparable bsTHC emissions of ~1g/kW-hr across the SOI sweep. The high-flow DI mode indicated the lowest bsTHC emissions during these tests with 0.68g/kW-hr at 180 deg bTDC at which SOI the piston would be at bottom dead center. It was possible that this piston location combined with the short injection duration of the high-flow injector significantly reduced the volume of crevice-trapped vapors.

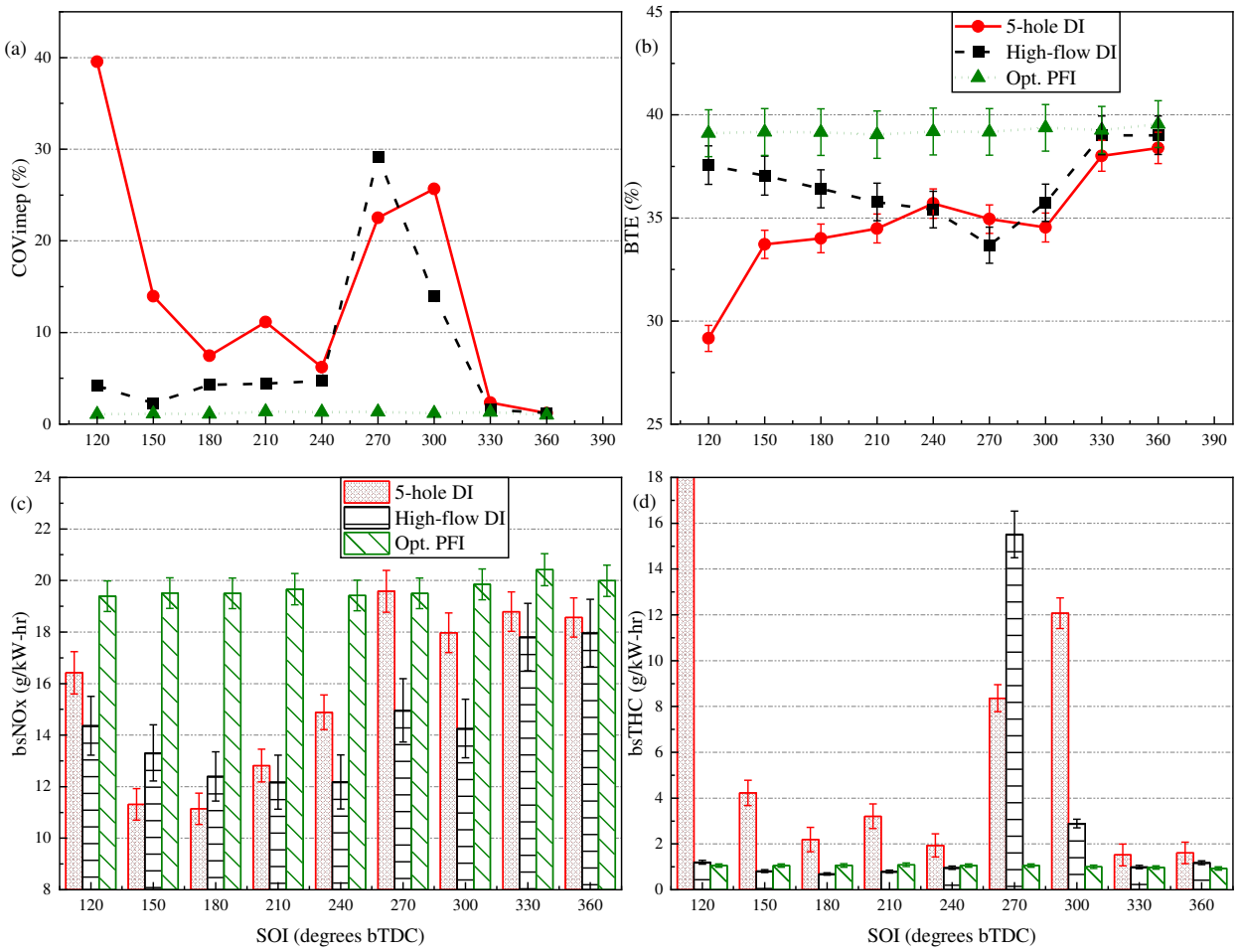

Figure 6.10. Plots of the (a) COVimep (%) (b) BTE (%) (c) bsNOx (g/kW-hr) (d) bsTHC (g/kW-hr) vs SOI (deg bTDC) for all three injection configurations.

Figure 6.11 illustrates the influence of varying the combustion phasing on key combustion, performance and emissions metrics for all three injection configurations. Following the SOI tests, the earliest SOI timing 360 deg bTDC was demonstrated the highest efficiency, best combustion

stability and acceptable levels of emissions was chosen for the combustion phasing tests. As combustion phasing in terms of CA50 was advanced towards TDC in Figure 6.11a, the BTE increased for all modes, with the optimized PFI and high-flow DI indicating similar engine efficiencies. The limitations of the 5-hole modified injector were now becoming more apparent as it consistently indicated about 0.8% lower efficiencies than the other two injection configurations in absolute terms. In terms of knock presented in Figure 6.11b, all three injection modes performed similarly, transitioning from incipient knock to light to medium knock at the most advanced timing. The 5-hole injector began to diverge from the other two modes and showed lower and lower knock intensities as CA50 was advanced possibly due to its longer injection duration reducing residence time for the LPG spray in the cylinder and improving the charge cooling effect closer to combustion. Again, the DI modes showed superior qualities in terms of bsNOx plotted in Figure 6.11c with ~11% and 15% reduction in bsNOx for the 5-hole and high-flow DI configurations respectively when compared to the 20.16g/kW-hr measured for the optimized PFI configuration. For the bsTHC emissions during these CA50 tests, the order was generally observed to be optimized PFI < high-flow DI < 5-hole modified DI. For example, as illustrated in Figure 6.11d the optimized PFI mode indicated a 32% reduction in bsTHC compared to the 5-hole modified DI configuration at CA50 18 deg bTDC. Finally, the bsTHC was observed to reduce with retarded CA50 for all injection configurations due to the increased late cycle temperatures which was expected as combustion happened later and later.

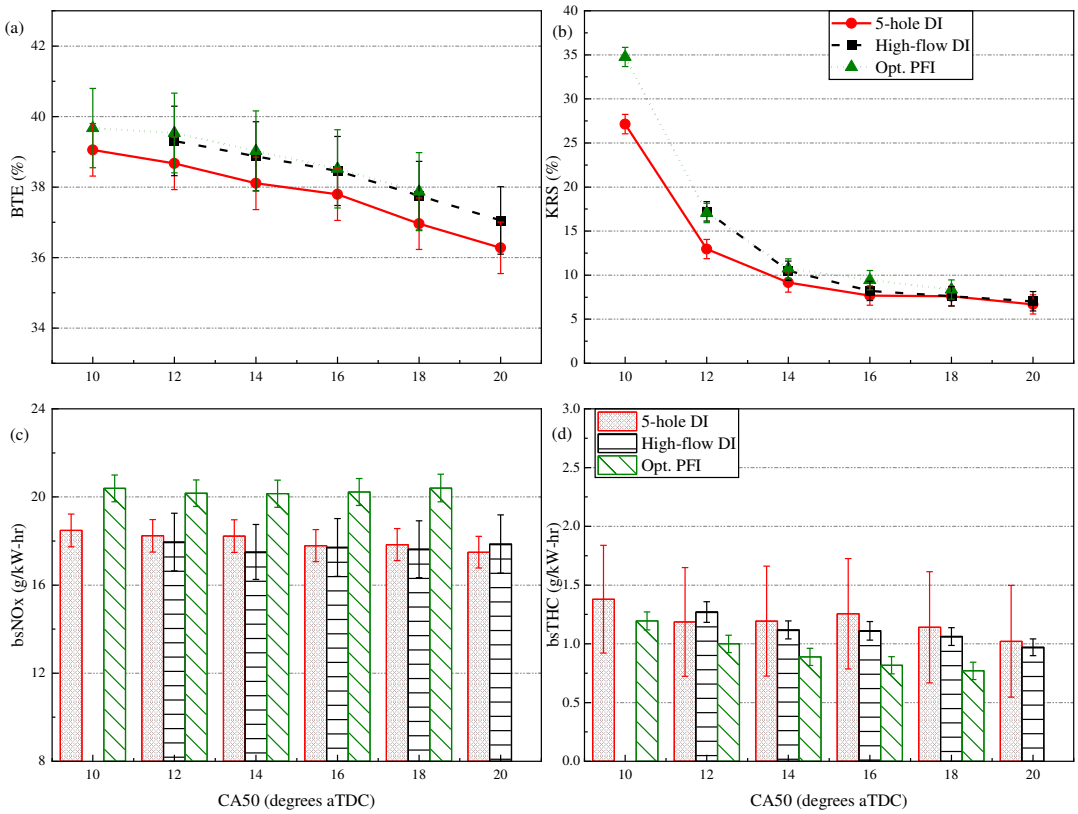

Figure 6.11. Plots of the (a) BTE (%) (b) KRS (%) (c) bsNOx (g/kW-hr) (d) bsTHC (g/kW-hr) vs CA50 (deg aTDC) for all three injection configurations.

Next, the injection configurations were tested with EGR at different engine operating conditions to better understand their overall performance and limits. First, EGR was introduced at low load conditions (900kPa BMEP) on the 11.9 'natural gas' piston with the baseline 5-hole modified injector and the 3-prong spark plug. The results are shown in Figure 6.12a for the EGR sweep at an early direct injection SOI timing (EDI) of 360 deg bTDC and a late direct injection SOI timing (LDI) of 120 deg bTDC. Two observations from Figure 6.12a are that the EGR_{peak} defined earlier in this chapter and introduced in chapter 3 for the CFR LPG engine also exists for the heavy-duty LPG engine just as the COV is about to cross its set limit of 3% for the COV_{imep} as shown in Figure 6.12a and 10% for the $COV_{peak\ pressure}$ shown previously. The second key observation was that the EGR_{peak} at LDI was found to be around 7%, which was then more than tripled to over 22% at the early DI condition. This had a knock-on effect on BTE as the BTE at EGR_{peak} for the EDI case

was 37.4%, ~11% relatively higher than the BTE at EGR_{peak} for the LDI scenario. Figure 6.12b shows the BTE, KRS and bsNOx as EGR was increased up to its limit at 360 deg SOI with the optimized PFI, the high squish 14:1 compression ratio piston and the prechamber spark plug configuration. The tests were conducted at low loads (1MPa BMEP). EGR has been shown to mitigate knock and NOx on the CFR engine in chapter 3 and 4 and in the literature [10], however, it was imperative to demonstrate this on the heavy-duty LPG engine in order to understand the EGR limitations and define an EGR_{peak} value. The EGR_{peak} for this configuration was measured to be 29% shown in Figure 6.12b at the inflection point after which BTE starts to trend downwards. Similar values were measured for the high-flow DI injector using the 14:1 compression ratio and prechamber spark plug engine configuration at the same engine operating conditions. In terms of bsNOx and knock mitigation, the results showed an 88% and 68% reduction respectively as EGR was increased from 15% to the EGR_{peak} value of 29%. This reduction continued beyond the EGR_{peak} point but BTE started to trend downwards as combustion stability began to suffer.

Finally, the baseline 5-hole DI configuration was compared with the other two injection configurations at high load and high EGR conditions and at 360 deg bTDC SOI. In Figure 6.13a, the baseline 5-hole modified injector is compared to the high-flow direct injector with the high squish 14:1 piston and prechamber configuration. Similar to the experiment design described in section 6.3.2, the BMEP is swept from 900kPa to 1200kPa to 1500kPa as EGR and spark advance was controlled to maintain a KRS ≤15% and a $COV_{peak\ pressure}$ ~10% for EGR_{peak}. The biggest difference between the DI modes was indicated at mid-loads (1200kPa) where the high-flow DI mode achieved a BTE of 43.2%, a 3% improvement on the BTE for the 5-hole modified mode in absolute terms. This was as a result of the increased EGR tolerance of the high-flow injector due to its shorter injection duration as shown also in Figure 6.13a. The high-flow injector cut the

injection duration by almost half at 1200kPa, thus allowing more time for the mixing with the recirculated exhaust gases to occur before relying on the added combustion stability benefits of the prechamber spark plug to ignite the mixture completely. At this mid-load 1200kPa point, the EGR_{peak} for the high-flow DI configuration was 21% compared to the 13% EGR_{peak} for the 5-hole modified direct injector at the same condition. Overall, the high-flow DI configuration showed significantly lower injection durations and thus longer mixture preparation times compared to the 5-hole DI configuration all low, mid and high conditions. It is important to note that the lower EGR_{peak} values recorded here were a direct result of the restriction on spark advance by the KRS 15% limit which meant the engine was more likely to run into misfire quicker. It will be shown in the final discussion in this chapter that advancing the combustion phasing allows more EGR to be added within the prescribed stability limits of the engine ($COV_{imep} < 3\%$ and $COV_{peak\ pressure} \leq 10\%$). Figure 6.13b presents the comparison of the optimized PFI and the 5-hole DI configuration using the same experiment design as above (EGR_{peak} at KRS 15%) but with the 11.9:1 natural gas piston and the 3-prong configuration. The BMEP sweep was conducted from low loads (900kPa BMEP) up until high engine loads (1800kPa BMEP) on the engine. Again, the 5-hole modified DI configuration was outperformed in terms of EGR_{peak} and BTE shown in Figure 6.13b. The optimized PFI achieved a BTE of 43% at 1500kPa BMEP with an EGR_{peak} of 26%. The increased injector flow with the double-injector system and the longer distance and time for mixing gave the optimized PFI the obvious edge over the 5-hole DI mode in terms allowing more EGR which in turn increased the efficiency of the engine. A possible explanation for the very high optimized PFI BTE achieved at this lower 11.9 compression ratio was that the more homogenous mixture from the PFI mode prevented rich pockets from forming at the cylinder and piston walls which would have more easily been auto-ignited, along with the charge cooling behavior of the vaporized liquid

LPG spray reducing the combustion temperatures and consequently mitigating knock. This allowed combustion phasing to be advanced to ~CA50 10 deg aTDC (close to MBT) for the high load conditions (1500kPa BMEP) before the KRS 15% limit was reached. The discussions so far in this chapter point to the high squish 14:1 compression ratio piston, the prechamber spark plug, and the optimized PFI and high-flow DI configurations as potential combinations to achieve the target 44% efficiency on the heavy-duty LPG engine.

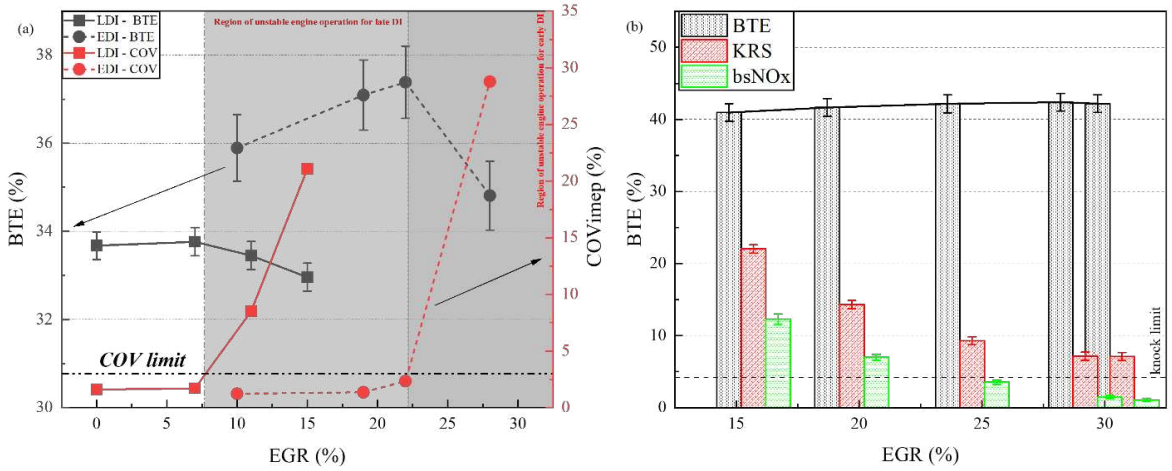

Figure 6.12. Plots of (a) BTE (%) and COV_{imep} (%) vs EGR (%) at late (120) and early (360) SOI timings (deg bTDC) for the 5-hole modified direct injector on the 11.9:1 compression ratio engine with the 3-prong spark plug and (b) BTE (%), KRS (%) and bsNOx (g/kW-hr)) vs EGR (%) for the 14:1 compression ratio engine with the prechamber spark plug, at early SOI 360 deg bTDC.

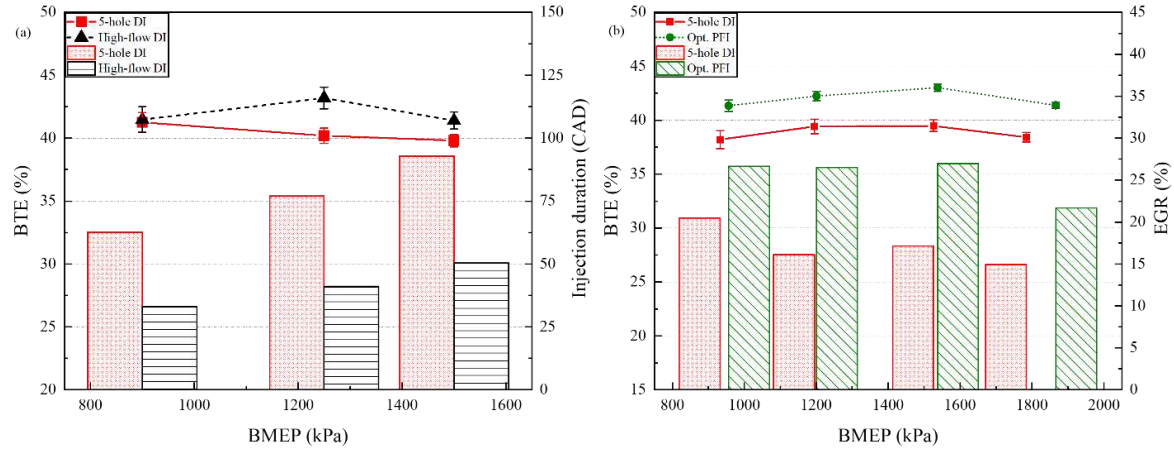

Figure 6.13. Plots of (a) BTE (%) and Injection duration (CAD) vs BMEP (kPa) for the DI comparison on the 14:1 compression ratio engine with the prechamber spark plug and (b) BTE (%) and EGR (%) vs BMEP (kPa) for the 11.9:1 compression ratio engine with the 3-prong spark plug, at constant engine conditions: 1200RPM, Phi:1, MAT:38 deg C, and SOI: 360 deg bTDC

Having narrowed the compression ratio, ignition source, and injection configurations to the best possible candidates, the engine was operated using the strategies that have now been shown to improve efficiency i.e., at engine conditions with EGR_{peak} and early SOI timings (single injection strategy). Maintaining the EGR_{peak} at 26% < EGR_{peak} 29% for all tested engine loads and the SOI at 360 deg bTDC, the CA50 was advanced at each engine load (BMEP) until the knock limit was reached on the left and retarded until misfire region was approached on the right of the 3-D plots in Figure 6.14. This was done using the optimized double-injector PFI and high-flow DI injection strategies with the prechamber spark plug and the 14:1 piston engine configuration. As the CA50 was advanced in Figures 6.14a and e, the BTE was shown to increase as BMEP was increased up until the desired 44% BTE in the region between 1500 and 1700kPa and CA50 9 – 12.5 deg aTDC for both the high-flow DI and the optimized PFI configuration. As the CA50 was retarded the engine crossed into misfire for both injection configurations at such high EGR rates. A key feature of both 3-D plots for the BTE was the shortened region of operation at higher loads which could possibly be due to the longer time now required to mix the larger air, fuel and EGR mixture required to produce the higher loads. Thus, further shortening the injection durations for the LPG injection hardware could be advantageous in achieving even higher loads and expanding the region of operability of the LPG engine. Figures 6.14b and f simply depict the trend towards end-gas auto-ignition as the region of operation of the LPG engine was shifted upwards and to the left (high BMEP, advanced CA50). In this regard, there was a possible competing effect of charge cooling with the direct injected liquid LPG spray for the high-flow DI configuration and the superior mixing of the optimized PFI configuration which would improve homogeneity in the combustion chamber. The DI charge cooling would likely reduce combustion temperatures and mitigate knock while the PFI mixing time and distance would possibly reduce the occurrence of locally rich

regions at the cylinder and piston wall that would more easily auto-ignite. The better mixture preparation time and distance was also likely responsible for the slightly higher EGR_{peak} observed for the optimized PFI configuration at all tested BMEPs. Figures 6.14b and f would suggest that these PFI benefits slightly edged out the DI one as the PFI was able to achieve slightly more advanced CA50s and the knock intensities observed with the PFI mode at the same condition as the DI were also slightly lower. For example, at 1400kPa BMEP and CA50 9, the optimized PFI recorded a KRS of 30.7%, 2.1% lower than the 32.8% recorded for the high-flow DI configuration. The bsNOx emissions are presented in Figures 6.14c and g for the high-flow DI and the optimized PFI configurations respectively. Both 3-D plots show the previously discussed tendency of the NOx emissions to increase with advanced CA50. However, of the two injection modes, the high-flow DI configuration produced higher bsNOx emissions despite the described charge cooling effect of the LPG spray vaporizing in the combustion chamber. It is important to put the numbers into context however as the highest bsNOx shown in Figures 6.14c (3.33g/kW-hr) was still over 83% lower than the ~20g/kW-hr bsNOx reported for the baseline PFI configuration in chapter 5. Even more significant was the fact that at the most efficient conditions on the engine the bsNOx reported was 1.7g/kW-hr for the high-flow DI configuration and 1.99g/kW-hr for the optimized PFI configuration. Finally, the bsTHC emissions are shown in Figures 6.14d and h for both injection configurations. The bsTHC was observed to be maximized in the mirror opposite direction to the bsNOx for both configurations, at the most retarded timings and low engine loads. This was counterintuitive as the THC trends have been shown to reduce with retarded CA50 due to the higher late cycle temperatures and their more effective oxidation of the crevice volume HC. However, in this scenario the tendency for poor, partial burns and misfires as CA50 was retarded at such high EGR dilution rates was most likely responsible for the uptick in the bsTHC in the

CA50 retard direction. In similar mirror opposite fashion to the bsNOx trends in Figure 6.14c and g, the bsTHC was minimized at higher loads and advanced CA50 for both configurations. Finally, the high-flow DI outperformed the optimized PFI configuration in terms of the bsTHC emissions, for example, at the most efficient operating condition for both configurations, the high-flow DI mode reported 9% lower bsTHC emissions than the optimized PFI configuration.

6.5 Conclusions

This final chapter presented the optimization of the heavy-duty LPG engine efficiency using the tools that have been developed over the preceding chapters and a response surface technique. These tools include the developed fuel delivery systems for the PFI and DI modes on the engine, the modification of a Delphi 7-hole OEM injector to a 5-hole design with nozzles aligned for central distribution of the LPG fuel in the combustion chamber considering the off-center location of the injector, the design of an optimized double-injector PFI adapter capable of achieving high loads on the engine. They also include the introduction of exhaust gas recirculation at high amounts, the modification of a high-flow off-the-shelf injector for installation and use in the heavy-duty LPG engine. Combining all these tools, the engine was operated in a number of different configurations and the results analyzed.

Engine compression ratio was optimized using the CFD models to produce the high squish 14:1 piston that achieved a ~13% relative improvement in BTE over the baseline 9.3:1 piston at 360 deg bTDC. The 14:1 piston achieved a peak BTE of 39.1% compared to the 34.4% baseline efficiency at naturally aspirated, stoichiometric conditions for the heavy-duty engine operated with the baseline 5-hole DI configuration. Despite indicating the highest in-cylinder pressures at all tested start of injection timings, the 14:1 high-squish piston maintained similar exhaust gas temperatures to the 11.9 ‘natural gas’ piston and also produced the lowest bsNOx for the start of

injection tests with 11.14g/kW-hr at SOI 180 deg bTDC which was 12% lower than the bsNOx for the 11.9:1 piston at the same condition. This pointed to better thermal management properties for the 14:1 piston unlike the 9.3 and 11.9 pistons and indicated the importance of properly designing the piston and compression ratio of the heavy-duty engine for LPG combustion.

The use of robust advanced ignition systems such as the prechamber spark plug was shown to be beneficial for LPG combustion on the heavy-duty engine allowing stable engine operation at higher EGR rates, higher compression ratios and higher loads when compared to regular ignition systems. The prechamber spark plug was responsible for a 3% improvement in EGR_{peak} values over the 3-prong spark plug, ~29% compared to ~26%, which then translated to a 1.2% absolute increase in BTE and a 47% reduction in knock intensities at the same operating conditions. However, the prechamber spark plug demonstrated a slight disadvantage in terms of bsTHC, generating 9% higher bsTHC when compared to the 3-prong spark plug at retarded conditions, due in part to its higher EGR tolerance. The regular J-gap spark plug showed some encouraging results at low loads on the 14:1 piston with comparable efficiencies to the prechamber spark plug but showed limitations in terms of high compression ratios as it ran into knock at low loads and advanced CA50 timings on the 14:1 piston.

Mixture preparation time, affected by injection duration and location, was established to be a key factor in LPG engine operation as it determined engine performance, combustion, and emissions. In this regard, the baseline 5-hole modified injector with the longest injection duration was outperformed by both the high-flow DI and optimized PFI configuration. For example, the optimized PFI configuration which was located much further upstream and had the longer mixing distance when compared to the DI modes indicated stable combustion at all tested start of injection timings while the DI modes showed best combustion stability at only the early start of injection

timings 330 and 360 deg bTDC. The optimized PFI mode was responsible for a ~2% and 3% relative improvement in BTE over the high-flow and 5-hole DI respectively at 360 deg bTDC (after EVC) and as air and fuel residence time increased for the optimized PFI and mixture preparation reduced for the DI with start of injection timing set after IVC (120 deg bTDC), the relative improvement became more substantial with ~6% and ~16% respectively. Compared just to the 5-hole modified DI configuration at CA50 18 deg bTDC and naturally aspirated conditions, the optimized PFI mode indicated a 32% reduction in bsTHC. For the DI modes, the high-flow direct injector indicated a 3% absolute improvement in BTE over the 5-hole modified mode at mid-loads (1.2MPa) where the high-flow DI cut the injection duration by almost 50%, thus allowing higher EGR_{peak}, 21% compared to the 13% EGR_{peak} for the 5-hole modified injector.

In DI configuration, the single, early injection strategy was found to be sufficient to achieve the 44% thermal efficiency goals of the project with liquid LPG. This simple strategy avoided the complexity of designing a more involved strategy while achieving the 44% target. The early single injection strategy (360 deg bTDC) was found to increase EGR_{peak} values by over 300% from 7% to 22% as well as achieving ~11% higher BTE at EGR_{peak} and generally more stable combustion when compared to the late single injection strategy (120 deg bTDC). Using this early single injection strategy, the high-flow DI configuration was coupled with the prechamber spark plug and engine load was increased up to 1.8MPa BMEP at EGR_{peak} and stoichiometric conditions. With this configuration, the 44% BTE target was achieved in the region between 1.5MPa and 1.7MPa BMEP and CA50 9 – 12.5 deg aTDC at EGR_{peak} of 28 – 29%.

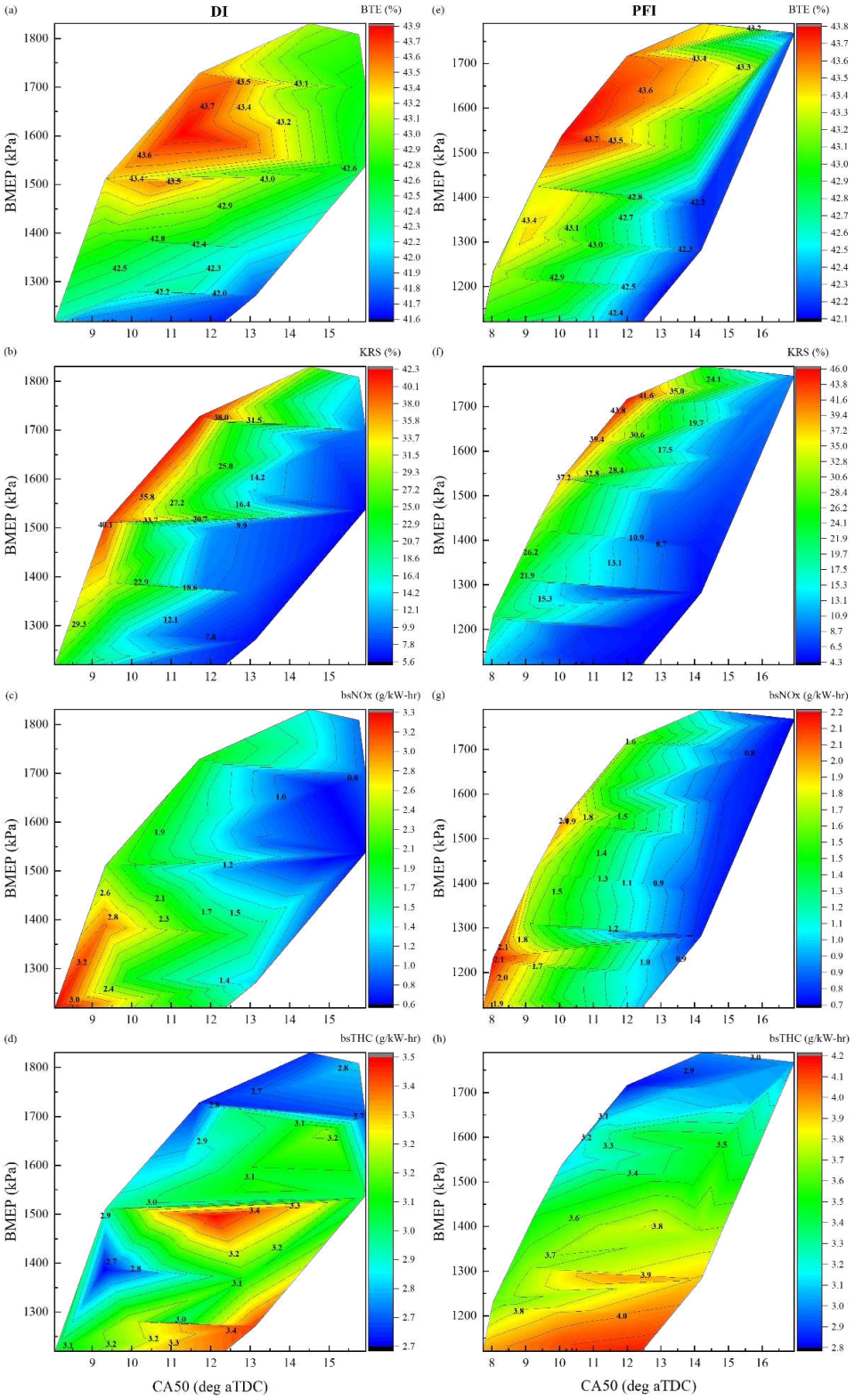

Figure 6.14. 3-D plots showing the relationship between BMEP (kPa) and (a) BTE (%) (b) KRS (%) (c) bsNOx (g/kW-hr) (d) bsTHC (g/kW-hr) for the high-flow DI configuration and (e) BTE (%) (f) KRS (%) (g) bsNOx (g/kW-hr) (h) bsTHC (g/kW-hr) for the optimized PFI configuration at EGR_{peak} and SOI 360 deg bTDC with the 14:1 and prechamber spark plug on the heavy-duty LPG engine.

In PFI configuration, designing a double-injector system with valve targeting was required to achieve the 44% thermal efficiency goals of the project. The double injector system was designed to achieve the higher loads and peak pressures associated with the target efficiency on the engine by simultaneously spraying liquid LPG onto the intake valves using the early 'single' injection event strategy. Like the high-flow DI mode, the optimized PFI configuration was combined with the prechamber spark plug and the high squish 14:1 compression ratio piston and achieved the target 44% BTE at BMEP > 1.5MPa, advanced CA50s and EGR_{peak} of 29%. The optimized PFI configuration demonstrated a slight advantage in terms of knock mitigation, achieving more advanced CA50s, generally lower bsNOx emissions but with higher bsTHC than the high-flow DI configuration as a result of its slightly higher EGR_{peak} values.

The response surface method optimization results demonstrated the viability of using design of experiments to cut down engine test time and resources while optimizing the objective function, as BTE was increased by over 16% from ~37% to near-diesel efficiencies at ~43% in just 3 iterations. Critically, the optimization technique showed that while increasing injector flow rate and reducing injection duration was paramount to increasing mixture preparation time and engine performance in direct injection configuration, consideration must be given to operating at optimal injection pressures. This was evident in the optimization results as the RSM technique showed that the direction of increasing efficiency for the DI modes was in the direction of reducing injection pressure. This finding played a huge role in achieving the 44% target efficiency on the engine as the high-flow DI configuration was operated at 13MPa injection pressure compared to 17MPa for the 5-hole modified injector.

The results from this chapter demonstrate the existence of several pathways to achieving the 44% target efficiency with LPG on a heavy-duty engine. The results also show the importance of

properly designing the critical engine components tailored for LPG operation to properly harness its potential and prevent knock and misfire. The pistons, ignition source, EGR system, fuel injection hardware, fuel delivery system, and injection strategies to mention a few were designed, developed or adopted throughout the course of this work. Finally, this chapter provides resolution on research questions 2, 3, 4 and 5 and successfully completes the work that was laid out at the beginning of the project which was to achieve near diesel efficiency on a heavy-duty engine platform using LPG.

CHAPTER 7. CONCLUSIONS AND RECOMMENDATIONS

7.1 Overview

This work began by showing the potential of LPG fueling in an SI engine. The strategies that were identified as key to achieving diesel performance parity on the heavy-duty platform were studied in detail on the CFR engine in this phase of the research. The experiments were conducted in comparison with CNG and LPG showed higher efficiencies compared to CNG but indicated higher knock intensities. Knock, which was more likely at higher loads and compression ratios was shown to be counteracted by the introduction of EGR as a diluent in the combustion chamber. EGR also mitigated NOx. Again, LPG indicated higher EGR dilution tolerance when compared to CNG, thus extending the region of knock-free operation, allowing further NOx mitigation, and improvement of the engine efficiency. The CIM tool was recalibrated for LPG operation and showed combustion benefits as well as the possibility of controlling end-gas auto-ignition to a desired fraction.

Next, the influence of LPG composition was studied on the CFR engine to determine how much effect this variability may have in practical operation. It was found that the typical components found in their varying amounts in different blends of LPG around the world had little to no effect on the performance of the engine. These components are typically ethane, propylene, and n-butane. The experiments however showed that the blend composition did have some effect on combustion and emission behavior of the engine. High amounts of n-butane made knock more likely to occur and the H:C ratio of the blend affected the carbon emissions.

The findings were then transferred to the heavy-duty engine where an experimental fuel delivery system was designed for the baseline study which consistently delivered liquid LPG at 16bar required for the baseline PFI configuration. A baseline piston was also successfully designed to

mimic the current LPG buses in operation and used for this evaluation. This baseline operation indicated a baseline efficiency of 34% on the heavy-duty LPG engine platform. It was shown that SOI had an insignificant effect on the combustion and performance behavior of the engine in baseline PFI mode. A knock study was done to determine the knock threshold of the engine in this configuration and to further understanding of the knock behavior of the LPG engine.

Further investigations were then carried out at this baseline 9.3:1 piston using the first generation of the LPG direct injector that was developed from a gasoline direct injector and modified for high pressure liquid LPG flow on this project. Based on the successful application of the PFI fuel delivery system concept, an improved version capable of delivering liquid LPG at 200bar was designed and installed. The same test conditions were run as with the baseline PFI configuration. The tests showed a noteworthy effect of SOI on the efficiency of the LPG engine in DI mode. It was discovered that mixture preparation time played a critical role in the performance of the LPG heavy-duty engine. The prohibitive injection duration required by the first-generation injector to deliver the amount of fuel was found to be a severe limitation to engine performance. The charge cooling effect, however, was shown in the mitigation of NOx by the DI configuration by almost half at retarded spark timings and the extension of the knock limit beyond the PFI value thus indicating the possibility of even higher compression ratios, loads, and consequently EGR with a more efficient direct injector.

The concluding phase of the research focused on the optimization process of the heavy-duty LPG engine to achieve the 44% target efficiency. Learnings from the preceding phases were streamlined to create configurations capable of achieving the desired efficiency. A new piston was designed using the CFD tool and the models that had been developed and validated over the course of the project. Advanced ignition systems were introduced to ensure combustion stability at high loads

and high EGR dilution rates. A high-flow direct injector that shortened injection durations by about half compared to the first-generation injector was modified for LPG operation on the heavy-duty engine. A second-generation direct injector with shorter durations compared to the first-generation injector and optimized in-cylinder fuel distribution was conceptually developed using the CFD tools but remains untested on a practical engine. The baseline PFI configuration was optimized for higher engine loads and injection location so as to take advantage of the rapid vaporization and charge cooling properties of the LPG fuel. A response surface optimization technique using a full factorial design of experiments was applied with five choice variables in DI mode and four in optimized PFI mode. Finally, engine load, EGR rates, and combustion phasing were varied at the developed engine configurations. A summary of the key findings is presented in section 7.2.

7.2 Conclusions

The most important outcome of this work is that it demonstrated that is possible to achieve diesel efficiencies with LPG on a heavy-duty engine in both direct injection and port fuel injection configuration. Both modes indicated specific advantages that can be harnessed depending on the application of the LPG engine to be developed. The high-flow direct injector achieved an engine high BTE of 43.85% at 1.6MPa BMEP and CA50 11.3 deg aTDC. This was achieved with the high squish 14:1 compression ratio piston, the prechamber spark plug and 29% EGR. At this condition, the bsNOx emissions were 1.73g/kW-hr, 91% lower than the baseline 9.3:1 bsNOx emissions, however, the bsTHC emissions were measured to be 2.86g/kW-hr, about 3 times higher than the baseline PFI values. Similarly, the optimized PFI configuration achieved an engine high BTE of 43.77% at 1.54MPa BMEP and CA50 10 deg aTDC using the 14:1 piston and the prechamber spark plug. The optimized PFI LPG engine indicated bsNOx emissions of 1.99g/kW-hr at this point and 3.14g/kW-hr of bsTHC emissions. For both configurations at these two

conditions, there was some level of end-gas auto-ignition, but in both cases the LPG engine was operated away from both the troublesome uncontrollable heavy knock and the misfire regions. A time-history plot of the BTE improvements during this research is shown in Figure 7.1. The plot tracks significant milestones in the efficiency improvements all the way from the initial CFR engine tests through the baseline 9.3:1 evaluation to the 11.9:1 piston configuration operated with DI and PFI, up until the 14:1 compression ratio points within the target region described above for the high flow DI and optimized PFI configurations.

In finer details, the research results showed that mixture preparation time is the most important factor in LPG heavy-duty engine performance. This was apparent with the high-flow direct injector which cut injection durations by about half at even lower injection pressures when compared to the 5-hole modified injector. Although the 5-hole injector nozzle pattern was modified specifically for this engine to improve in-cylinder fuel distribution, the influence of the disparity in injection durations overwhelmingly favored the high-flow injector even with its unmodified nozzle patterns. The RSM optimization results also showed that operating at an optimal injection pressure was critical to engine performance, as despite the desired higher injector flow rates at higher injector pressures, the likelihood of liner and piston impingement and fuel residing unmixed at the bottom of the piston bowl meant that engine efficiency was optimized in the direction of reducing injection pressure. For the optimized PFI configuration, this mixture preparation time was optimized in two ways as it had longer mixing distances due to its location upstream of the cylinder and thus had longer time to interact with the incoming EGR and air mixture. Shorter durations were also guaranteed with the double-injector system designed for the LPG heavy-duty engine. This two-fold attack on mixture preparation time showed some advantages for optimized PFI configuration as it extended the EGR limit slightly compared to the high-flow DI mode during the optimization

experiments. As a result, both the high-flow DI and optimized PFI configurations were able to achieve higher efficiencies than the 5-hole modified injector. Given this dependence on mixture preparation time, it was determined and shown that the early single injection event strategy was adequate and simple enough to meet the goals of the project. Still, even though mixture preparation time was determined to be the key factor in combustion stability and performance, the behavior of the LPG engine in DI mode at 270 and 300 deg bTDC start of injection timings compared to retarded timings such as 150 deg bTDC suggested that there were other important factors to be considered in LPG engine operation and injection strategy design such as piston location, combustion chamber design, valve position etc.

The use of advanced ignition systems took center stage in the latter stages of the research and the passive prechamber technology from Woodward was shown to encourage an increase in compression ratio, EGR dilution rates and efficiency, The prechamber spark plug outperformed the 3-prong spark plug by enabling stable combustion at higher EGR dilutions which was then translated to an ability to further advance CA50 at high loads and compression ratio and the attendant efficiency benefits. At similar engine conditions, the prechamber spark plug was responsible for as much as a 3% absolute increase in the EGR limit of the LPG heavy-duty engine and as much as a 1.2% absolute improvement in BTE. The prechamber spark plug was also robust enough to withstand the knock events triggered by the aggressive design of the high squish 14:1 piston which was one of the downfalls of the regular J-gap spark plug which showed comparable efficiencies to the prechamber spark plug at low loads and retarded timings but suffered severely at advanced timings even at low loads. This illustrated the critical role advanced ignition systems such as the prechamber and the 3-prong spark plug can play in the design of high compression ratio heavy-duty engines for LPG combustion.

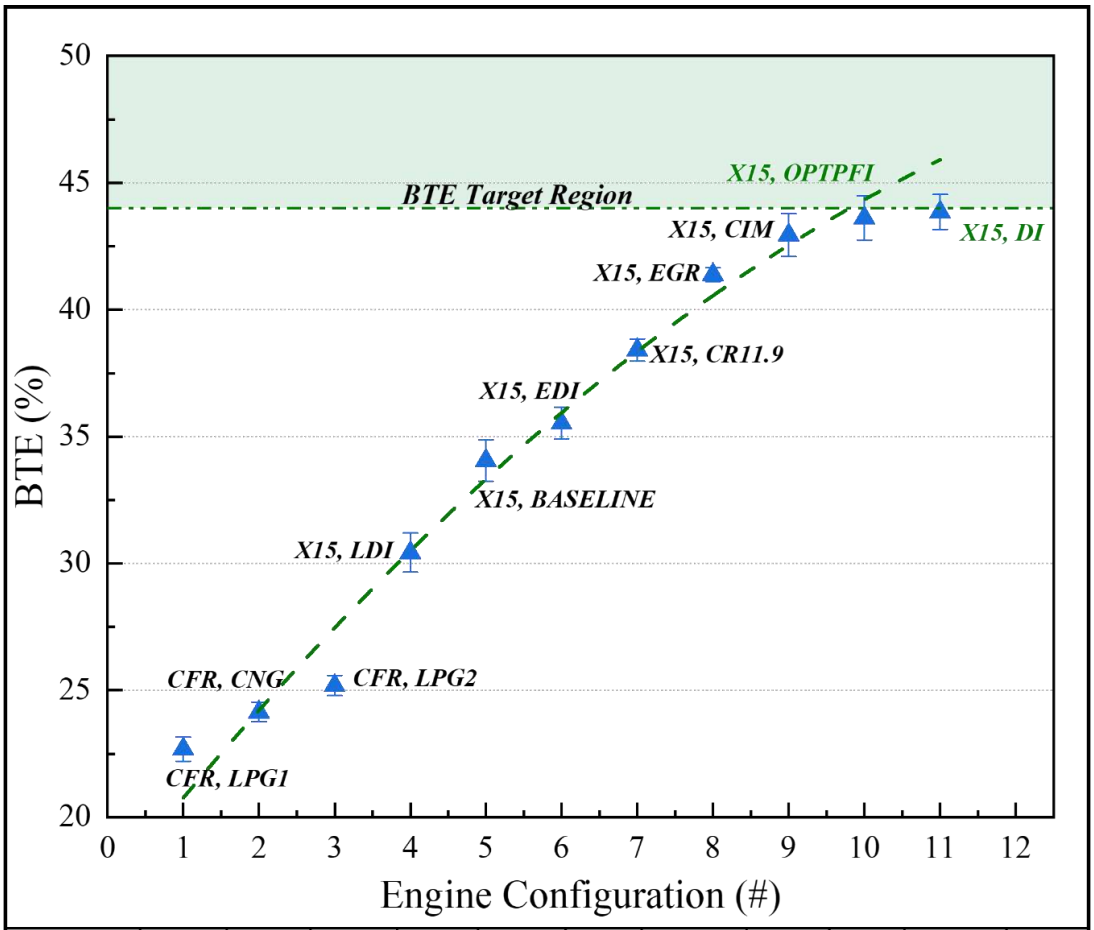

DETAIL	CFR, LPG1	CFR, CNG	CFR, LPG2	X15, LDI	X15, BASE LINE	X15, EDI	X15, CR11.9	X15, EGR	X15, CIM	X15, OPTPFI	X15, DI
BMEP (kPa)	528	724	736	815	900	1298	1784	1866	1271	1521	1605
EGR (%)	-	-	30	-	-	-	15	22	21	29	29
CA50 (deg aTDC)	9.6	9.4	8.8	15.5	8.8	9.3	16.2	16.5	10.7	11.5	11.3
CR	10	8	9	9.3	9.3	9.3	11.9	11.9	14	14	14
SPEED (RPM)	900			1200							
SOI (deg bTDC)	Premixed-gaseous			150, DI	120, PFI	360, 5-hole DI		360, PFI	360, DI	360, PFI	360, DI

Figure 7.1.Time-history of BTE for key engine operating conditions over the course of the study

Finally, proper compression ratio and piston design was shown to be critical in meeting the 44% efficiency target on the engine. The high squish 14:1 piston was developed using CFD and optimized for high loads and high EGR with direct injected liquid LPG. The aggressive 14:1 piston

design improved BTE by ~13% relative to the baseline 9.3:1 piston at 360 deg bTDC start of injection timing by attaining a BTE of 39.1% at naturally aspirated, stoichiometric conditions. The 14:1 piston indicated slightly higher bsTHC emissions linked to its high squish design but more importantly, the effect of a superior piston designed specifically for LPG combustion was apparent as the 14:1 compression ratio piston produced the lowest bsNOx compared to the CR 9.3 and 11:9 piston with the DI configuration. For example, for DI operation and at start of injection 360 deg bTDC and CA50 ~13 deg aTDC, the high squish 14:1 piston reduced bsNOx by ~1% and ~9% compared to the baseline 9.3:1 and 11.9 pistons respectively. Despite enduring higher in-cylinder pressures and consequently temperatures, the CR 14:1 piston indicated similar exhaust gas temperatures to the CR 11.9 piston at all tested CA50s.

7.3 Recommendations

The pathway to reaching the desired efficiency on the engine has opened several possible direction for future work. The most pertinent would be to improve LPG direct injector design for higher flow and shorter injection durations at lower pressures while optimizing nozzle patterns for proper fuel distribution depending on injector location. In this work, the injector had to be installed off-center in the cylinder as the spark plug was centrally located, a different set-up would require a different nozzle design. One way to quantify the benefits of developing an LPG direct injector with optimized nozzle patterns and higher flow would be to test the second-generation injector developed during the course of this project but not covered in this work.

Related to this would be the design of more involved injection strategies to determine benefits in terms of combustion, performance and emissions. In this work, the early single injection event strategy was used for both PFI and DI configurations. One possible strategy is the stratified DI injection with one early injection event to improve mixture preparation times and oner late

injection event to capitalize on the charge cooling properties of the rapidly vaporizing LPG spray. Another possible strategy is a mixed DI/PFI combination, where the benefits of improved mixing with PFI and the possibly higher EGR tolerance can be combined with either a late or early DI single injection event.

For PFI specifically but also a consideration with for the high-pressure pump in DI liquid LPG system, designing a system that is fitted to the heavy-duty engine unit while avoiding two-phase flow would fast-track the development of heavy-duty LPG engines as the results in this research work have demonstrated the immense benefits of the fuel in terms of engine performance, combustion, and emissions on a heavy-duty engine platform. A durability test stand that was used to characterize the modified LPG injector used in the larger LPG project which this research work was a part of introduced a cooling loop into the fuel supply system that was successful in curbing cavitation and pump failure. On a final note, the CIM which was calibrated for LPG operation on the CFR engine and the heavy-duty engine was used sparingly on the heavy-duty engine despite its combustion benefits as it was found to be susceptible to signal noises on the test cell, specifically, spark plug signal noises. The tool can be programmed more robustly to detect and disregard signal noises and therefore enable even more control of end-gas auto-ignition on the heavy-duty LPG engine leading to higher engine efficiencies.

References

1. US Energy Information Administration, Monthly energy review - December 2022 (2022)
2. Fuels Europe: Statistical report (2019)
3. Alternative Fuels Data Center (2019). [Accessed 20-Jun-2023]. Alternative Fuels Data Center: Maps and Data - Energy Use by Transportation Mode and Fuel Type
4. Kalghatgi, G. (2018). Is it really the end of internal combustion engines and petroleum in transport? In Applied Energy (Vol. 225, pp. 965–974). Elsevier Ltd. https://doi.org/10.1016/j.apenergy.2018.05.076
5. C. Bae, J. Kim, Alternative fuels for internal combustion engines, Proceedings of the Combustion Institute 36 (2017) 3389–3413.
6. M. Campbell, Łukasz P Wyszynski, R. Stone, Combustion of LPG in a spark-ignition engine, Source: SAE Transactions 113 (2004) 628–637
7. T. Fosudo, T. Kar, A. Marchese, B. Windom, D. Olsen. (2022). The Impact of LPG Composition on Performance, Emissions, and Combustion Characteristics of a Pre-mixed Spark-Ignited CFR Engine. SAE Technical Paper 2022-01-0476, 2022. doi:10.4271/2022-01-0476.
8. H. E. Saleh. Effect of variation in LPG composition on emissions and performance in a dual fuel diesel engine, Fuel 87 (2008) 3031–3
9. E. Elnajjar, M. Y. Selim, M. O. Hamdan. Experimental study of dual fuel engine performance using variable LPG composition and engine parameters. Energy conversion and management 76 (2013) 32–42.
10. J. B. Heywood, Internal Combustion Engine Fundamentals, 2nd Edition, McGraw-Hill Education, 2018.
11. J. P. Szybist, S. Busch, R. L. McCormick, J. A. Pihl, D. A. Splitter, M. A. Ratcliff, C. P. Kolodziej, J. M. Storey, M. Moses-DeBusk, D. Vuilleumier, M. Sjoberg, C. S. Sluder, T. Rockstroh, P. Miles. What fuel properties enable ¨ higher thermal efficiency in spark-ignited engines? Progress in Energy and Combustion Science 82 (2021).
12. D. Splitter, A. Pawlowski, R. Wagner. A historical analysis of the coevolution of gasoline octane number and spark-ignition engines, Frontiers of Mechanical Engineering 1 (2016)

13. M. Malenshek, D. B. Olsen, Methane number testing of alternative gaseous fuels, Fuel 88 (2009) 650–656.
14. D. M. Wise, D. B. Olsen, M. Kim, Development of a lean burn methane number measurement technique for alternative gaseous fuel evaluation, in: Internal Combustion Engine Division Fall Technical Conference, Vol. 56109, American Society of Mechanical Engineers, 2013, p. V002T02A014.
15. BS EN 16726:2015+a1:2018: Gas infrastructure. quality of gas. group H (2018).
16. Hampson, High efficiency natural gas engine combustion using controlled auto-ignition, in: Internal Combustion Engine Division Fall Technical Conference, Vol. 59346, American Society of Mechanical Engineers, 2019, p. V001T03A019
17. J. Mohr, The effect of fuel reactivity and exhaust gas recirculation on knock propensity of natural gas, master's thesis, Colorado State University (2020).
18. Bestel, S. Bayliff, A. Marchese, D. Olsen, B. Windom, H. Xu, Multidimensional modeling of the CFR engine for the investigation of SI natural gas combustion and controlled end-gas autoignition, in: Internal Combustion Engine Division Fall Technical Conference, Vol. 84034, American Society of Mechanical Engineers, 2020, p. V001T06A012.
19. J. Felipe Rodriguez, H. Xu, G. Hampson, B. Windom, A. Marchese, D. B Olsen, Heavy duty natural gas single cylinder research engine installation, commissioning, and baseline testing, Energy and Power Engineering 14 (06) (2022) 217–232.
20. S. M. Bayliff, Evaluation of controlled end gas auto ignition with exhaust gas recirculation in a stoichiometric, spark ignited, natural gas engine, master's thesis (2020)
21. M. Krieck, M. Gunther, S. Pischinger, U. Kramer, M. Thewes, Effects of LPG "Fuel formulations on knock and pre-ignition behavior of a DI SI engine, SAE International Journal of Engines 9 (2015) 237–251.
22. T. Kar, T. Fosudo, C. Slunecka, A. Marchese, B. Windom, D. Olsen, A study of propane combustion in a spark-ignited cooperative fuel research (CFR) engine, SAE Technical Papers (2022).
23. K. J. Morganti, M. J. Brear, G. D. Silva, Y. Yang, F. L. Dryer, The autoignition of liquefied petroleum gas (LPG) in spark-ignition engines, Proceedings of the Combustion Institute 35 (2015) 2933–2940.

24. Fosudo, T., Kar, T., Windom, B., Olsen, D. (2024). Low-carbon fuels for spark-ignited engines: A comparative study of compressed natural gas and liquefied petroleum gas on a CFR engine with exhaust gas recirculation. Fuel (360) 2024, 130456. https://doi.org/10.1016/j.fuel.2023.130456.
25. Nutu, N. C., Pana, C., Negurescu, N., Cernat, A., & Mirica, I. (2017). LPG as a Fuel for Diesel Engines-Experimental Investigations. IOP Conference Series: Materials Science and Engineering, 252(1). https://doi.org/10.1088/1757-899X/252/1/012079
26. Cinar, G., Eldamanhory, A., Akansu, S. O., Enes Fil, H., & Ilhak, M. I. (2020). Experimental Study On An SI Engine Fueled By LPG/Acetylene Mixtures. International Journal of Automotive Technology, 21(5), 1323–1331. https://doi.org/10.1007/s12239–020–0125–5
27. Selim, M. Y. E., Radwan, M. S., & Saleh, H. E. (2008). Improving the performance of dual fuel engines running on natural gas/LPG by using pilot fuel derived from jojoba seeds. Renewable Energy, 33(6), 1173–1185. https://doi.org/10.1016/j.renene.2007.07.015
28. Szybist, J. P., Busch, S., McCormick, R. L., Pihl, J. A., Splitter, D. A., Ratcliff, M. A., Kolodziej, C. P., Storey, J. M. E., Moses-DeBusk, M., Vuilleumier, D., Sjöberg, M., Sluder, C. S., Rockstroh, T., & Miles, P. (2021). What fuel properties enable higher thermal efficiency in spark-ignited engines? In Progress in Energy and Combustion Science (Vol. 82). Elsevier Ltd. https://doi.org/10.1016/j.pecs.2020.100876
29. Boronat, V., Splitter, D., & Dal Forno Chuahy, F. (2020). Achieving Diesel-Like Efficiency in a High Stroke-to-Bore Ratio DISI Engine under Stoichiometric Operation. SAE Technical Papers, 2020-April(April). https://doi.org/10.4271/2020-01-0293
30. Ravi, K., Bhasker, J. P., Alexander, J., & Porpatham, E. (2017). Influence of cooled exhaust gas recirculation on performance, emissions and combustion characteristics of LPG fuelled lean burn SI engine. IOP Conference Series: Materials Science and Engineering, 263(6). https://doi.org/10.1088/1757-899X/263/6/062069
31. Kar, T., Fosudo, T., Marchese, A., Windom, B., & Olsen, D. (2022). Effect of fuel composition and EGR on spark-ignited engine combustion with LPG fueling: Experimental and numerical investigation. Fuel, 327. https://doi.org/10.1016/j.fuel.2022.125221

32. Ge, W., D. F. Chuahy, F., Zhang, P., Sankaran, R., Splitter, D., DelVescovo, D., Lu, T., & Zhao, P. (2023). A direct numerical simulation study of the dilution tolerance of propane combustion under spark-ignition engine conditions. Combustion and Flame, 247. https://doi.org/10.1016/j.combustflame.2022.112495
33. Sawut, U., Tohti, G., Takigawa, B., Yamaguchi, S., Konagai, G., & Tsuji, T. (2009). Identification and Robust Control of LPG Fuel Supply System.
34. Tuan, N. T., & Dong, N. P. (2021). Theoretical and experimental study of an injector of LPG liquid phase injection system. Energy for Sustainable Development, 63, 103–112. https://doi.org/10.1016/j.esd.2021.06.002
35. Pradeep Bhasker, J., & Porpatham, E. (2016). LPG gaseous phase electronic port injection on performance, emission and combustion characteristics of Lean Burn SI Engine. IOP Conference Series: Earth and Environmental Science, 40(1). https://doi.org/10.1088/1755-1315/40/1/012069
36. Pradeep, V., Bakshi, S., & Ramesh, A. (2015). Direct injection of gaseous LPG in a two-stroke SI engine for improved performance. Applied Thermal Engineering, 89, 738–747. https://doi.org/10.1016/j.applthermaleng.2015.06.049
37. Watson, Harry & Pham, Phuong. (2007). Why Liquid Phase LPG Port Injection has Superior Power and Efficiency to Gas Phase Port Injection. 10.4271/2007-01-3552.
38. Tukiman, Mohd & Mustaffa, Norrizal & Mohd Ali, Mas Fawzi & Osman, Shahrul & Madon, Rais. (2016). A Comparative Study of an Lpg- Spark Ignition Engine using Liquid Sequential Injection Technique. MATEC Web of Conferences. 78. 01050. 10.1051/matecconf/20167801050.
39. Splitter, D., Boronat, V., Chuahy, F. D. F., & Storey, J. (2021). Performance of direct injected propane and gasoline in a high stroke-to-bore ratio SI engine: Pathways to diesel efficiency parity with ultra-low soot. International Journal of Engine Research, 22(12), 3Siere5–3488. https://doi.org/10.1177/14680874211006981
40. Dube, A., Vivekanand, M., & Ramesh, A. (2019). Experimental Studies on Liquid Phase LPG Direct Injection on a Two-Stroke SI Engine. SAE International Journal of Engines, 12(3). https://doi.org/10.4271/03-12-03-0023
41. Krieck, M., Günther, M., Pischinger, S., Kramer, U., Heinze, T., & Thewes, M. (2016). Future Specification of Automotive LPG Fuels for Modern Turbocharged DI SI Engines

with Today's High Pressure Fuel Pumps. SAE International Journal of Fuels and Lubricants, 9(3), 575–592. https://doi.org/10.4271/2016-01-2255

42. De Ojeda, W. and Wu, S.H. (2023). Development of a High-Pressure Fuel Injection System for Use with Propane-DME. SAE Technical Paper 2023-01-0403. doi:10.4271/2023-01-0403.
43. Sungha Baek, Kangjin Kim, Jaeho Cho, Cha-Lee Myung, Simsoo Park. (2021). Assessment of gaseous, particulate, and unregulated emissions from diesel compression ignition and LPG direct injection spark ignition minibus vehicles under the world harmonized vehicle cycle on a chassis dynamometer. Fuel (294) 120392. https://doi.org/10.1016/j.fuel.2021.120392.
44. Cha-Lee Myung, Kwanhee Choi, Juwon Kim, Yunsung Lim, Jongtae Lee, Simsoo Park. (2012). Comparative study of regulated and unregulated toxic emissions characteristics from a spark ignition direct injection light-duty vehicle fueled with gasoline and liquid phase LPG (liquefied petroleum gas). Energy (Volume 44) 1, 189-196. https://doi.org/10.1016/j.energy.2012.06.039.
45. Xu, B., Zhang, X., Xu, J., Qi, Y., Cai, S. (2013). Numerical analysis of homogeneous mixture formation for a direct injection liquid LPG engine. International Journal of Automotive Technology. 14. 857-865. 10.1007/s12239-013-0094-z.
46. Xu, B, Qi, Y.L., Sun, C.D., Ma, J.Z. (2016). Numerical Investigation on Mixture Formation of Two-Stroke LPG Direct Injection Engine Used as Range Extender for Electric Car. Proceedings of the ASME 2016 Internal Combustion Engine Division Fall Technical Conference. ASME 2016 Internal Combustion Engine Division Fall Technical Conference. Greenville, South Carolina, USA. October 9–12. V001T06A007. ASME. https://doi.org/10.1115/ICEF2016-9334
47. Boyan, X., Longlong, J., Chaodong, S., Ma, J.Z. (2018). Numerical Analysis of the Mixture Formation in a Two-Stroke Wall-Guided LPG DI Engine for Extended-Range Electric Vehicle. Int .J Automot. Technol. 19, 313–321. https://doi.org/10.1007/s12239-018-0030-3
48. Boretti, Albert & Watson, Harry. (2009). Development of a Direct Injection High Efficiency Liquid Phase LPG Spark Ignition Engine. SAE International Journal of Engines. 2. 1639-1649. 10.4271/2009-01-1881.

49. US. Department of Energy Vehicles Technologies Office. (2018). Advanced Combustion Engines and Fuels 2018 Annual Progress Report
50. Davis, S. C., & Boundy, R. G. (2022). Transportation Energy Data Book: Edition 40. ORNL/TM-2022/2376
51. Melaina, M. W., Heath, G., Sandor, D., Steward, D., Vimmerstedt, L., Warner, E., & Webster, K. W. (2013). Transportation Energy Futures Series: Alternative Fuel Infrastructure Expansion: Costs, Resources, Production Capacity, and Retail Availability for Low-Carbon Scenarios.
52. Sloan, M. M. (2016). Propane Market Outlook Key Market Trends, Opportunities, and Threats Facing the Consumer Propane Industry Through 2025. www.icfi.com
53. Rengarajan, S., Liu, Z., Lerin, C., Stetter, J. et al. (2020). LPG Direct Injection Engine for Medium Duty Trucks. SAE Technical Paper 2020-01-5008. doi:10.4271/2020-01-5008.
54. AEGPL. (2013). Autogas in Europe, The Sustainable Alternative. An LPG Industry Roadmap.
55. Renewable Propane. [Online]. Available: Environment | PERC (propane.com) [Accessed 18-Jul-24]
56. T. Kar, T. Fosudo, B. Windom, D. Olsen, J. Hoke, J. Rogers, Development of a liquid-phase LPG delivery system for direct injection, spark-ignited engines, in: Internal Combustion Engine Division Fall Technical Conference, Vol. 86540, American Society of Mechanical Engineers, 2022, p. V001T07A005
57. Grondin, Oskar. Moulin, Peter. Chauvin, James. (2009). Control of a turbocharged Diesel engine fitted with high pressure and low-pressure exhaust gas recirculation systems." Proceedings of the 48h IEEE Conference on Decision and Control (CDC) held jointly with 2009 28th Chinese Control Conference, Shanghai, pp. 6582-6589.
58. Compression ratio [Online]. Available: https://www.autoprotips.com/what-is-compression-ratio-petrol-and-diesel-engine/ [Accessed 19-March-23]
59. Felipe, J., Rueda, R., Olsen, D. B., Windom, B., Baker, D., & Quinn, J. (2023). Expanding The Knock/Emissions Limits for The Realization of Ultra-Low Emissions, High-Efficiency Heavy-Duty Natural Gas Engines. Colorado State University, PhD Dissertation.

60. Fosudo, T., Kar, T., Windom, B., Schlagel, J. et al. (2023). Performance, Combustion and Emissions Evaluation of Liquid Phase Port-Injected LPG on a Single Cylinder Heavy-Duty Spark Ignited Engine. SAE Technical Paper 2023-01-0245. doi:10.4271/2023-01- 0245
61. Altronic, “Ignition Accessories,” [Online]. Available: https://www.altronic-llc.com/wp-content/uploads/Ignition-Accessories.pdf [Accessed 13-Jul-24]
62. Woodward Inc, "FTI-Family FAST TURBULENT IGNITER," [Online]. Available: https://www.woodward.com/en/shop/woodward44-electronic-controls/fti-family. [Accessed 13-Jul-24].
63. Mizushima, N., Sato, S., Ogawa, Y., Yamamoto, T. et al., “Combustion Characteristics and Performance Increase of an LPG-SI Engine with Liquid Fuel Injection System,” SAE Technical Paper 2009-01-2785 (2009), https://doi. org/10.4271/2009-01-2785.
64. Kim, Y., Lee, Y., Kim, C., and Shin, M., “Effects of Shape and Surface Roughness on Icing and Condensation Characteristics of an Injector in a Liquid Phase LPG Injection System,” Fuel 132 (2014): 82-92, https://doi. org/10.1016/j.fuel.2014.04.010.
65. Battino, R., Rettich, R., and Tominaga, T., “The Solubility of Nitrogen and Air in Liquids,” Journal of Physical and Chemical Reference Data 13, no. 2 (1984): 563-600, https:// doi.org/10.1063/1.555713
66. Urban, C., and Sharp, C., “Computing Air/Fuel Ratio from Exhaust Composition,” Natural Gas and Alternative Fuels for Engines ASME 1CE-Vol. 24, 1994.
67. J. Wheeler, A. R. A. R. Ganji, Introduction to engineering experimentation / Anthony J. Wheeler, Ahmad R. Ganji; with contributions by V. V. Krishnan, Brian S. Thurow, 3rd Edition, Pearson Higher Education, Upper Saddle River, N.J., 2010.
68. C. Slunecka. (2023). Autoignition and flame speed of premixed liquefied petroleum gas in a rapid compression machine: Experimental results and reduced chemical kinetic mechanism. Master’s thesis, Colorado State University.
69. BS EN 16726:2015+a1:2018: Gas infrastructure. quality of gas. group H (2018).
70. Alternative Fuels Data Center: Fuel Properties Comparison [Online]. Available: https://afdc.energy.gov/fuels/properties [Accessed 12-Jun-2023]

71. M. Moussavi, M. AI-Turk. (1993). Compressed natural gas and liquefied petroleum gas as alternative fuels, J. Energy Eng 119 168–179.
72. G. T. Kalghatgi. (2014). The outlook for fuels for internal combustion engines, International Journal of Engine Research 15 383–398.
73. P. Bielaczyc, A. Szczotka, J. Woodburn. (2016). A comparison of exhaust emissions from vehicles fueled with petrol, LPG and CNG, IOP conference series. Materials Science and Engineering 148 (1) 12060
74. U¨mit Ag˘bulut, M. Karago¨z, S. Sarıdemir, A. O¨ztu¨rk. (2020). Impact of various metal-oxide based nanoparticles and biodiesel blends on the combustion, performance, emission, vibration and noise characteristics of a CI engine. Fuel 270 117521.
75. T. Kar, Z. Zhou, M. Brear, Y. Yang, M. Khosravi, J. Lacey. (2022). A comparative study of directly injected, spark ignition engine combustion and energy transfer with natural gas, gasoline, and charge dilution, SAE International Journal of Fuels and Lubricants 15 (04-15-02-0009) 199–220.
76. Bayliff, S, Windom, B, Marchese, A, Hampson, G, Carlson, J, Chiera, D, & Olsen, D. (2020). Controlled End Gas Auto Ignition with Exhaust Gas Recirculation on a Stoichiometric, Spark Ignited, Natural Gas Engine. Proceedings of the ASME 2020 Internal Combustion Engine Division Fall Technical Conference. ASME 2020 Internal Combustion Engine Division Fall Technical Conference. November 4–6, 2020. V001T03A011. ASME. https://doi.org/10.1115/ICEF2020-2979
77. Gomez, J.E., Walker, B. (2019). National Propane Survey 2017 – 2018 Final Report. Southwest Research Institute, San Antonio, TX. Prepared for Propane Education and Research Council, Docket No. 21257, SWRI Project No. 08.23448.
78. Amador Diaz, J.G., Gomez Montoya, J.P., Corredor Martinez, L.A., Olsen, D.B et al. (2019). Influence of Engine Operating Conditions on Combustion Parameters in a Spark Ignited Internal Combustion Engine Fueled with Fuel Blends of Methane and Hydrogen. Energy Conversion and Management 181:414-424.
79. Kumar, D., Sonawane, U., Chandra, K., & Agarwal, A. K. (2022). Experimental investigations of methanol fumigation via port fuel injection in preheated intake air in a single cylinder dual-fuel diesel engine. *Fuel*, *324*. https://doi.org/10.1016/j.fuel.2022.124340

80. Ramalingam, A., Panigrahy, S., Fenard, Y., Curran, H., Heufer, K.A. (2021). A chemical kinetic perspective on the low-temperature oxidation of propane/propene mixtures through experiments and kinetic analyses. Combustion and Flame 223:361-375.
81. Wendeker, M., Jakliński, P., Czarnigowski, J., Boulet, P., & Breaban, F. (2007). Operational Parameters of LPG Fueled SI Engine-Comparison of Simultaneous and Sequential Port Injection. SAE International, SAE 2007-01-2051.
82. Loganathan, M., & Ramesh, A. (2007). Study on manifold injection of LPG in two stroke SI engine. Journal of the Energy Institute, 80(3), 168–174. https://doi.org/10.1179/174602207X216255
83. Hofeldt, D. (1993). Alternative Fuel Technologies for Heavy Duty Vehicles: Performance, Emissions, Economics, Safety, and Development Status. SAE Technical Paper 930731, https://doi.org/10.4271/930731
84. Lee, Y., Kim, C., Oh, S., & Kang, K. (2004). Effects of Injection Timing on Mixture Distribution in a Liquid-Phase LPG Injection Engine for a Heavy-Duty Vehicle. JSME International Journal, Series B, Vol. 47, No. 2.
85. Kim, K., Kim, J., Oh, S., Kim, C., & Lee, Y. (2017). Lower particulate matter emissions with a stoichiometric LPG direct injection engine. Fuel, 187, 197–210. https://doi.org/10.1016/j.fuel.2016.09.058
86. Hyun, G., Oguma, M., and Goto, S. (2002). CFD Study of an LPG DI SI Engine for Heavy Duty Vehicles. SAE Technical Paper 2002-01-1648. https://doi.org/10.4271/2002-01-1648.
87. Sierens, R., "An Experimental and Theoretical Study of Liquid LPG Injection," SAE Technical Paper 922363, 1992, https://doi.org/10.4271/922363.
88. Windell, B., Sharma, M., Nocivelli, L., Asztalos, K. et al. (2022). Bulk Spray and Individual Plume Characterization of LPG and Iso-Octane Sprays at Engine-Like Conditions. SAE Technical Paper 2022-01-0497. https://doi.org/10.4271/2022-01-0497.
89. Lacey, J., Poursadegh, F., Brear, M. J., Gordon, R., Petersen, P., Lakey, C., Butcher, B., & Ryan, S. (2017). Generalizing the behavior of flash-boiling, plume interaction and spray collapse for multi-hole, direct injection. Fuel, 200, 345–356. https://doi.org/10.1016/j.fuel.2017.03.057

90. Churchill, R., Windom. B. (2024). Numerical investigation of mixture formation at different start of injection timings for a direct injection LPG engine. Proceedings of the Western States Section of The Combustion Institute Spring Technical Meeting.
91. S. R. Turns, An Introduction to Combustion Concepts and Applications, 3rd Edition, McGraw-Hill Education, 2012.
92. McGee, M., Curtis, W., Russ, G., Lavoie, A. (2000). The Effects of Port Fuel Injection Timing and Targeting on Fuel Preparation Relative to a Pre-Vaporized System. SAE Technical Paper 2000-01-2834.
93. Kar, T., Zhou, Z., Brear, M., Yang, Y., Khosravi, M., Lacey, J. (2021). A Comparative Study of Directly Injected Spark Ignition Engine Performance and Emissions with Natural Gas, Gasoline and Charge Dilution. Fuel (304) 121438 https://doi.org/10.1016/j.fuel.2021.121438.
94. Woo, S., Lee, J., & Lee, K. (2021). Experimental study on the performance of a liquefied petroleum gas engine according to the air fuel ratio. Fuel, 303. https://doi.org/10.1016/j.fuel.2021.121330
95. Choi, G. H., Chung, Y. J., & Han, S. bin. (2005). Comparison study between mixer and liquefied petroleum injection system fuel supply methods in a heavy-duty single cylinder engine. Proceedings of the Institution of Mechanical Engineers, Part D: Journal of Automobile Engineering, 219(9), 1119–1123. https://doi.org/10.1243/095440705X34748
96. Singh, S. B., Dhar, A., & Agarwal, A. K. (2015). Technical feasibility study of butanol-gasoline blends for powering medium-duty transportation spark ignition engine. Renewable Energy, 76, 706–716. https://doi.org/10.1016/j.renene.2014.11.095
97. Sharma, M., Windom, B., Yalin, A., & Yost, D. (2023). Thesis Diagnostics and Characterization of Direct Injection of Liquified Petroleum Gas for Development of Spray Models at Engine-Like Conditions. Masters' Thesis, Colorado State University.
98. Rodriguez, J.F., Xu, H., Hampson, G., Bestel, D. et al. (2023). Innovative Piston Design Performance for High Efficiency Stoichiometric Heavy Duty Natural Gas Engine. SAE Technical Paper 2023-01-0288. doi:10.4271/2023-01-0288.

99. Goto, Shinichi., Lee, Daeyup., Harayama, Naoya., Honjo, Fumitaka., Ueno, Hiroki., Honma, Hidekazu., Wakao, Yoshitaka., Mori, Makihiko. (2000). Development of LPG SI and CI engines for heavy duty vehicles. 2000-05-0166.
100. Kalghatgi, G. T. (2015). Developments in internal combustion engines and implications for combustion science and future transport fuels. Proceedings of the Combustion Institute, 35(1), 101–115. https://doi.org/10.1016/j.proci.2014.10.002
101. Srivastava, D., & Agarwal, A. K. (2013). Laser ignition of single cylinder engine and effects of ignition location. SAE Technical Papers. https://doi.org/10.4271/2013-01-1631
102. Toulson, E., Huisjen, A., Chen, X., Squibb, C. et al. (2012) Visualization of Propane and Natural Gas Spark Ignition and Turbulent Jet Ignition Combustion. SAE Int. J. Engines 5(4):1821-1835. https://doi.org/10.4271/2012-32-0002.
103. Montgomery, D., Design and Analysis of Experiments: Fifth Edition, John Wiley and Sons, Incorporated, New York, 2001. ISBN: 0471316490
104. Brown, J., On-Engine Investigation of a Micro-Liter Quantity Pilot Ignition System for a Large Bore Natural Gas Engine, Master's Thesis, Colorado State University, 2003.
105. Olsen, D. B., & Kirkpatrick, A. K. (2008). Experimental examination of prechamber heat release in a large bore natural gas engine. Journal of Engineering for Gas Turbines and Power, 130(5). https://doi.org/10.1115/1.2906182
106. Benajes, J. & Novella, R. & Gomez-Soriano, J. & Martinez-Hernandiz, P.J. & Libert, C. & Dabiri, M. (2019). Evaluation of the passive pre-chamber ignition concept for future high compression ratio turbocharged spark-ignition engines. Applied Energy, Elsevier, vol. 248(C), pages 576-588.

APPENDIX

As described in section 2.5.4, nominal repeat tests were conducted for every day of testing on the CFR and the X15 heavy-duty engine to ensure the repeatability and consistency of engine data. The trends are presented in this appendix section for both engines. On the CFR engine, the repeat tests were conducted at 900RPM, 9.5:1 compression ratio, 60 deg C mixture temperature, and at naturally aspirated (101.3kPa), stoichiometric conditions with compressed natural gas filled in a gas bottle (average methane number - 73). The CA50 was set at 10.3 deg aTDC, with coolant temperature, oil pressure, and temperature maintained at 95 deg C, 186kPa and 55 – 60 deg C respectively. The CFR engine was also operated in the hot motoring configuration as described in Heywood [10] at the beginning and end of each test day at compression ratio 9.5:1 and 900RPM. The Coriolis meter fuel flow rate, which is a critical measurement in the determination of engine efficiency, from the repeat tests on the CFR engine are shown in Figure Appendix – 1 and the In-cylinder pressure traces for the hot motoring engine operation over the test days are shown in Figure Appendix – 2.

A similar procedure was followed for the X15 heavy-duty LPG engine, however, as the engine configuration changed frequently in terms of compression ratio, injection configuration, etc., only the repeat tests that were conducted while the engine was held at the final 14:1 compression ratio piston and high-flow direct injection configuration are presented here. The engine was operated at 1200RPM, 38 deg C intake manifold air temperature, and at naturally aspirated (101.3kPa), stoichiometric conditions with liquid DI LPG injected at 13MPa. The CA50 was set at 14 deg aTDC to avoid knock, with coolant temperature, oil pressure, and temperature maintained at 85 deg C, 290kPa and 110 deg C respectively. The X15 engine was also operated in the hot motoring

configuration as described earlier, but at 1200RPM. The Coriolis meter fuel flow rate, and in-cylinder pressure traces for the hot motoring engine operation are presented in Figures Appendix – 3 and 4 respectively.

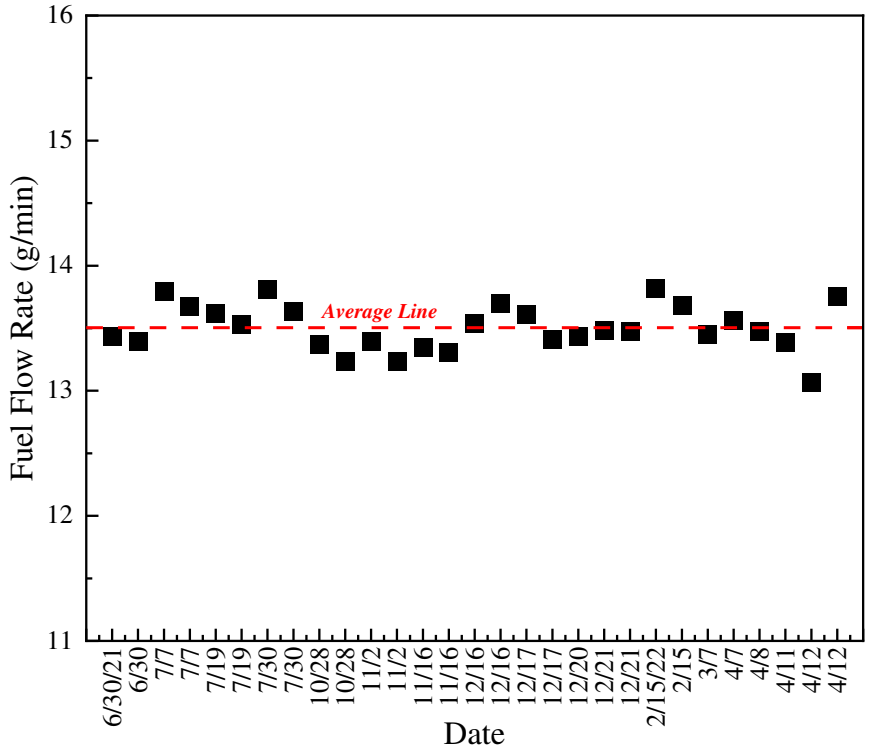

Figure Appendix – 1. Measured fuel flow rate (g/min) for the repeat tests conditions over the duration of CFR engine operation.

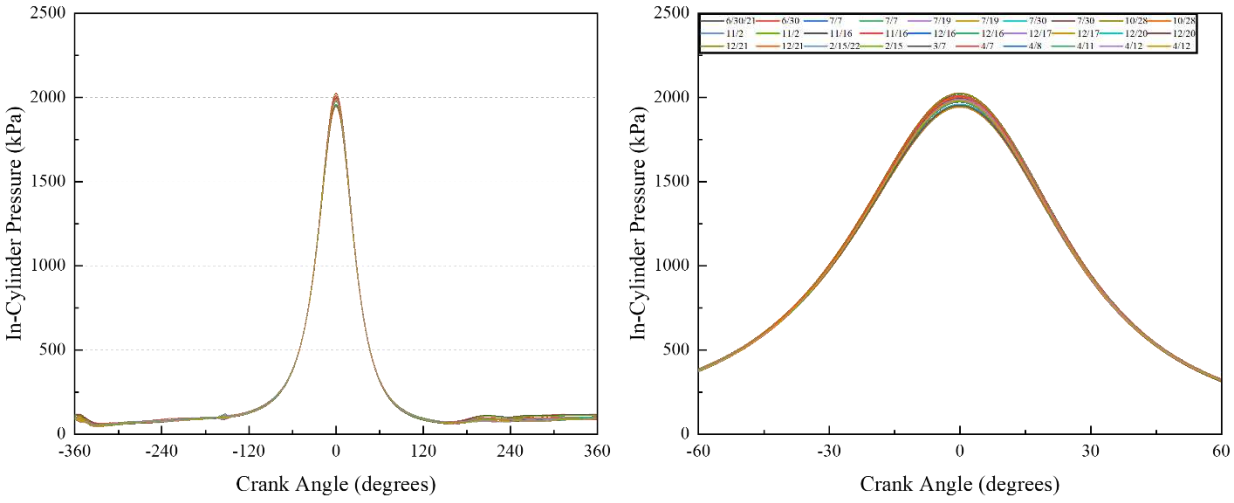

Figure Appendix – 2. In-cylinder pressure traces (zoomed in on the right) for the hot motoring engine operation over the duration of CFR engine operation.

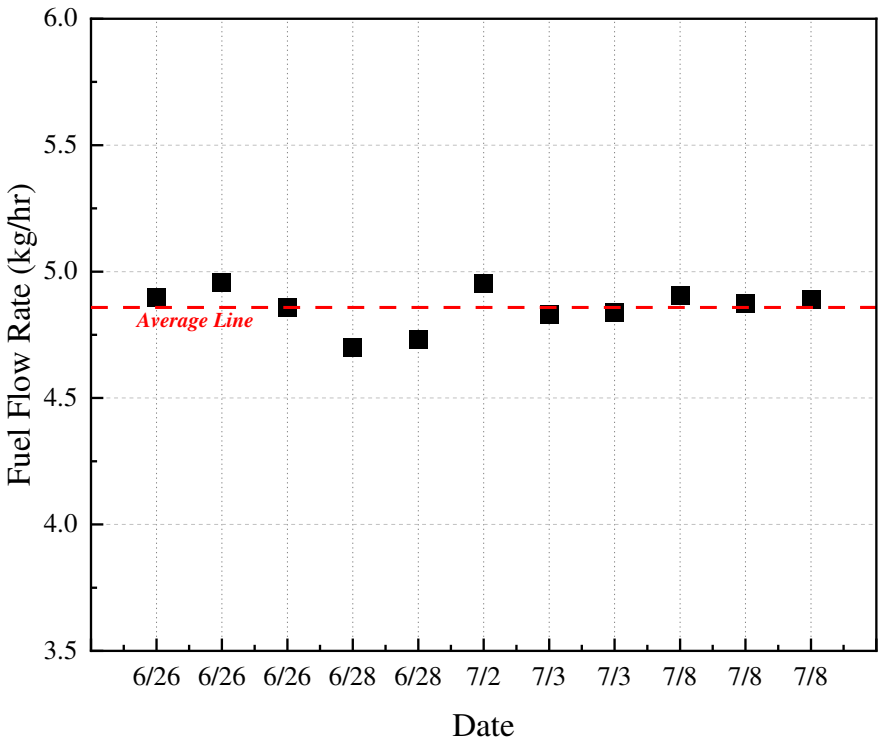

Figure Appendix – 3. Measured fuel flow rate (g/min) for the repeat tests on the X15 LPG engine

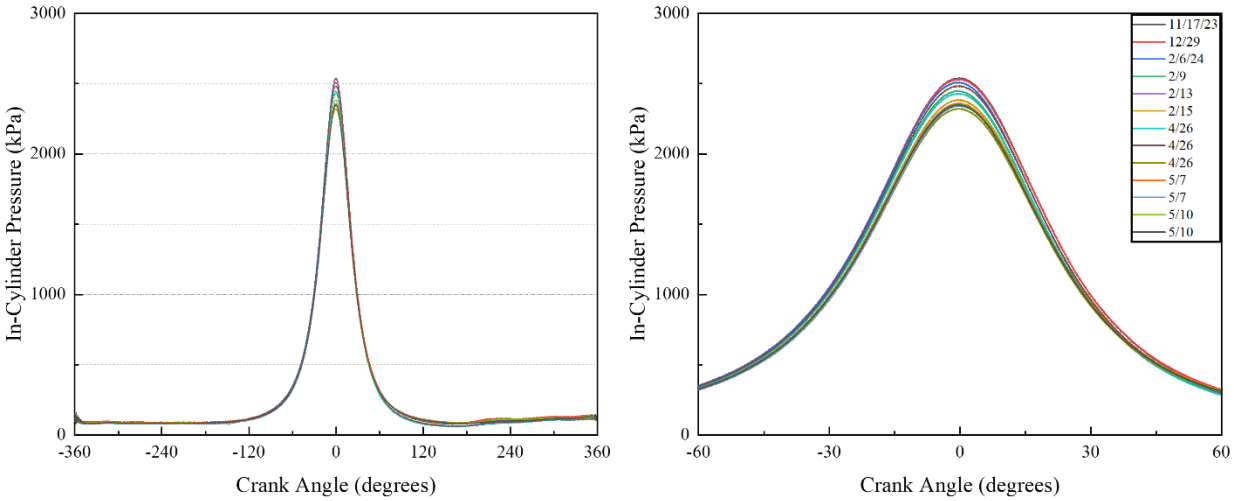

Figure Appendix – 4. In-cylinder pressure traces (zoomed in on the right) for the hot motoring engine operation of the heavy-duty LPG engine with the 14:1 high squish, high-flow DI configuration.